October 2010

Numerical Assessment of Roof Panel Uplift Capacity under Wind Load

Weixian He, *The University of Western Ontario*

Supervisor: Hanping Hong, *The University of Western Ontario*

A thesis submitted in partial fulfillment of the requirements for the Doctor of Philosophy degree in Civil and Environmental Engineering

Numerical Assessment of Roof Panel Uplift Capacity under Wind Load

(Spine title: Roof Panel Uplift Capacity under Wind Load)

(Thesis format: Integrated-Article)

by

Weixian He

Department of Civil and Environmental Engineering
Graduate Program in Engineering Science

A thesis submitted in partial fulfilment
of the requirements for the degree of
Doctor of Philosophy

School of Graduate and Postdoctoral Studies
The University of Western Ontario
London, Ontario, Canada
July, 2010

THE UNIVERSITY OF WESTERN ONTARIO
FACULTY OF GRADUATE STUDIES

CERTIFICATE OF EXAMINATION

Supervisor	Examiners
_____	_____
Dr. Hanping Hong	Dr. Ashraf A. El Damatty
	_____
	Dr. Craig Miller
	_____
	Dr. Liying Jiang
	_____
	Dr. Ying Hei Chui

The thesis by

Weixian He

entitled:

Numerical Assessment of Roof Panel Uplift Capacity under Wind Load

is accepted in partial fulfillment of the
requirements for the degree of
Doctor of Philosophy

Date_____ _____
Chair of the Thesis Examination Board

ABSTRACT

The integrity of the roof system is essential for ensuring the safety of inhabitants and preventing excessive damage to light-frame wood structures. The uplift capacity of fastened roof panels has been investigated using experimental tests and numerical models, where monotonic uniform static pressures are often applied to the roof panel models. The verification is needed for the adequacy of using static uniformly distributed pressure representing the wind load. Moreover, the uncertainty of nail withdrawal behaviour has not been included in existing numerical models, and the effect due to construction errors has not been addressed rationally.

A nonlinear Finite Element model is developed in this study to incorporate the nail withdrawal uncertainty in terms of maximum withdrawal force, initial stiffness, proportional limit, and the displacement at maximum force of the nail withdrawal behaviour. This model is used to investigate the statistical characteristics of the panel uplift capacity. The effect of spatial varying wind load is discussed by using the pressure coefficient obtained from wind tunnel model test at the Boundary Layer Wind Tunnel at the University of Western Ontario.

Furthermore, the impact of construction error is investigated, in terms of missing nail effects, with first-hand survey information. The detailed survey was carried out at the IRLBH (The Insurance Research Lab for Better Homes) facility to inspect the quality of construction, specifically for the statistical information of missing nails on roof panels.

Finally, the evaluated statistical characterization of panel uplift capacity is used for the reliability analysis of a typical panel considering or ignoring the missing nail effects.

Both code specified pressure-gust coefficient from NBCC (2005) and the peak pressure coefficients obtained from wind tunnel test are used. Results suggested that the nonlinear pushover analysis using the proposed nonlinear Finite Element model is adequate for estimating the panel uplift capacity. A more stringent fastening schedule with a spacing of 150 mm for the edges and intermediate supports is suggested for the construction of light frame wood houses.

Keywords: Uplift capacity, roof panel, wind pressure, spatial varying, nail spacing, nonlinear dynamic analysis, human error, missing nail, reliability

DEDICATION

To my father

Jun He

ACKNOWLEDGEMENTS

I would like to express my sincere and deep gratitude to my supervisor Professor Hanping Hong for his endless guidance, encouragement and moral support throughout this study. It is my honour to work with a mentor with such wisdom and graciousness.

A debt of gratitude is also owed to all the individuals and organizations who generously gave their time, funds, and ideas to this work. I am thankful to Dr. J. K. Galsworthy and Dr. G. A. Kopp for providing the wind pressure data in this study. The Civil and Environmental Engineering department provided me the opportunities to serve as an instructor and a teaching assistant in the past four years during my study, which provided not only financial support but also valuable experience. My fellow graduate students shared with me their ideas and happy time, which are treasures to cherish in my life. Special thank is given to Mr. Thomas Mara for his proofreading and valuable comments.

None of these works would have been possible without the supports of my family. I would like to express my truly appreciation to my father, Jun He, and my mother, Yanlin Li, for their constant source of love and concern. My deep gratitude is also to my brother, Peiyuan He, for his generous support. Last but not least, I am very grateful to my wife, Rui Zhao, for her precious love and unwavering encouragement.

Financial support from NSERC and the University of Western Ontario is very much appreciated.

TABLE OF CONTENTS

LIST OF TABLES

LIST OF FIGURES

LIST OF NOTATIONS

F	The nail withdrawal force used to define the force-displacement of nail withdrawal behaviour
d	The nail withdrawal displacement used to define the force-displacement of nail withdrawal behaviour
f_m	The maximum nail withdrawal force
f_p	The proportional limit of nail withdrawal force
d_m	The displacement corresponding to the maximum withdrawal force
d_p	The displacement corresponding to the proportional limit of withdrawal force
k_0	The initial stiffness of the nail withdrawal behaviour
Q_0	A constant model parameter used to define nail withdrawal curve, and to be determined with nail withdrawal test
Q_1	A constant model parameter used to define nail withdrawal curve, and to be determined with nail withdrawal test
Q_2	A constant model parameter used to define nail withdrawal curve, and to be determined with nail withdrawal test
Q_3	A constant model parameter used to define nail withdrawal curve, and to be determined with nail withdrawal test
Q_4	A constant model parameter used to define nail withdrawal curve defined by Equation (1b)
k	The secant stiffness used to define a equivalent linear nail model
γ	A variable to define the relationship between f_m and f_p
E	The modulus of elasticity of timber
A	The assumed contact area between sheathing and supporting frame

Y_i	A general random variable used to generate correlated random variables with Y_j
Y_j	A general random variable used to generate correlated random variables with Y_i
ρ_{ij}	The correlation coefficient of Y_i and Y_j
Y_0	A global random variable that independent of X_i
X_i	A local random variable that independent of Y_0
ρ	The correlation of nail withdrawal behaviour
m_{Y0}	The mean of random variable Y_0
v_0	The coefficient of variation of Y_0
m	The mean of a random variable
σ	The standard deviation of a random variable
v_X	The coefficient of variation of X_i
f	The sampling frequency
D	The length scale of a structure
U	The reference mean wind speed
FS	Short abbreviation for Full Scale
MS	Short abbreviation for Model Scale
R	The uplift capacity of roof panel
ρ_c	The correlation coefficient of pressure between two pressure taps
d_c	The distance between two pressure taps
λ	The correlation length
C_p	The pressure coefficient on roof measured at wind tunnel
ρ_a	The air density

A_T	The total area for a typical layout roof panel
F_T	The total uplift force of wind load at panel failure point
U_{CR}	The critical wind mean speed corresponding to F_T
C_i	The pressure coefficient of *i*-th pressure tap
A_i	The tributary area corresponding to *i*-th pressure tap
C_E	The equivalent pressure coefficient
F_{TF}	The total uplift force of wind load at panel failure point considering spatial varying wind load
$F_{TF,E}$	The equivalent total uplift force of wind load at the panel failure point
R_n	The ratio between F_{TF} and $F_{TF,E}$
$p(.)$	The binomial probability density function
p	The nail missing rate
m_{cm}	The mean of the equivalent pressure coefficient C_E
σ_{cm}	The standard deviation of the equivalent pressure coefficient C_E
$\hat{C}_m$	The peak value of the equivalent pressure coefficient C_E
a_n	The location parameter of Gumbel distribution of the $\hat{C}_m$
α_n	The dispersion parameter of Gumbel distribution of the $\hat{C}_m$
n	The number of time points of pressure data in one hour
C_pC_g	The external peak composite pressure-gust coefficients defined in NBCC
P_f	The probability of failure of a panel
$\Phi^{-1}(.)$	The inverse cumulative function of Normal distribution
β	The reliability index

CHAPTER 1

INTRODUCTION

1.1 Background

Damaging wind events, which include hurricanes, tornadoes, and other windstorms, occur year round and can strike most places in the United States and Canada. When specifically considering the insured property losses, wind probably is one of the highest natural disasters. Based on the post disaster investigations, the integrity of roofs is essential to the residential houses subjecting extreme wind events. It ensures the safety and prevents excessive damages to those light-frame wood structures. The loss of even one roof panel or window could cause insured losses increasing dramatically, and insured loss can reach up to 80% of total insured value of the house due to water penetration during a wind storm (Sparks et al. 1994). Studies showed that the partially enclosed buildings suffer much higher wind loads than an enclosed one, and keeping the integrity of a house is critical for reducing insured losses in wind storms (Rosowsky 1996). The uplift capacity of fastened roof panels is of great interest since the roof is one of the weakest links in building envelope. Experiment tests and numerical models are the two main approaches to evaluating its capacity.

Studies on the test results were reviewed by Datin and Prevatt (2009), indicating that monotonically increasing uniform static pressure is often applied in experiment investigation to find the uplift capacity of typical panels, and the panel failure is defined as the failure of the first nail, or a permanent separation between the fastened panel and supporting frames (Sutt 2000). As a summary of those test results, the mean of panel uplift capacity for plywood sheathing (11.9 mm (15/32 in) thickness) is ranged from

2.9~6.2 KPa (60~130 psf), or 8.6~18.5 KN in terms of total uplifting force. Those panels are all fastened on framing members with 8d common nails (the length and the diameter of the nail are 63 mm (2.5 in) and 3.4 mm (0.133 in), respectively) at the nail spacing of 150 mm along the framing members at panel edges and 300 mm along the interior supports. Such a big range of the panel capacity is mainly due to the variation of the nail withdrawal capacity, which can be affected by the type of wood, the wood moisture content, and the nail installing method, and the fore-mentioned tests are carried out with different type of wood framing member. Since there is no standard test protocol for determining the uplift capacity of wood framed roof structures, the obtained results can not compare to each other. Moreover, the numbers of the samples used in the tests are small (mostly less than 10 samples have been used), which make the test results statistically unreliable.

Numerical methods are used to predict the panel system failure from the nail withdrawal capacity, which can be obtained from tests that following the procedures described in ASTM D1761, Standard Test Method for Mechanical Fasteners in Wood (ASTM, 2005a). Nail withdrawal tests results usually based on hundreds of samples, such as Sutt (2000) reported the test results based on 593 samples, and the mean and coefficient of variation (cov) values of nail withdrawal equal 996N and 19% COV, respectively. However, most test reports available in the literature are focused on the maximum nail withdrawal force. Only Groom and Leichti (1993) reported the statistical test results for the initial stiffness, proportional limit, and the displacement at the maximum force, as well as the capacity of the nail withdrawal behaviour, which are very important for developing nonlinear model of nail withdrawal behaviour. It also makes the

analyzing of load sharing among nails possible when considering all nails within a panel as a system.

The spatial varying wind load effect on panel uplift capacity remains a mystery under wind loads. The theory has been well developed for linear structures, and there are extensive studies for ductile nonlinear structures in earthquake engineering. Datin and Prevatt (2009) provided the methodology of using equivalent pressure traces for a typical sized roof panel that accounts for the spatial varying wind load, but there is no further analysis carried out for the evaluation of the panel uplift capacity.

In the United States, significant building code revisions have also been conducted after hurricane Andrew in 1992. However, the post hurricane survey found out that the roof damage remains high in newer homes built to modern building code(Gurley et al. 2006). As Surry (Surry et al. 2005) pointed out:

"We know enough about the wind loads on low buildings now, so that disastrous failures (such as those seen during Hurricane Andrew) to storms other than severe tornadoes, are much more likely to be due to faults in codes, or construction and inspection practices, than due to a lack of basic wind engineering knowledge."

Human error effect on panel capacity was brought up to attention and a good opportunity was provided by the lab of the Insurance Research Lab for Better Homes in the project called "three little pigs". A detailed survey of the fastening of the roof panel was constructed, panel-by-panel and nail-by-nail, for the full-scale two-story test house at the IRLBH facility (Surry et al., 2005; Bartlett et al., 2007; Kopp et al., 2010). The statistical characteristic of panel uplift capacity was then carried out based on the Finite Element model that was developed in chapters 2 to 3.

1.2 Objectives

The main objective of the present study is to assess the statistical characteristics and to assign probability distribution of the uplift capacity of the roof panel under stochastic wind pressure and considering several factors: the uncertainty in nail withdrawal behaviour, the spatial varying effects of wind load, and the human error effects.

1.3 Organization of the thesis

This dissertation consists of five chapters. The subsequent four chapters are summarized briefly in the following.

Chapter 2 develops a nonlinear Finite Element model for evaluation of the roof panel uplift. This model is used to assess the statistical characteristics of the uplift capacity for the roof panel under stochastic wind pressure incorporating the uncertainty in nail withdrawal behaviour. The results have shown that the nonlinear behaviour of nail withdrawal needs to be considered to improve the accuracy of the estimated uplift capacity. The statistics and the probability model of the uplift capacity are affected by the degree of correlation of the fasteners' behaviour within the panel; the nail spacing and missing nail on the uplift capacity affect the uplift capacity significantly.

Chapter 3 focuses on the assessment of the statistics of and probability model for the uplift capacity of the roof panel under spatio-temporally varying wind pressure. The assessment considers the uncertainty in the spatial variation of nonlinear nail withdrawal behaviour and the impact of the possible missing nails.

Chapter 4 investigates the construction error effect on the panel uplift capacity. The statistical information of construction error is obtained by a detailed construction roof

survey on an “as build” two story typical Canadian residential house.

Chapter 5 summarizes conclusions obtained from the preceding chapters. Based on the conclusions, future research topics related to roof panel uplift capacity, risk, and codification for low rise residential roofs are suggested.

1.4 Thesis format

This thesis is prepared in a manuscript format as specified by the School of Postgraduate Studies at the University of Western Ontario. Each chapter is presented in a manuscript format with its own list of references.

Reference:

Bartlett F.M., Galsworthy, J.K., Henderson, D., Hong, H.P., Iizumi, E., Inculet, D.R., Kopp, G.A., Morrison, M.J., Savory, E., Sabarinathan, J., Sauer, A., Scott, J., St. Pierre, L.M., Surry, D. (2007). The Three Little Pigs Project: A New Test Facility for Full-Scale Small Buildings. In: International Conference on Wind Engineering, Cairns.

Groom, K.M. and Leichti, R.J. (1993). Load withdrawal displacement characteristics of nails, Forest Products Journal, 43(1), pp. 51-54.

Gurley K., Davis Jr. R.H., Ferrera S.P., Burton J., Masters F., Reinhold T., Abdullah M. (2006), Post 2004 Hurricane field survey - An evaluation of the relative performance of the standard building code and the Florida building code, Proceedings of the Structures Congress and Exposition, pp.8.

Hill, K., Datin, P., Prevatt, D.O., Gurley, K. and Kopp, G.A. (2009). A Case for Standardized Dynamic Wind Uplift Pressure Test for Wood Roof Structural Systems, 11th Americas Conference on Wind Engineering, San Juan, Puerto Rico.

Kopp, G.A., Morrison, M.J., Gavanski, E., Henderson, D. and Hong, H.P. (2010). The "Three Little Pigs" Project: Hurricane Risk Mitigation by Integrated Wind Tunnel and Full-Scale Laboratory Tests, Natural Hazards Review, http://dx.doi.org/10.1061/(ASCE) NH.1527-6996.0000019.

Surry, D., Kopp, G.A., and Bartlett, F.M. (2005). Wind load testing of low buildings to failure at model and full scale, ASCE Natural Hazards Review, vol. 6: 121-128.

Sutt, E.G. (2000). The Effect of Combined Shear and Uplift Forces on Roof Sheathing Panels, PhD thesis, Dept. of Civil Engineering, Clemson University, Clemson, S. C.

CHAPTER 2

PROBABILISTIC CHARACTERIZATION OF ROOF PANEL UPLIFT CAPACITY UNDER WIND LOADING

2.1 Introduction

The integrity of roof system is essential for residential houses subjected to extreme wind events. It could ensure the safety of inhabitants and prevent excessive damages to the light-frame wood structures. The loss of even a single panel or window has the potential to cause a dramatic increase in insured losses, which can reach up to 80% of the total insured value of the house in the event of water penetration during a wind storm (Sparks et al. 1994). Studies have shown that partially enclosed buildings or structures with openings suffer much higher wind pressure than an enclosed one (Kopp et al. 2008), and that maintaining the integrity of a house is critical for reducing insured losses in wind storms (Rosowsky and Schiff 1996).

The uplift capacity of fastened roof panels is therefore of great interest as the roof is one of the weakest links in building envelope, and has been investigated using both test results and numerical models. In previous experimental investigations, monotonically increasing uniform static pressure has often been applied to obtain the uplift capacity of typical panels, and the panel failure is defined as the failure or "pullout" of the first nail, or a permanent separation (6 to 12 mm) between the fastened panel and supporting frames (Sutt 2000). As panel tests can be costly, numerical models have been employed to estimate the capacity of panels considering the nail withdrawal capacity (Cunningham 1992, Mizzell 1994, Rosowsky and Schiff 1996, Kallem 1997, Sutt 2000). For example,

Cunningham (1992) considered that the uplift capacity of the panel can be estimated from the largest tributary area associated with a fastener in the panel, while Mizzell (1994) modeled the panel using shell element in a finite element model, with the nail connections represented by linear elastic springs to predicting the uplift capacity under static wind (load) pressure. The latter showed that the predicted uplift capacity using tributary area approach differs from that predicted by using the finite element model, and that the difference decreases with decreased nail spacing between fasteners. However, the nail withdrawal capacity is uncertain, and this uncertainty propagates to the estimated uplift capacity of panel under negative wind pressure (suction). Incorporation of this uncertainty to assess the uplift capacity by using the tributary area approach was presented by Rosowsky and Schiff (1996) and Sutt (2000).

The tributary area approach assumes that each nail in the panel shares the wind load, proportional to its tributary area, until failure. Therefore, the load sharing and redistribution caused by the differences in stiffness and withdrawal capacities of the fasteners cannot be considered. Murphy et al. (1996) carried out two types of tests: 30 typical panel tests and 40 single 8d (the length and the diameter of the nail are 63 mm (2.5″) and 3.4 mm (0.133″), respectively) common nail withdrawal tests on southern yellow pine (SYP) studs. They compared the results of single nail tests to the nail withdrawal capacities estimated from panel test based on panel failure pressures. Their findings indicated that the use of tributary area approach may not accurately predict panel capacity, especially in evaluating its statistical characteristics, and that a modification factor is needed to account for system effects. However, a modification factor derived for a particular fastening schedule and panel may not necessarily be applicable to panels

with different fastening schedules or panel thickness. Furthermore, in almost all previous studies, static uniformly distributed wind pressure is assumed even though natural wind pressure is spatio-temporarily varying; verification of the adequacy of applying static uniformly distributed load in assessing the panel uplift capacity is needed.

In housing construction, it has often been observed that nails may not be fastened properly or simply missing. Sutt (2000) estimated the missing nail effect on the uplift capacity of the panel using the tributary area approach (by excluding the missing nail), and suggested that tests need to be carry out to verify the missing nail effect. In addition, construction in different geographic regions may adopt different fastening schedules for roofing, which could affect the uplift capacity of the panels as well.

The main objective of the present study is to assess the statistical characteristics and to assign probability distribution of the uplift capacity of the roof panel under stochastic wind pressure while considering the uncertainty in nail withdrawal behaviour. For the uncertainty analysis, the simple Monte Carlo technique is employed, and the temporal variability of wind pressure is considered. The panel is modeled using a finite element model, and the nail connections are modeled using linear or nonlinear springs. Sensitivity of the statistics of panel uplift capacity to the nail spacing and missing nail(s), and to static and dynamic wind pressure, is also investigated. The material properties and geometrical variables of the considered panels and fasteners, numerical modeling and analyses, as well as the obtained statistics of the uplift capacity of the panels are presented in the following sections.

2.2 Modeling of the panel and wind load and analysis procedure

2.2.1 Model for roof panel

A typical roof panel with a fastening schedule for residential houses, shown in Figure 2.1, is considered for this study. The panel is composed of plywood sheathing with a thickness of 11.5 mm (3-plies) and a size of 1.22 m × 2.44 m (i.e., 4 ft × 8 ft); and is fastened to the framing members with 8d common nails. The length and the diameter of the nails are 63 mm (2.5 in) and 3.4 mm (0.133 in), respectively. The framing members, such as trusses and rafters, consist of 38 mm × 89 mm (2 in ×4 in) lumbers, often Douglas-fir, and are spaced 610 mm (24 in) on center. The nail spacing along the framing member shown in Figure 2.1 follows the roof panel fastening schedule for wind uplift recommended in APA (1995), the Engineered Wood Association. The schedule shown in Figure 2.1 is also recommended in NBCC (2005) and some jurisdictions in the United States; NBCC (2005) requires a nail spacing of 150 mm along the framing members at panel edges and 300 mm along the interior supports. More stringent fastener requirements are warranted for regions with significant wind hazard. For example, Florida Building Code (Florida Building Code 2007) requires a spacing of 152 mm (6 in) at panel edges and intermediate supports, except at gable ends where a spacing of 102 mm (4 in) is specified. However, nail spacing less than 76 mm (3 in) is not recommended as it is likely to split the wood.

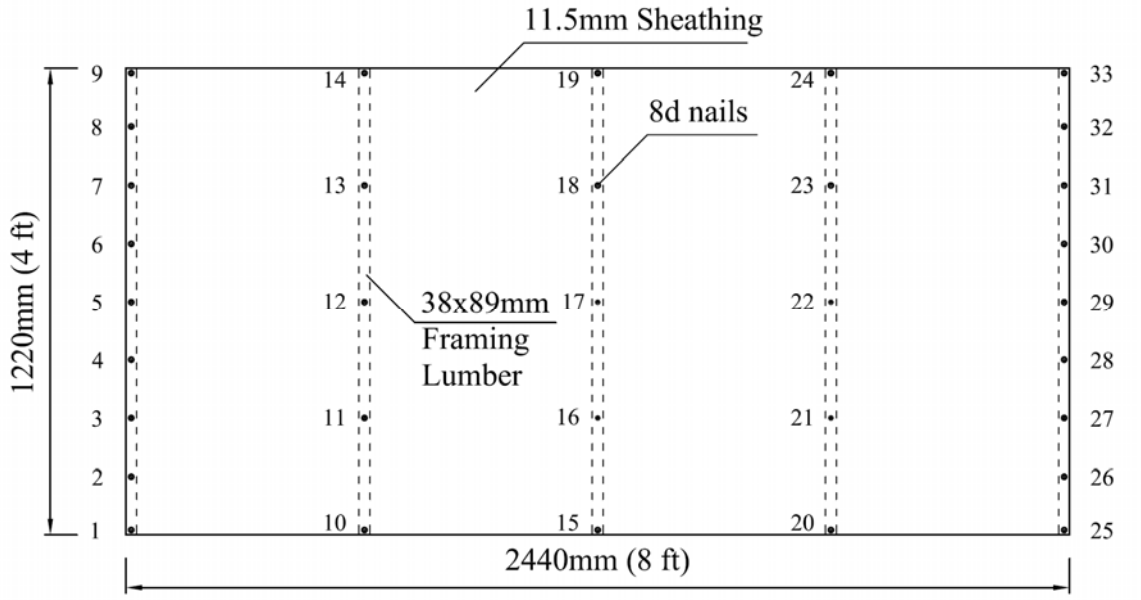

Figure 2.1 Typical roof panel and nail schedule.

In the present study, the panel is modeled using 4–node shell element with 6 degree of freedoms at each node, considering both bending and membrane stiffness to allow for large deflections. The mesh of the finite element model for the panel is shown in Figure 2.2, where the mesh is generated using ANSYS (ANSYS Inc. 2005). The element type used for nails is summarized in Table 2.1. It is assumed that the modulus of elasticity of Douglas-fir along the longitudinal grain, which equals 10.45 GPa, could be employed to represent that for the panel as Douglas-fir is the common wood specie used to manufacture plywood panels (Canadian Plywood Association 2005). It is noted that the wood is isotropic material, and the modulus of elasticity along the longitudinal, radial, and tangential axes of wood can be varying in a large range. While the plywood is a composite material with overlays, and the orientation of the plies are well balanced. The panel uplift capacity only reduces less than 2% if the modulus elasticity reduces to a half. Therefore, the modulus of elasticity along longitudinal grain is used, and treated as a

deterministic value.

Table 2.1 Elements used for the finite element modeling.

	ANSYS Element	Description
Roof Panel	Shell63	Large displacement, bending & membrane stiffness
Nail (Linear)	Combin14	1D linear spring
Nail (Nonlinear)	Combin39	1D nonlinear spring

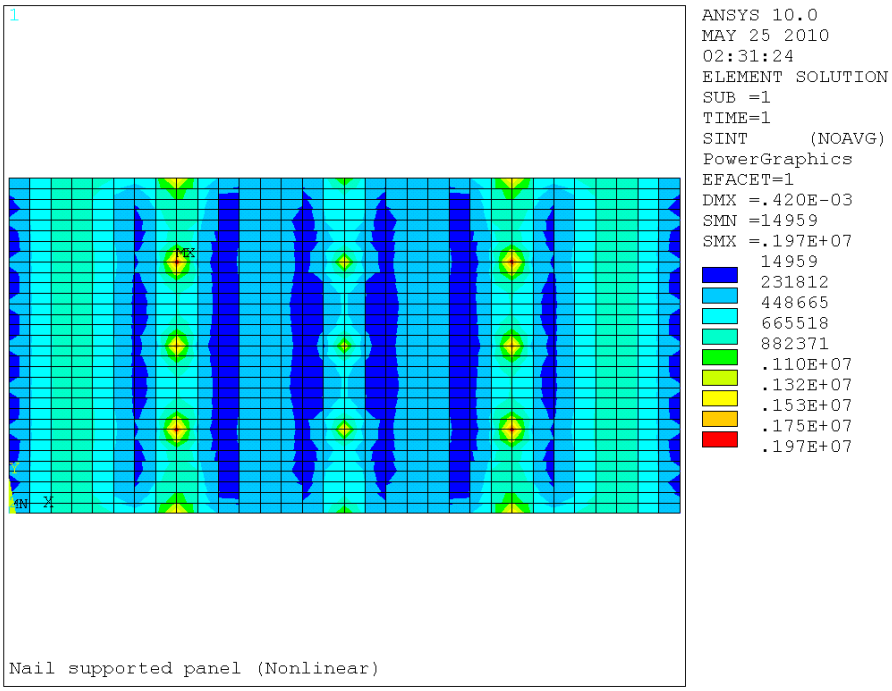

Figure 2.2 Finite element model mesh of the panel with fasteners.

As the nail withdrawal capacity is not significantly affected until the shear loading approaches the ultimate shear capacity of the nail (Sutt 2000), the shear effect on the nail withdrawal capacity is neglected in this study. The available nonlinear force-deformation curves used to model the nail withdrawal behaviour include elastoplastic model (Chui et

al. 1998) and tri-linear model (Groom and Leichti 1993). These models do not consider strain softening effect (i.e., negative stiffness after maximum load) to simplify the numerical treatment. More recently, Dao and van de Lindt (2009) proposed a new nonlinear roof panel fastener model that incorporates bending moment effect. They showed that the nail withdrawal behaviour can be modeled using nonlinear springs, and the moment rotation has an effect on external nail supports. However, the panel fastening schedule used in their study differs from that shown in Figure 2.1, and as the panel uplift capacity for the typical panel shown in Figure 2.1 is governed by the withdrawal capacity of the nails on internal supports, the moment rotation effect on nail withdrawal behaviour is neglected in the present study. To model nail withdrawal capacity, nonlinear springs with force-displacement curve illustrated in Figure 2.3 is adopted, where f_m, f_p, d_m, d_p and k_0 are the ultimate withdrawal force, proportion limit, displacement corresponding to the ultimate withdrawal force, displacement at proportional limit, and initial stiffness, respectively. The curve is based on the studies reported by Groom and Leichti (1993) and Foschi (2000). The force, F, and displacement, D, relation follows a linear relation from O up to the proportional limit (Point b). After Point b, the force-displacement relation is described by,

$$F = f_p + \left(Q_0 + Q_1 d\right)\left(1 - \exp\left(-k_0 d / Q_0\right)\right) \tag{1a}$$

for $d_p < D \le d_m$ where $d = D - d_p$, and

$$F = f_m \exp\left(Q_4 \left(D - d_m\right)^2\right) \tag{1b}$$

for $D > d_m$ where $Q_4 = \ln\left(Q_2\right) / \left[d_m \left(Q_3 - 1\right)\right]^2$.

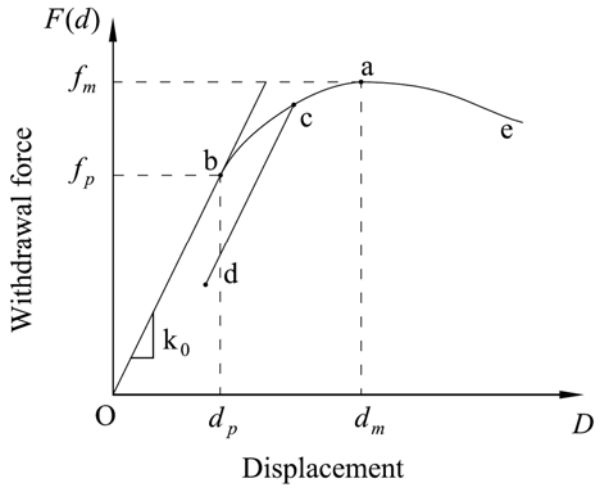

Figure 2.3 Force-displacement curve for nail withdrawal behavior.

The model parameters in the above equation (Q_0, Q_1, Q_2, Q_3) are determined using test results with monotonically increasing displacement. The displacement d_m corresponding to f_m for given Q_0, Q_1, f_p, and k_0 can be evaluated by letting F equal to f_m in Eq. (1a). If a roof panel is subjected to positive pressure, the nail is modeled using a linear spring with the stiffness equal to AE where E (= 10.45 GPa) is the modulus of elasticity of timber, and A (=0.0052 m^2) represents the contact area of panel with the 38 × 89 mm (2″×4″) stud. As negative wind pressures dominate throughout the roof, the nail model under positive pressure provides an equivalent restoring force only, and has no effects on panel uplift capacity.

For dynamic analysis, the loading and unloading behaviour needs to be considered. According to He et al. (2001), as an approximation, the initial stiffness can be used for the stiffness of unloading and reloading as shown in Figure 2.3. It is noteworthy that Foschi (2000) considered that the model is adequate for in plane displacement, whereas the displacement D in Eq. (1) represents the displacement along nail shank. The model

does not include the stiffness degradation of nail withdrawal capacity due to cyclic dynamic loads. To assess the difference between using linear and nonlinear nail connection models, a linear brittle spring is also considered. For the linear spring, it is considered that the stiffness equals the secant stiffness k defined as $k = f_m / d_m$, and the ultimate withdrawal capacity equals f_m.

Table 2.2 Parameters used to model the nail withdrawal behaviour.

Parameter	Mean value	Coefficient of variation
Initial stiffness, K_0 (N/m)	4171521.2	0.39
Proportional limit, f_p (N)	680.6	0.20
Maximum load, f_m (N)	805.1	0.17
Displacement corresponding to maximum laod, d_m (mm)	0.254	0.38
Ratio, r	0.183	0.44
Q_0*	121	-
Q_1*	1×10^5	-
Q_2*	0.9	-
Q_3*	2.6	-

* Values of Q_0 to Q_3 are determined by fitting Eq(1) to the mean capacity curve reported by Groom and Leichti (1993) through regression analysis.

Although it is acknowledged that the material properties for both the panel and nail withdrawal capacity are uncertain, only uncertainty in nail withdrawal capacity is considered to assess the panel uplift capacity. This is because that this study is focused on the nail withdrawal rather than the nail punching failure model, and no pull-through failures were observed in entire panel tests with 8d common nails and plywood sheathing for the test conducted by Sutt (2000). The uncertainty in the nail withdrawal capacity is influenced by the wood density, moisture content, nail installation method and the

statistical inhomogeneity in timber or lumber. Following Groom and Leichti (1993), the uncertainty in nail withdrawal capacity (i.e., the relation shown in Figure 2.3) can be characterized by the uncertainties in f_m, f_p, d_m, and k_0 where their means and standard deviations are shown in Table 2.2. Also shown in the table are the model parameters (Q_0, Q_1, Q_2, Q_3) for 8d common nail suggested by Foschi (2000).

Note that Sutt (2000) analyzed the ultimate withdrawal capacity from tests of 8d common nails fastened to SYP, and concluded that f_m can be modeled as lognormal variate with mean of 206.65 N/cm (118 lb per inch) and a coefficient of variation (cov) of 0.33. However, there is insufficient information available in the literature to investigate the appropriate probability model for f_p and k_0. As k_0 is non-negatively defined, it is assumed that it can be adequately modeled as a lognormal variate with the mean and cov shown in Table 2.2.

For a given nail, as f_m must be greater than f_p by definition, the ratio $(f_m\text{-}f_p)/f_p$, denoted by γ, must be non-negatively defined. It is considered that this ratio is lognormally distributed with mean of 0.183 and cov of 0.08, where these values are estimated using first-order second moment approximation (Madsen et al. 1986, Melchers 1999) and the statistics shown in Table 2.2.

For the simulation analysis, once values of f_m, k_0 and γ are sampled from their probability distributions, the force-deformation curve for nail withdrawal is completely defined if Q_0, Q_1, Q_2, and Q_3 are given, as f_p and d_p can be estimated using,

$$f_p = f_m / (1 + \gamma) \tag{2a}$$

and

$$d_p = f_p / k_0 \tag{2b}$$

and d_m can be evaluated using Eq. (1a).

The nail withdrawal behaviour within a panel could be correlated as they serve under similar environment and are fastened to similar timber species. Let Y_i denote the random variable of interest such as f_m, k_0 or γ for the i-th nail. As test results are not available to assess the correlation between Y_i and Y_j, the following multiplicative model is adopted to investigate the impact of the correlation of nail withdrawal behaviour on the estimated panel uplift capacity. The model considers that Y_i can be expressed as,

$$Y_i = Y_0 \times X_i,\ i = 1, \cdots, n, \tag{3}$$

where Y_0 and X_i are independent random variables. This model considers that the variable controlling the nail withdrawal capacity for each nail depends on a common or "global" variable Y_0 and on a "local" variable for the i-th nail, X_i, where X_i, $i = 1, \cdots, n$, are independent and identically distributed. If Y_0 is lognormally distributed with a mean of m_{Y0} and a cov of v_0 (i.e., $Y_0 \in LN(m_{Y0}, v_0 m_{Y0})$ where the symbol $LN(m, \sigma)$ is used to denote a lognormal variate with a mean of m and a standard deviation of σ), and $X_i \in LN(1, v_X)$, it can be shown that Y_i is lognormally distributed with mean m_{Yi} equal to m_{Y0}, and the correlation coefficient between Y_i and Y_j for $i \neq j$, ρ_{ij}, is given by,

$$\rho_{ij} = \frac{v_0^2}{v_0^2 v_X^2 + v_0^2 + v_X^2} \tag{4}$$

and the cov of Y_i, v_i, equals $\sqrt{v_0{}^2 v_X{}^2 + v_0{}^2 + v_X^2}$. This shows that the correlation for this multiplicative model is completely defined by the cov of the random variable Y_0 that is common to all nails, and by the cov of the independent identically distributed random variables X_i. The correlation is uniform in that it is distance (and nail location)

independent. The use of this model is advantageous because the degree of correlation and the cov of Y_i are completely defined by v_0 and v_X (or vice versa). In particular, if v_X equals zero, the correlation coefficients are equal to one; if v_0 equals zero, the correlation coefficients are equal to zero. This probabilistic model is adopted for f_m, k_0 and γ in section below to describe the fasteners. An illustration of the force-displacement curve simulated for 20 nails using the probabilistic models and with a correlation coefficient equals 0.5 is given in Figure 2.4.

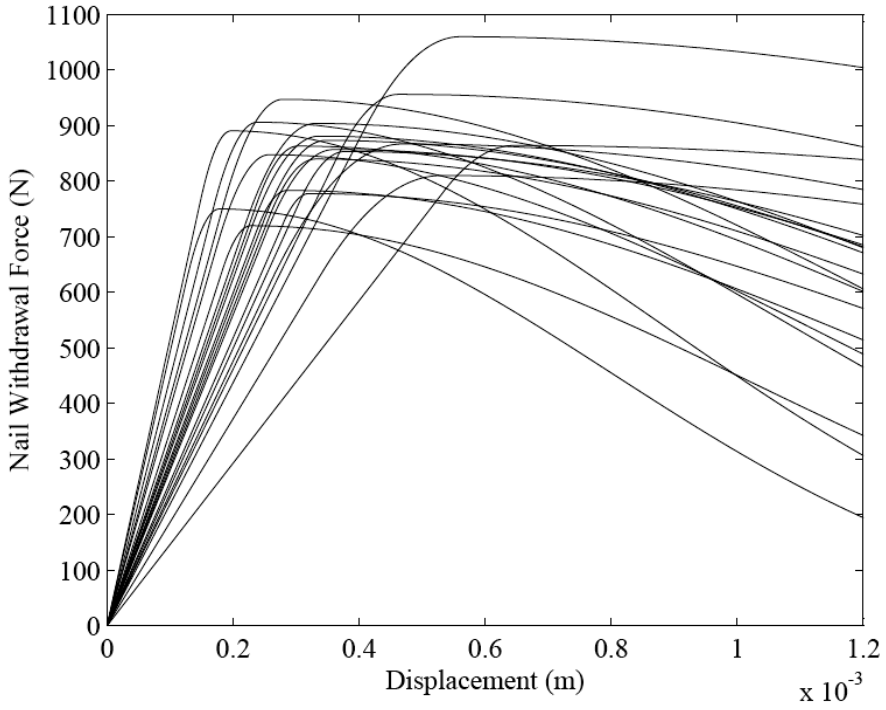

Figure 2.4 Samples of the force-displacement curve for nail withdrawal.

2.2.2 Wind Load Model

Wind pressure on low-rise buildings and houses is complex and varies spatio-temporarily. The variation is influenced by their geometry and orientation with respect to wind direction, and by their proximity to the adjacent structures (e.g. Simiu and

Stathopoulos 1997). For simplicity, the analyses are focused on fragility curves or the panel uplift capacities often consider that the wind pressure can be approximated as uniform and static, and that the panel uplift capacity can be estimated using tributary area method (Sutt 2000, Lee and Rosowsky 2005). The validity of this simplifying assumption and its associated accuracy in estimating the panel uplift capacity is unknown. Furthermore, as time-history of the wind pressure coefficients are available from boundary layer wind tunnel (Rigato et al. 2001), it is desirable, at least, to validate such assumption by comparing the uplift capacity obtained from time-varying wind pressure and that obtained under static uniform wind pressure, including nonlinear dynamic effects of the fasteners.

For the present study, the wind pressure time histories obtained from a test model carried out at the Boundary Layer Wind Tunnel laboratory at the University of Western Ontario are considered. The test model with the length scale of 1:50 represents a typical domestic dwelling with 4:12 gable roof, 8 m roof eave height. Locations of the pressure taps on the roof are shown in Figure 2.5, and the wind pressure coefficient time histories C_p, sampled at a frequency of 400Hz, for open country terrain (z_0=0.01 m) and a reference mean wind speed of 13.7 m/s (45 ft/s).

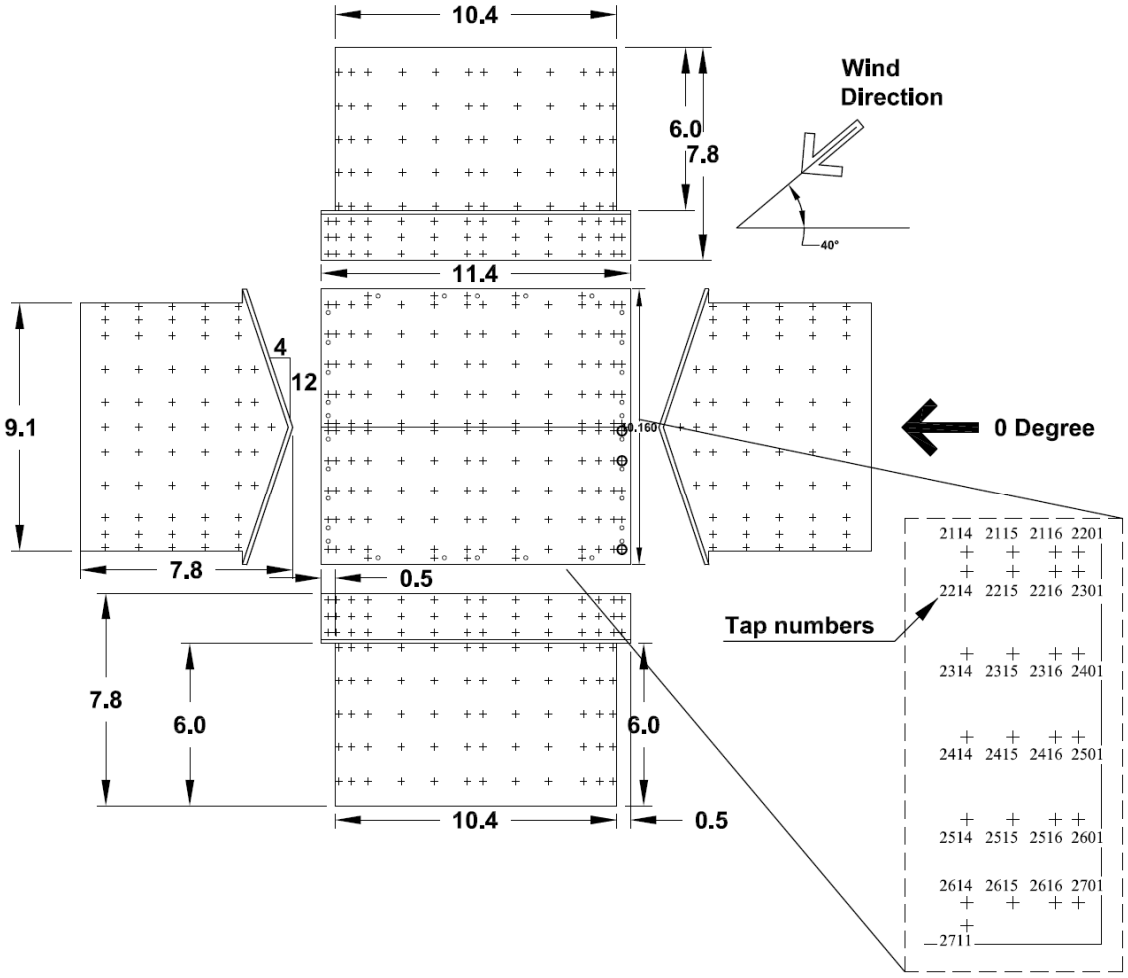

Figure 2.5 Identification of taps on test model.

The total number of samples for each tap is 71871, representing about 3 minutes time history for the model scale that corresponds to about one hour full-scale wind load history for a 30 m/s reference mean wind speed. The sampling frequency for full-scale is related to model scale as follows (Simiu and Scanlan 1996),

$$\left(\frac{fD}{U}\right)_{MS} = \left(\frac{fD}{U}\right)_{FS} \tag{5}$$

where D is the length scale, f is the sampling frequency, U is the mean wind velocity at the eave height, and the subscript FS and MS denote the quantities associated with full-scale and model scale, respectively. For example, if the reference mean wind speed is 30

m/s, the full scale sampling frequency f_{FS} determined by using Eq. (5) equals 17.5 Hz (i.e., $f_{FS} = \frac{f_{MS}U_{FS}}{U_{MS}} \times \frac{D_{MS}}{D_{FS}} = \frac{400 \times 30}{13.7} \times \frac{1}{50}$), and the wind pressure time histories on the roof are calculated by multiplying the time histories of C_p and the reference pressure.

2.2.3 Analysis Procedure

Both static and dynamic analyses are carried out on a typical roof panel subjected to static and time-varying wind pressure. The results are used to assess the dynamic load effects on the characteristics of panel uplift capacity. The numerical evaluation of the capacity by using the finite element model discussed previously is straight forward, if the wind pressure is modeled as a static uniform pressure, and the uncertainty in nail withdrawal capacity and material properties of panel is ignored. Furthermore, the resistance or capacity curve defined by the uplift force (or the total reacting force) versus displacement of a critical nail of the panel can be obtained using the nonlinear static pushover (NSP) analysis (Krawinkler and Seneviratna 1998). In fact, the term nonlinear static pushover analysis, perhaps, could be more appropriately termed as nonlinear static pullover analysis as the uplift or suction force is of concern. The uplift capacity (or capacity at incipient failure) is defined by the applied wind pressure or the point, where there is non-convergence for an increased wind pressure, provided that a stable and reliable numerical method is used for the analysis.

If deterministic nonlinear dynamic responses for a given time-varying wind pressure are of interest, the incremental dynamic analysis (IDA) (Vamvatsikos and Cornell 2002) which is developed in earthquake engineering, can be used. The method was adopted to evaluate transmission tower capacity under fluctuating along wind excitations (Banik et

al. 2010). To assess the capacity curve of the panel using the IDA, a series of nonlinear dynamic analyses needs to be carried out, each with increased reference wind speed and the same set of samples of the wind pressure coefficients. It must be emphasized that although the magnitude of the wind pressure coefficients for the time history measured from wind tunnel test is the same, the sampling frequency for the full-scale needs to be estimated using Eq. (5) for the given reference mean wind speed. Again, the results of nonlinear dynamic analysis can be used to obtain the capacity curve, defined in terms of maximum displacement of a critical nail and its corresponding total reaction force for each of the dynamic analysis, and to find the uplift capacity of the panel.

Furthermore, if the uncertainties in nail withdrawal capacity as well as different samples of pressure time history are considered, the simple Monte Carlo technique (Melchers 1999) can be employed to evaluate samples of the uplift capacity of the panel. In such a case, the finite element analyses are carried out repeatedly for simulated withdrawal behaviour of the nails. The samples of capacity curve and the uplift capacity of the panel obtained from each analysis can be used to statistically characterizing the capacity curve and uplift capacity of the panel.

2.3 Panel Uplift Capacity

2.3.1 Dynamic effect on panel capacity

A simple dynamic analysis of the panel is considered with the material properties equal to their corresponding means shown in Table 2.2 and the fastener modeled as linear elastic spring leading to the fundamental vibration frequency of 57.3 Hz. To investigate the uplift capacity of the panel under uniform but time-varying wind pressure, nonlinear

dynamic analysis is first carried out according to the procedure outlined in the previous section. For the dynamic analysis, the viscous damping ratio of 2% is considered throughout this study; the sample time history of wind pressure coefficients taken from tap 2301 (see Figure 2.5) is considered. For the evaluation, the sampling frequency for the full-scale is equal to 17.5 Hz (see previous section). Wind pressure time history of one minute shown in Figure 2.6a, has a mean wind pressure of -0.71 kPa (negative indicates suction). By using this wind pressure time history, the obtained displacement time history for the nail labelled 11 (see Figure 2.1) is shown in Figure 2.6b. The responses at nail 11, as well as nails 13, 21 and 23, shown in Figure 2.1 (the response at these nails are the same due to symmetry) are of interest, as they were found to be critical nails under uniform wind pressure. Inspection of the results of other nails indicates that the reacting force and displacement at these nails are larger than those associated with the remaining nails, implying that the wind demand on these nails is highest. To investigate the dynamic effect on the response of the panel, a time history static analysis was also carried out(i.e., static analysis but considering the magnitude of wind pressure obtained at each sampling point of the time history), which for simplicity will be referred to as quasi-static analysis. The obtained results are also shown in Figure 2.6b. The figure shows that the results obtained by quasi-static analysis are only very slightly greater than those obtained by the dynamic analysis. The difference is attributed to the inertial force and damping effect.

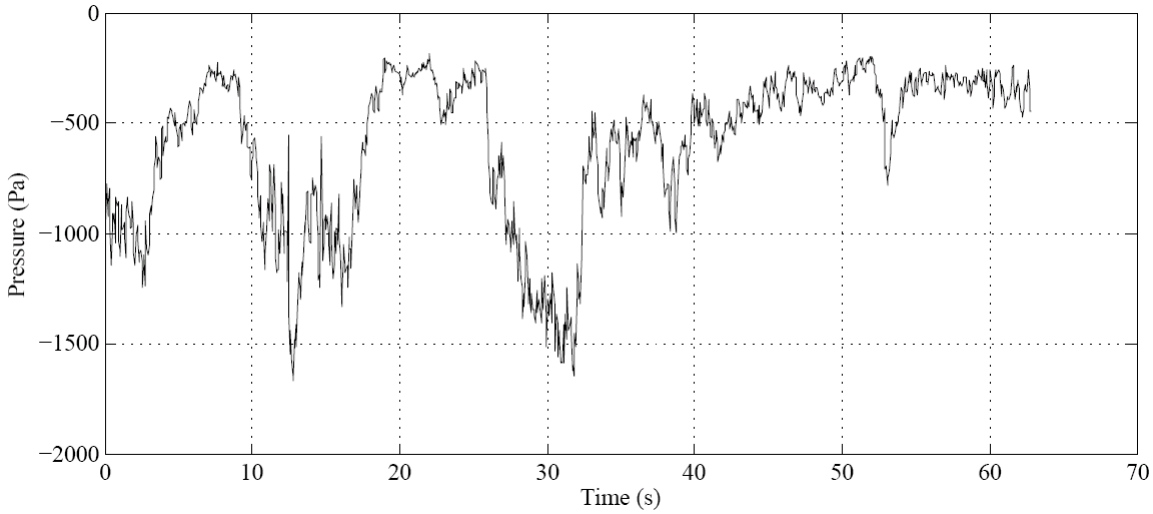

a). Pressure time history

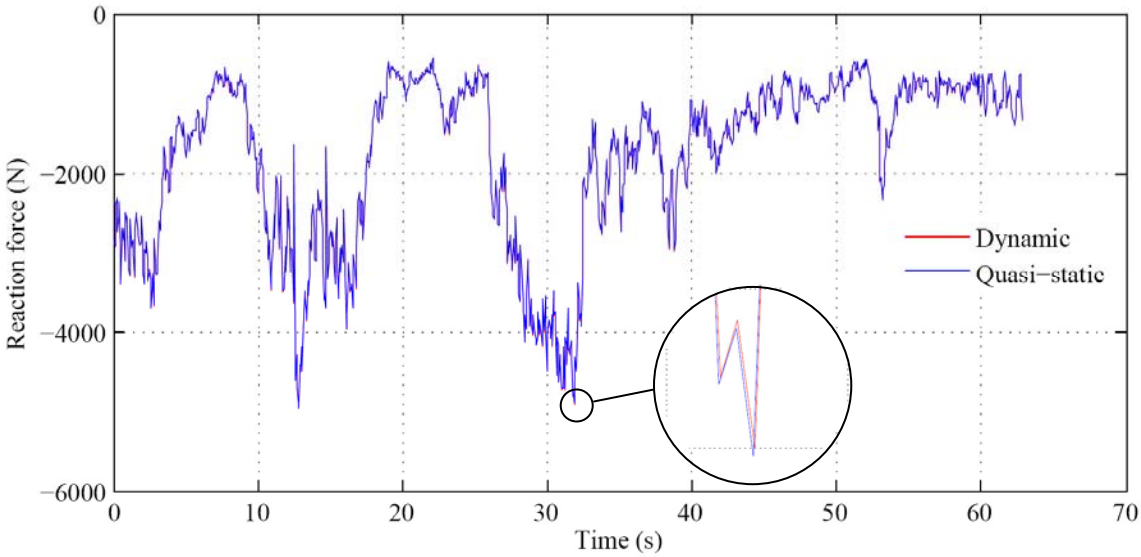

b) Time history of the total reaction force

Figure 2.6 Time histories of wind pressure and responses.

To completely characterize the uplift capacity of the panel under dynamic loads, a series of nonlinear dynamic analyses (i.e., IDA), each with an increased wind speed, is carried out. The obtained maximum total reacting force and the corresponding displacement of nail 11 for each nonlinear dynamic analysis are collected and plotted in Figure 2.7. Note that the identified total reacting force is independent of whether the displacement of nail 11 is used to represent the ordinate to draw the capacity curve. The

use of one minute (full scale) wind pressure time history to characterize the capacity curve is adequate (Banik et al. 2010). Since the wind pressure is time-varying and stochastic, the IDA is repeated using nine additional one-minute wind pressure records based on the pressure coefficients from the same tap to assess the effect of "record-to-record" variability. The obtained results are shown in Figure 2.7 as well, indicating that the record-to-record variability is not very significant, at least if the time history obtained from the same pressure tap is considered.

For the NSP analysis with uniformly distributed pressure over the panel instead of using nonlinear dynamic or quasi-static analysis, the obtained capacity curve is also shown in Figure 2.7. Unfortunately, the use of the NSP analysis could not obtain the descending branch of capacity curve (i.e., the part on the right side of point A shown in Figure 2.7) as in this case a force driven algorithm (as opposite to the displacement controlled algorithm) is adopted for the NSP analysis. To overcome this, a nonlinear dynamic analysis without the viscous damping is carried out by considering the panel subjecting to a ramp load defined by spatially uniformly distributed pressure whose magnitude increases linearly with time. For the analysis, the rate of increase of the pressure magnitude is considered to be equal to about the pressure associated with the yield capacity of the panel divided by twice of the first vibration period; the time increment used for the nonlinear dynamic analysis is considered to be equal to the first vibration period divided by 40. The obtained time histories of the total reacting force versus the displacement at nail 11 are shown in Figure 2.8.

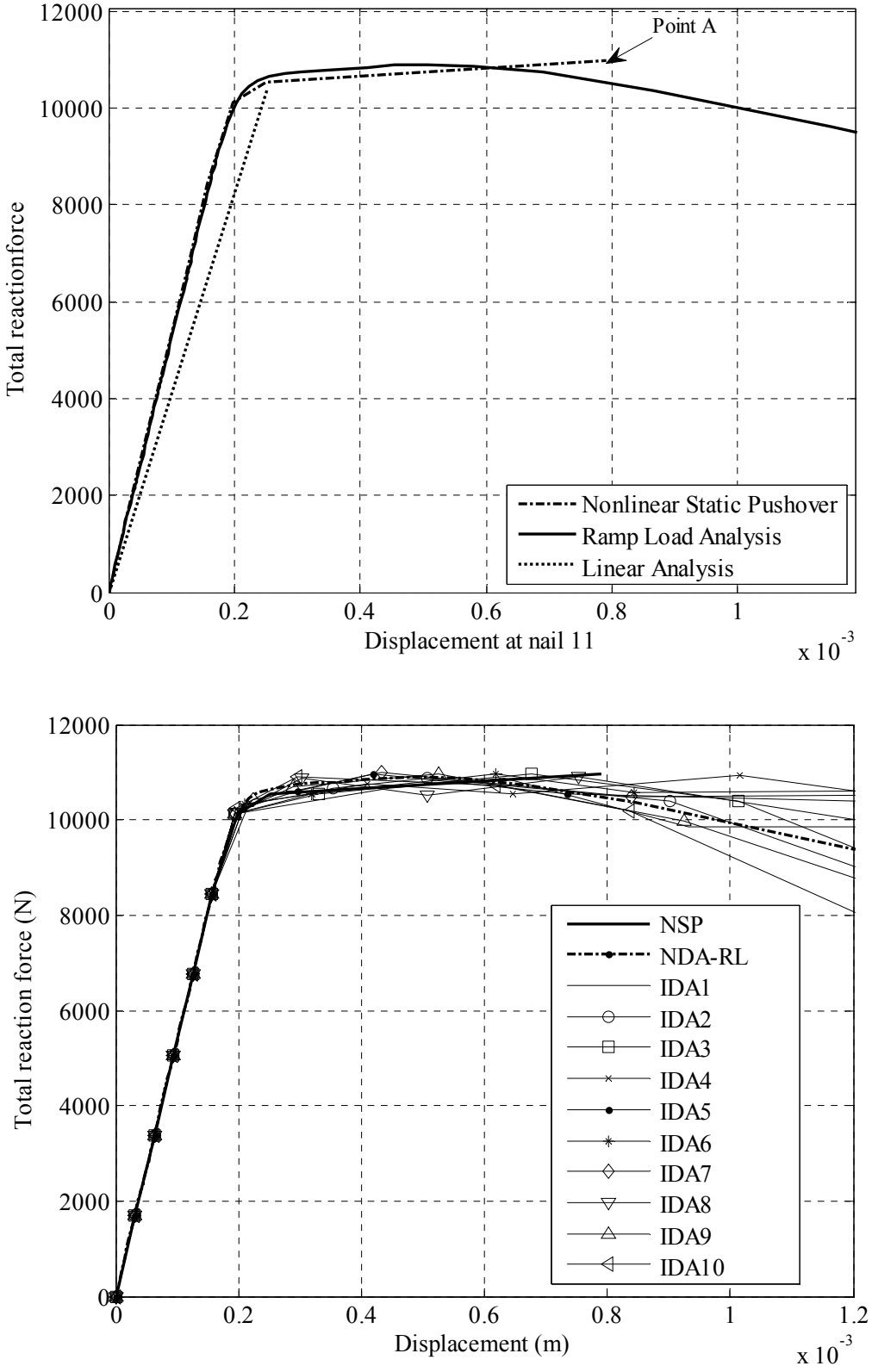

Figure 2.7 Estimated uplift capacity curves by different approaches.

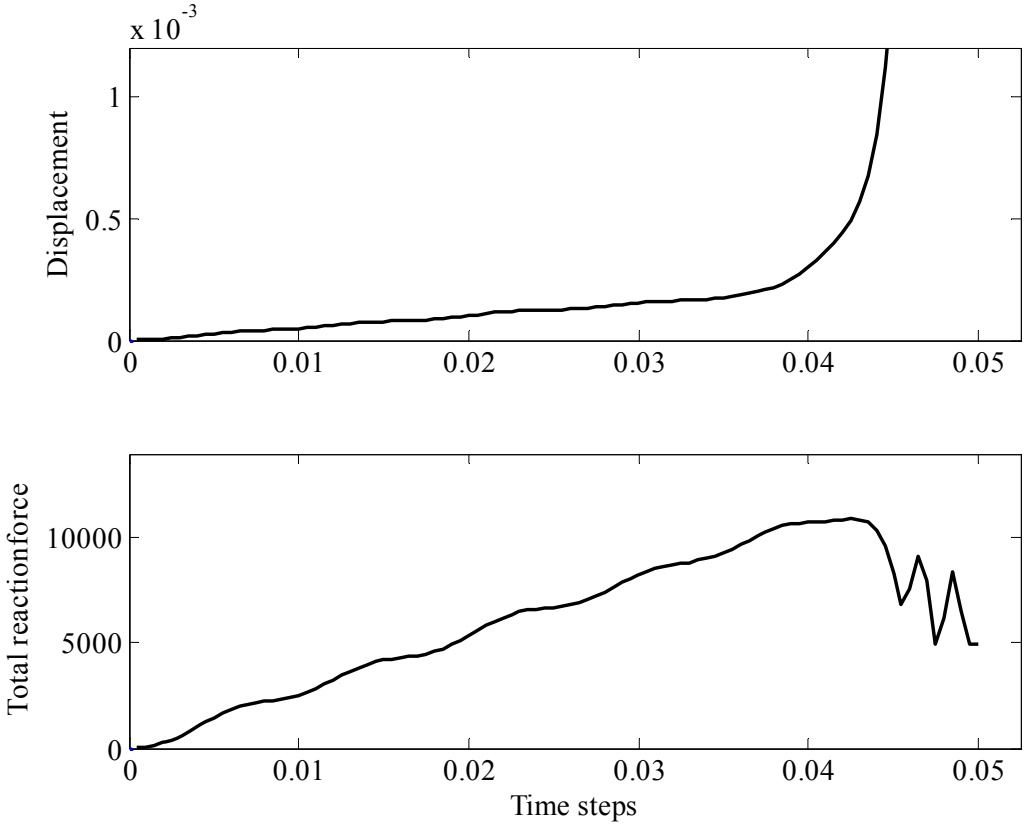

Figure 2.8 Time histories from nonlinear dynamic analysis for a constant wind pressure.

Since the total reacting force and displacement at each time instance is related, it is reasonable to use the force and displacement pair (for the same time instances) identified from Figure 2.8 to define the capacity curve. The curve obtained based on nonlinear dynamic analysis with the ramp load, termed as the NDA-RL curve, is presented in Figure 2.7 and compared with that obtained from the NSP analysis. During the analysis, it was observed that the NDA-RL curve is insensitive to the rate of increase of the pressure magnitude if the rate is sufficiently small. In fact, by varying this rate by 20% the identified maximum values from the NDA-RL curves differ by only 1%.

Comparison shown in Figure 2.7 indicates that the (maximum) panel uplift capacity obtained from the NSP curve is close to the average of the 10 IDA curves, and that the NDA-RL curve mimics well the average of the IDA curves. The use of the NDA-RL

curve as the panel uplift capacity curve is adopted below because it allows the identification of descending branch of capacity curve, it avoids the non-convergence problems that is often associated with the NSP analysis, and it requires significantly less computing time as compared to the evaluation of the average of the IDA curves.

2.3.2 Adequacy of linear-brittle approximation

To inspect whether the approach used in the previous section can be further simplified but still adequately predict the uplift capacity of the panel, instead of using the nonlinear force-deformation shown in Figure 2.3, we consider the linear-brittle model for the nail connection discussed earlier was used (i.e., with stiffness $k = f_m / d_m$ and the ultimate withdrawal capacity equal to f_m). The obtained results by using linear-brittle model are also shown in Figure 2.7. Comparison of the results shown in Figure 2.7 indicates that the predicted uplift capacity of the panel by using the linear-brittle model for the nails is 4.6% less than that by using the NDA-RL analysis. Furthermore, it is noted that if the uncertainty in nail withdrawal behaviour is considered, the panel uplift capacity estimated by the linear-brittle model could be directly proportional to the withdrawal capacity of the weakest nail among the critical nails (i.e., nails 11, 13, 21 or 23) as the linear-brittle model does not sustain any load after its capacity is reached, and the load redistribution may not occur. Therefore, the analysis by using the linear-brittle spring model will not be considered in the remaining part of this study.

2.3.3 Impact of uncertainty in nail withdrawal behaviour on panel uplift capacity

2.3.3.1 Fully correlated or independent cases

Roof panel uplift capacity (i.e., the maximum capacity identified from the capacity curve), R, depends on the properties characterizing nail withdrawal behaviour, which are uncertain. To incorporate this uncertainty in evaluating panel capacity, it is first assumed that each of f_m, γ and k_0 for all the nails is identically distributed. As discussed in Section 2, f_m, γ and k_0 are assumed to be lognormally distributed with the model parameters shown in Table 2.2.

To incorporate the uncertainty in nail behaviour in estimating the uplift capacity, first, samples of the nail properties (f_m, γ and k_0) are generated, and are used to evaluate values of f_p, d_p, and d_m according to Eqs. (1) and (2) to define the force-displacement curve. Using this sample force-displacement curve for all nails in the panel and applying the NSP analysis as was done in the previous section, the uplift capacity of the panel is evaluated. By carrying out this procedure 500 times, samples of R are obtained and plotted on lognormal probability paper in Figure 2.9. Visual inspection of the plot suggests that the samples can be approximated by a straight line, and R could be modeled as a lognormal variate. A Kolmogorov-Smirnov goodness-of-fit test (Benjamin and Cornell 1970) indicates that the hypothesis that R is lognormally distributed could not be rejected at a significance level of 5%. For comparison, the statistics of R are summarized in Table 2.3 and identified as the case with correlation coefficient ρ equal to 1 (i.e., $\rho = 1$). The magnitude of the cov of R which equals 0.154 is comparable to that of f_m, which equals 16.5% (see Table 2.1).

Table 2.3 Effect of correlation of nail withdrawal behaviour on the panel uplift capacity.

Condition		Mean (N)	Coefficient of variation
Fully correlated	ρ=1	10893	0.154
Partially correlated	ρ=0.9	10691	0.151
	ρ=0.8	10575	0.147
	ρ=0.5	10350	0.132
Independent	ρ=0	10138	0.074

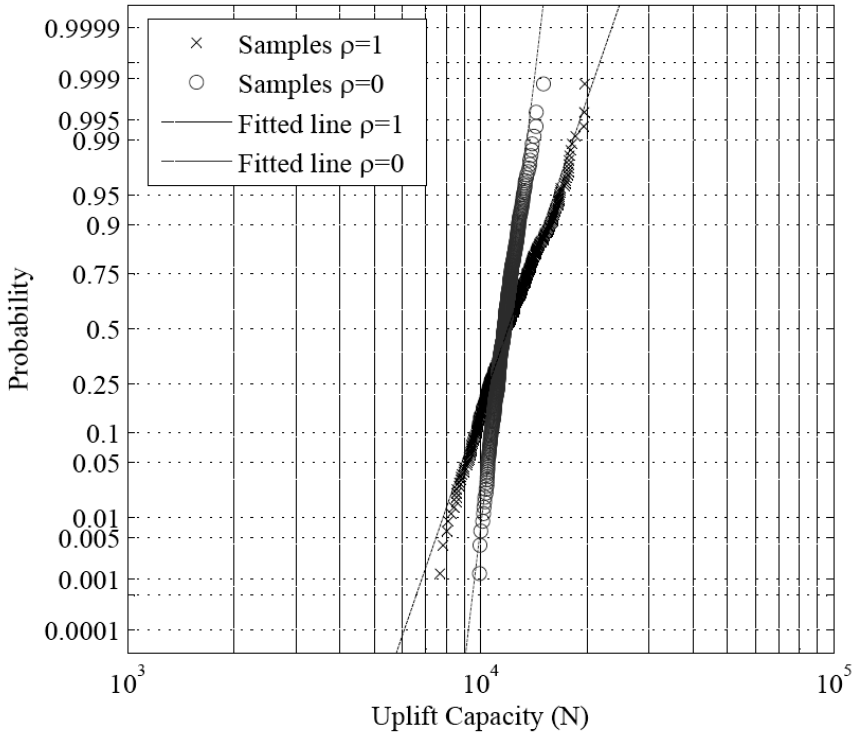

Figure 2.9 Simulated samples of uplift capacity presented on lognormal probability paper.

Rather than assuming that each of the variables f_m, γ and k_0 is identically and lognormally distributed for all nails, one can consider, as another extreme case, that each of the variables f_m, γ and k_0 is independent, identically and lognormally distributed for all

nails. By considering this case, and repeating the simulation analysis, the obtained samples are also plotted in Figure 2.9, and the mean and cov of samples of *R* are listed in Table 2.3. Comparison of the statistics of this case (i.e., case identified with $\rho = 0$) to those for the case with $\rho = 1$ indicates that the cov of *R* for the former is significantly less than that of the latter, although the mean of *R* is similar. The Kolmogorov-Smirnov goodness-of-fit test for the samples shown in Figure 2.9 (identified as $\rho = 0$) indicates that, again, *R* is lognormally distributed could not be rejected at a significance level of 5%.

Note that the means of *R* for the cases with $\rho = 1$ and $\rho = 0$ shown in Table 2.3 are lower than the mean of *R* determined from 7 experimental tests reported by Sutt (2000), which equals 11.4 kN (80 psf). This difference can be explained by noting that the mean of nail withdrawal capacity in the tests is 957 N while the mean of nail withdrawal capacity adopted in this study is 805.1 N. Furthermore, if the linear-brittle model (Mizzell 1994, Sutt 2000) is employed, which simplifies the analysis, the estimated mean of *R* is 10451 N and 8565 N for the cases with $\rho = 1$ and $\rho = 0$, respectively. The mean values are about 4.3% and 18% less than those shown in Table 2.3.

2.3.3.2 Effect of partial correlation of nail withdrawal behaviour on the uplift capacity of the panel

The nail withdrawal capacity for a panel is invariably and partially correlated since they serve under similar environment and fastened to similar or the same timber specie. As the values of the correlation coefficient or the experimental data for its assessment are not available, the multiplicative model discussed in Section 2.1 is employed for the

parametric analysis presented in this section. For the analysis, it is considered that the model described in Eq. (3) for Y_i can be used to model f_m, γ or k_0. For each of the random variables f_m, γ and k_0, as its mean and cov are already given in Table 2.2, by assigning the correlation coefficient ρ_{ij} equal to a selected value of ρ, v_0 and v_X for the model can be calculated using Eq. (4), as v_i, equals $\sqrt{v_0^2 v_X^2 + v_0^2 + v_X^2}$, and m_{Yi} and v_i are equal to the mean and cov of the variables of interest (i.e., f_m, γ or k_0).

Using the adopted model and following the procedure employed in the previous section, analyses are carried out for three selected cases: $\rho = 0.9$, $\rho = 0.8$, and $\rho = 0.5$. The obtained 500 samples of R for each case are shown in Figures 2.10a to 2.10c. The statistics of R are summarized in Table 2.3. The plots shown in the figure indicate that the use of the lognormal model for R is appropriate.

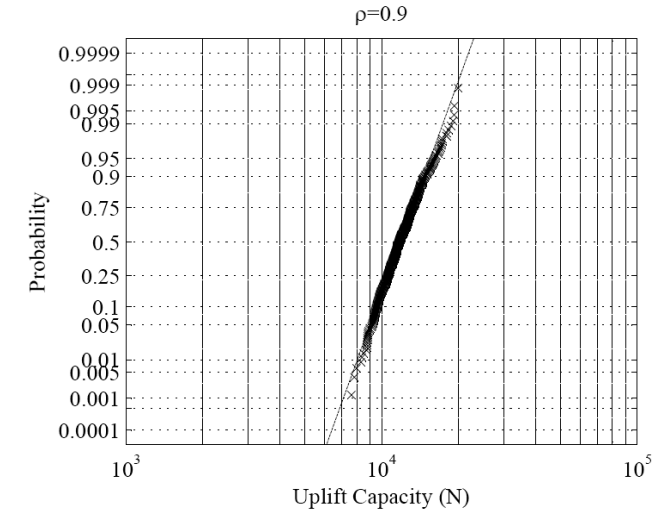

a) ρ = 0.9

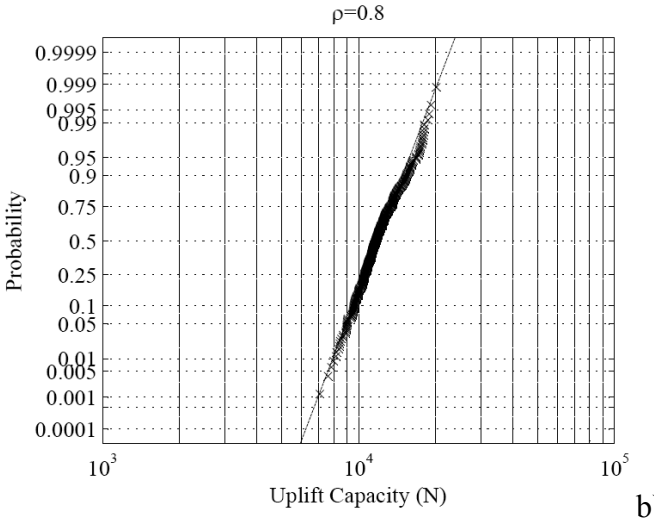

b) ρ = 0.8

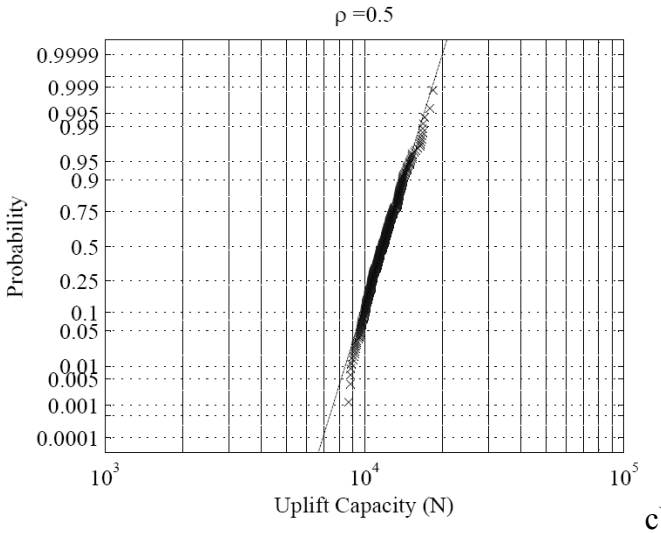

c) ρ = 0.5

Figure 2.10 Empirical probability distributions of the uplift capacity of the panel considering different degree of correlation of nail withdrawal behaviour.

Comparison of the results shown in Table 2.3 indicates that the mean of *R* is relatively insensitive to the value of ρ, while the cov of *R* decreases as the value of ρ decreases.

2.3.4 Effects of missing nail and nail schedule on the uplift capacity of the panel

As mentioned in the introduction, nails may not be fastened properly or simply missing in housing construction. To assess the impact of the missing nail effect on the uplift capacity of the roof panel, nails 5, 11 and 13 as shown in Figure 2.1 are considered missing one at time, or 2 at time, although it is acknowledged in construction practice the pattern of the missing nails are random.

Based on the above consideration and following the same analysis procedure employed in the previous sections, the obtained statistics of the uplift capacity of the panel for the cases with $\rho = 1$ and $\rho = 0$ are shown in Table 2.4 and the samples of *R* for each case are plotted in Figure 2.11. Visual inspection of the results shown in Figure 2.11 indicates that the lognormal model is still adequate for *R*. Table 2.4 shows that missing a single nail could reduce the mean of the panel uplift capacity by about 10%, missing two nails could reduce the mean of *R* by as much as 23%, and missing nails also can increase the cov of *R* for the case with $\rho = 0$ but slightly.

Table 2.4 Missing nail effects on panel uplift capacity.

Condition		Mean (N)	Coefficient of variation
Missing at nail #5	Fully correlated ρ=1	10833	0.154
	Independent ρ=0	10131	0.074
Missing at nail #11	Fully correlated ρ=1	9745	0.197
	Independent ρ=0	9426	0.082
Missing at nail #5 and #11	Fully correlated ρ=1	9383	0.182
	Independent ρ=0	9203	0.081
Missing at nail #11 and #13	Fully correlated ρ=1	8849	0.194
	Independent ρ=0	8759	0.087

One more issue that needs to be considered is the influence of the fastener schedule, as more stringent fastener requirements are warranted for regions with significant wind hazard. By considering the nail spacing of 6 inches on both internal and external supports, and repeat the analyses that were carried out to arrive at the results shown in Table 2.3, the obtained statistics of *R* are listed in Table 2.5. The mean uplift capacity of the panel shown in Table 2.5 is more than twice of those shown in Table 2.3. This is very significant as the number of nails is only increased from 33 to 45. In all cases, the differences between the cov value of *R* shown in Tables 3 and 5 are less than 20%.

Table 2.5 Uplift capacity for panel fastened with 6 inch nail spacing at panel edges and intermediate supports.

Condition		Mean (N)	Coefficient of variation
Fully correlated ρ=1		22156	0.154
Partially correlated	ρ=0.9	21623	0.152
	ρ=0.8	21309	0.148
	ρ=0.5	20710	0.127
Independent ρ=0		19683	0.063

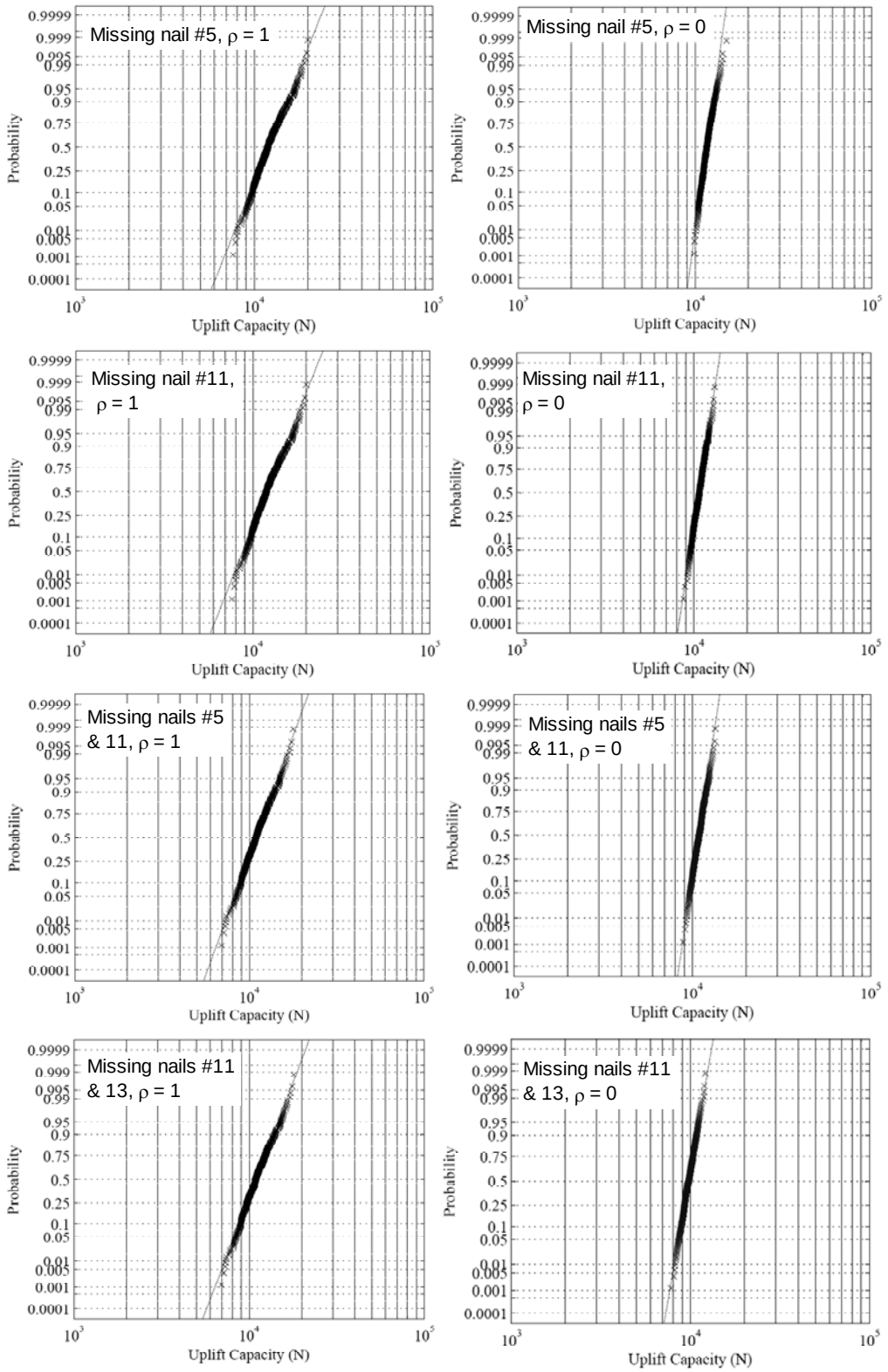

Figure 2.11 Empirical probability distributions of the uplift capacity of the panel considering the missing nail effect.

2.4 Conclusions

Statistical characterization of the uplift capacity of the roof panel under stochastic wind pressure has been carried out by considering the uncertainty in nail withdrawal behaviour. For the analysis, the panel is modeled using a finite element model and the nail withdrawal behaviour is modeled using a nonlinear spring. As the use of the nonlinear static pushover analysis could not identify the descending branch of capacity curve and often leads to non-convergence problem, and the application of the nonlinear incremental dynamic analysis is computing time consuming, the use of nonlinear dynamic analysis with a ramp load is adopted for estimating the uplift capacity of the panel, R. The numerical results show that the consideration of statistical correlation of nail withdrawal behaviour for the nails within the panel affects the mean of R negligibly, but it reduces the coefficient of variation (cov) of R as the degree of correlation between the nail behaviour decreases. In general, the use of the simple tributary area approach underestimates the mean of R by 5% to 23% as compared to that estimated using the NSP analysis. This underestimation is also about 10% if the panel is modeled using the finite element model and the nail withdrawal behaviour is modeled using (equivalent) linear-brittle spring.

Furthermore, sensitivity analysis indicates that missing a single nail could reduce the mean of the panel uplift capacity by 10%, and missing two nails could reduce the mean of R by as much as about 23%. Parametric analysis also indicates that by using a more stringent nail schedule with the nails spacing of 6 inches on the edge and intermediate supports, the mean of R is about twice of that obtained by using a nail spacing of 6 inches for edge supports and of 12 inches for intermediate support, which is a recommended

practice by the 2005 edition of the National Building Code of Canada (NBCC 2005).

In all cases, the uplift capacity of roof panel can be modeled adequately as a lognormal variate.

Reference:

ANSYS Inc. (2005), ANSYS User's Manual, Version 10.0, Canonsburg, PA.

APA – The Engineered Wood Association. (1995). Design capacities of APA performance rated structural use panels, Technical Note #N375B, Tacoma, WA.

Banik, S. Hong, H.P. and Kopp, G.A. (2010). Capacity curve of transmission under extreme wind load, Wind and Structures, Volume 13, Number 1, January, pp. 1-11.

Benjamin, J.R. and Cornell, C.A. (1970). Probability, Statistics and Decision for Civil Engineers, McGraw-Hill, New York.

Canadian Plywood Association (2005). Plywood Design Fundamentals, www.canply.org

Chui, Y.H., Ni, C., and Jiang, L. (1998). Finite element model for nailed wood joints under reversed cyclic load, Journal of Structural Engineering, ASCE, 124(1), pp 96-103.

Cunningham, T.P. (1992). Roof sheathing fastening schedules for wind uplift, APA Report T92-28, American Plywood Association, Tacoma, WA.

Dao, T.N. and van de Lindt, J.W. (2009). New nonlinear roof sheathing fastener model for use in finite-element wind load applications, Journal of Structural Engineering, ASCE, 134(10), pp1668-1674.

Datin, P.L., and Prevatt, D.O. (2009). Equivalent roof panel wind loading for full scale sheathing testing, 11th Americas Conference on Wind Engineering, San Juan, Puerto Rico.

Florida Building Code (2007). Florida Building Code -- Residential, International Code Council, Inc., FL.

Foschi, R.O. (2000). Modeling the hysteretic response of mechanical connections for

wood structures, Proc., World Conf. on Timber Engrg., Dept. of Wood Sci., ed., University of British Columbia, Vancouver.

Groom, K.M. and Leichti, R.J. (1993). Load withdrawal displacement characteristics of nails, Forest Products Journal, 43(1), pp. 51-54.

He, M., Lam, F. and Foschi, R.O. (2001). Modeling three-dimensional timber light-frame buildings, Journal of Structural Engineering, ASCE, 127(8), pp.901-913.

Hill, K., Datin, P., Prevatt, D.O., Gurley, K. and Kopp, G.A. (2009). A Case for Standardized Dynamic Wind Uplift Pressure Test for Wood Roof Structural Systems, 11th Americas Conference on Wind Engineering, San Juan, Puerto Rico.

Kallem, M.R. (1997). Roof Sheathing Attachment Sheathing Attachment for High Wind Regions: Comparison of Screws and Nails, MS thesis, Dept. of Civil Engineering, Clemson University, Clemson, S. C.

Kopp, G.A., Oh, J.H. and Inculet, D.R. (2008). Wind-Induced Internal Pressures in Houses, Journal of Structural Engineering, 134(7): 1129-1138.

Krawinkler, H. and Seneviratna, G.D.P.K. (1998). Pros and cons of a pushover analysis of seismic performance evaluation, Engineering Structures, 20(4-6), pp.452-464.

Lee, K.H. and Rosowsky, D.V. (2005). Fragility Assessment for Roof Sheathing Failure in High Wind Regions, Engineering Structures, 27, pp. 857-868.

Madsen, H. O., Krenk, S., and Lind, N. C. (1986). Methods of structural safety. Prentice-Hall, Englewood Cliffs, N.J.

Melchers, R.E. (1999). Structural Reliability Analysis and Prediction (2nd edition), Chichester, West Sussex, England: John Wiley and Sons Ltd.

Mizzell, D.P. (1994). Wind Resistance of Sheathing for Residential Roofs, MS thesis,

Dept. of Civil Engineering, Clemson University, Clemson, S. C.

Murphy, S., Schiff, S., Rosowsky, D. and Pye, S. (1996). System effects and uplift capacity of roof sheathing fasteners, Building an International Community of Structural Engineers, New York, NY, USA, pp.765-770.

Rigato, A., Chang, P. and Simiu, E. (2001). Database-assisted design, standardization, and wind direction effects, Journal of Structural Engineering, ASCE, 127(8), pp. 855-860.

Rosowsky, D.V. and Reinhold, T.A. (1999). Rate-of-load and duration-of-load effects for wood fasteners, Journal of Structural Engineering, ASCE, 125(7), pp.719-724.

Rosowsky, D.V. and Schiff, S.D. (1996). Probabilistic modeling of roof sheathing uplif capacity, Probabilistic Mechanics and Structural and Geotechnical Reliability, Proceedings of the Specialty Conference, pp.334-337.

Simiu E. and Scanlan R.H. (1996). Wind Effects on Structures, Fundamentals and Application to Design, New York: John Wiley.

Simiu, E. and Stathopoulos, T. (1997). Codification of wind loads on buildings using bluff body aerodynamics and climatological databases, J. Wind Eng. Ind. Aerodyn., Vol 69-71, pp.497–506.

Sparks, P.R., Schiff, S.D. and Reinhold, T.A., (1994). Wind damage to envelopes of houses and consequent insurance losses, J. Wind. Eng. Ind. Aerodyn., Vol. 53, pp. 145-155.

St. Pierre, L.M., Kopp, G.A., Surry D. and Ho T.C.E. (2005). The UWO contribution to the NIST aerodynamic database for wind loads on low buildings: Part 2 Comparison of data with wind load provisions, Journal of Wind Engineering and Industrial

Aerodynamics, Vol. 93 (1), pp. 31-59.

Sutt, E.G. (2000). The Effect of Combined Shear and Uplift Forces on Roof Sheathing Panels, PhD thesis, Dept. of Civil Engineering, Clemson University, Clemson, S. C.

Vamvatsikos, D. and Cornell, C.A. (2002). Incremental dynamic analysis, Earthquake Engineering and Structural Dynamics, Vol. 31, No. 3, pp. 491-514.

Zaitz, M.D. (1994). Roof sheathing racking effect on fastener withdrawal capacities, MS thesis, Dept. of Civil Engineering, Clemson University, Clemson, S.C.

CHAPTER 3

EFFECTS OF SPATIALLY AND TEMPORALLY VARYING WIND LOAD ON ROOF PANEL UPLIFT CAPACITY

3.1 Introduction

Strong winds result in significant external pressure on houses, including the roof sheathing panels. Media coverage and reconnaissance visits to the wind damage regions (Smith 2005) indicate that wind-induced failure often initiates at roof sheathing panels. Significant building code revisions (ASCE 7-95) have also been conducted after hurricane Andrew in 1992. More recent post-hurricane survey results continue to show that the occurrence of roof damage remains high even for newer homes built to more recent building codes (Gurley et al. 2006). Sheathing failure, especially at roof corners, is still common.

Wind pressure varies spatially and temporally, and its magnitude is a function of the wind speed, wind direction, roof pitch, and roof geometry. Experimental tests and numerical models (Mizzell 1994, Rosowsky and Schiff 1996, Sutt 2000) have been used to investigate the uplift capacity of typical roof sheathing panels, considering that the wind pressure can be treated as a time-invariante or static uniform pressure. This provided a workable assumption at the time, and led to valuable results for practice and building code revisions (Cunningham 1992). However, it does not incorporate the fact that the roof panels are actually experiencing non-uniform and dynamic wind loads. The impact of this simplifying assumption on the wind induced demand or on the probabilistic characterization of the uplift capacity of the panel is unknown. Progress for

full-scale testing of roofing system has been made by incorporating this spatially and temporally varying wind load (Surry et al. 2005, Bartlett et al. 2007, Hill et al. 2009, Kopp et al. 2010). This is done through the application of one or several innovative pressure actuators (or boxes), each covering an area ranging 610×610 mm to 2440×2440 mm (2′×2′ to 8′×8′). Numerical results of the uplift capacity of the panel under uniform time-varying uplift wind pressure indicate that this uplift capacity is affected by the nonlinear force-displacement behaviour of the fasteners (see Chapter 2). The results also indicate that the use of the tributary area method (Cunningham 1992, Murphy et al. 1996, Sutt 2000) could lead to an underestimation of the uplift capacity of a typical panel with 1220×2440 mm (4′×8′) that is fastened to the framing members using 8d common nails with a spacing of 150 mm (6″) along the framing members at panel edges and 300 mm (12″) along the intermediate supports by about 5%. However, the influence of the spatially varying wind pressure and the nonlinear nail withdrawal behaviour on the probabilistic characteristics of the panel uplift capacity is still unavailable, although such characterizations are of value for quantifying the fragility curve, as well as for reliability analysis and reliability-based design code calibration. Furthermore, it is often observed that panels may not be fastened properly or nails are simply missing. The improperly fastened or missing nails, and different nail schedules used in construction in different geographic regions, can also affect the statistics of the uplift capacity of the roof panel.

The assessment of the statistics of and probability model for the uplift capacity of the roof panel under spatio-temporally varying wind pressure forms the main task of this study. For the assessment, nonlinear dynamic analysis with a ramp load is considered. The application of the nonlinear dynamic analysis with a ramp load is justified because it

provides sufficiently accurate estimation of the panel uplift capacity as compared to that obtained by the incremental dynamic analysis method and it avoids the non-convergence problem that is often associated with the nonlinear static pushover analysis (see Chapter 2). Parametric investigation of the uplift capacity of the panel is carried out by considering nonlinear force-displacement behaviour of fasteners, and cases of possible missing nails. The uncertainty in the nail withdrawal behaviour, as well as in the wind pressure, is also incorporated in evaluating the statistics of the panel uplift capacity using the simple simulation technique.

3.2 Modeling the sheathing panel and fasteners

Consider the typical roof plywood sheathing panel for residential house shown in Figure 3.1. The panel has a thickness of 11.5 mm (3-plies) and a size of 1.22 m × 2.44 m (i.e., 4′×8′), and is fastened to the framing members using 8d common nails, each having a length of 63 mm (2.5″) and a diameter of 3.4 mm (0.133″). The framing members, such as trusses and rafters, consist of 38 mm × 89 mm (2″×4″) lumber, often Douglas-fir, and are at spaced 610 mm (24″) on centers. The panel depicted in Figure 3.1 is fastened to the frames following the roof sheathing fastening schedules for wind uplift that is recommended by APA- the Engineered Wood Association, which specifies a nail spacing of 150 mm (6″) along the framing members at panel edges and 300 mm (12″) at the intermediate supports. Such a fastening schedule is almost identical to that recommended in the NBCC (2005) and in the Ontario Building Code (OBC 2006), which considers a spacing of 150 mm along the framing members along edge supports and 300 mm along the intermediate supports. A more stringent fastener requirement for

geographic regions with significant wind hazard that requires a spacing of 150 mm (6″) for the edges and intermediate supports, except at gable ends, where a spacing of 100 mm (4″) has been recommended by the Florida Building Code (2007). A further reduction in the nail spacing to less than 75 mm (3″) is not recommended because of possible splitting of the framing member (Forest Products Laboratory 1999).

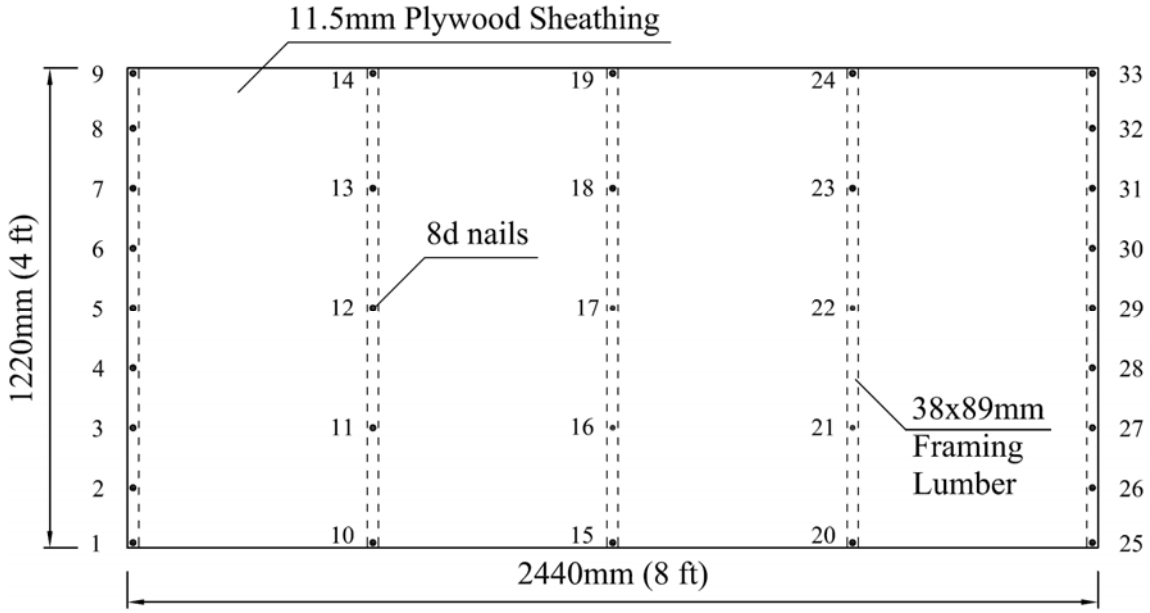

Figure 3.1 Typical roof panel layout

For numerical analysis, the sheathing panel is modeled using 4–node shell element with 6 degrees of freedom at each node, considering both bending and membrane stiffness to allow large deflection capability. The mesh generated using the finite element software package ANSYS (ANSYS Inc. 2005) is illustrated in Figure 3.2 and the element type used is described in Table 3.1.

Table 3.1 Element name in the ANSYS and its description for the finite element modeling.

	ANSYS Element	Property Description
Roof Panel	Shell63	Large displacement, bending & membrane stiffness
Nail (Linear)	Combin14	1D linear spring
Nail (Nonlinear)	Combin39	1D nonlinear spring

The software is employed for linear and nonlinear static analyses throughout the present study. It is assumed that the modulus of elasticity of Douglas-fir along the longitudinal grain equal to 10.45 GPa could be adopted to represent that for the sheathing panel, as the Douglas-fir is the common wood species used to manufacture plywood panels (Canadian Plywood Association 2005).

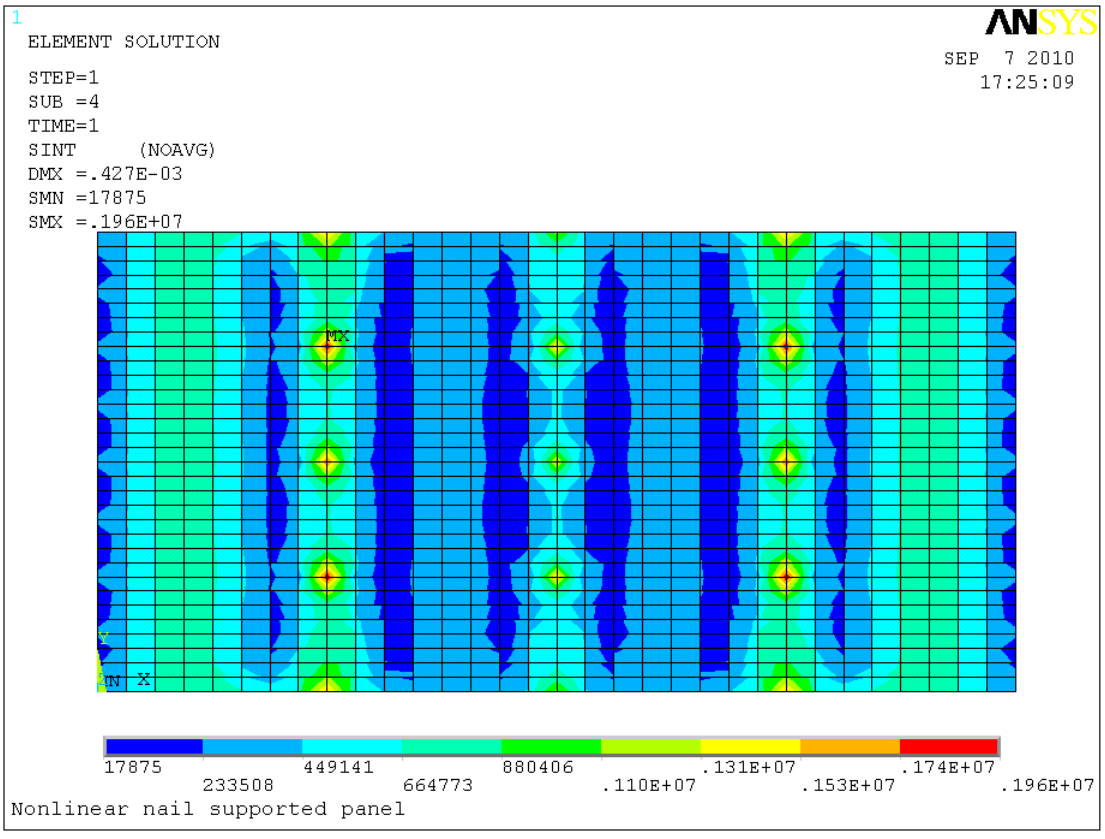

Figure 3.2 Finite element model representation of the panel and fasters.

The nonlinear force-displacement curves used to model the nail withdrawal behavior include elastoplastic model (Chui et al. 1998), tri-linear model (Groom and Leichti 1993), and a nonlinear model incorporating the bending moment effect (Dao and van de Lindt 2009). The adopted model for the nail withdrawal capacity in the current study is based on the test results reported by Groom and Leichti (1993) and a nail withdrawal model proposed by Foschi (2000), as this model allows more smooth transition from initial to post yield behaviour. The model is shown schematically in Figure 3.3, where f_m, f_p, d_m, d_p and k_0 are the ultimate withdrawal force, proportion limit, displacement corresponding to the ultimate withdrawal force, displacement at proportional limit, and initial stiffness, respectively. The relation between the force, F, and displacement along the nail shank direction, D, is given by

$$F = \begin{cases} k_0 D, & \text{for } D \le d_p \\ f_p + \left(Q_0 + Q_1 d\right)\left(1 + \exp\left(-k_0 d / Q_0\right)\right), & \text{for } d_p < D \le d_m \\ f_m \exp\left(Q_4 \left(D - d_m\right)^2\right), & \text{for } D > d_m \end{cases} \quad (1)$$

where $d = D - d_p$, $Q_4 = \ln\left(Q_2\right) / \left[d_m \left(Q_3 - 1\right)\right]^2$, the model parameters ($Q_0$, Q_1, Q_2, Q_3) are to be determined using test results with monotonically increasing displacement, and the displacement d_{m} is evaluated from the second equation for $F = f_{\mathrm{m}}$. The suggested values of (Q_0, Q_1, Q_2, Q_3) for 8d common nails based on the recommendations given in Foschi (2000) are shown in Table 3.2. Although Eq. (1) incorporates neither the shear effect (Sutt 2000) nor the edge bending moment effect (Dao and van de Lindt 2009), it is adopted in this study because these effects are considered to be negligible for the uplift capacity of panel under uplift wind pressure with the fastening schedule shown in Figure 3.1.

Table 3.2 Characterization of the parameters used to model the nail withdrawal behaviour.

Parameter	Mean value	Coefficient of variation
Initial stiffness, K_0 (N/m)*	4171521.2	0.39
Proportional limit, f_p (N)*	680.6	0.20
Maximum load, f_m (N)*	805.1	0.17
Displacement corresponding to maximum laod, d_m (mm)*	0.254	0.38
Ratio, r	0.183	0.44
Q_0^*	121	-
Q_1^*	1×10^5	-
Q_2^*	0.9	-
Q_3^*	2.6	-
Modulus elasticity, E (GPa)	10.45	-
Contact area, A (m^2)	0.0052	-

* Statistics are based on the nail withdrawal tests reported by Groom and Leichti (1993).

* Values of Q_0 to Q_3 are determined by fitting Eq(1) to the mean capacity curve reported by Groom and Leichti (1993) through regression analysis.

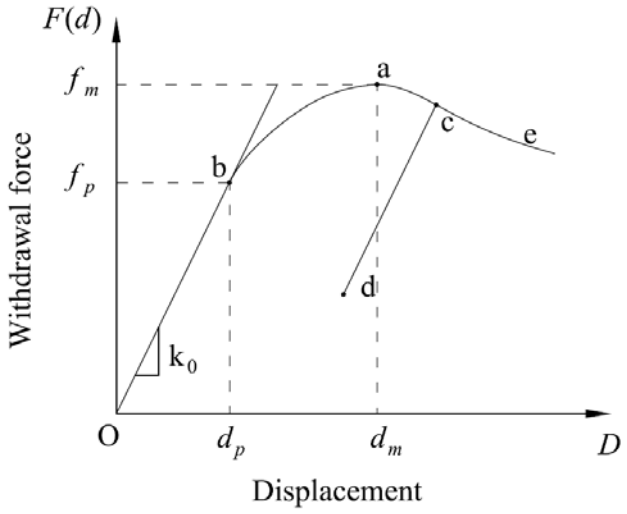

Figure 3.3 Illustration of force-displacement curve of nail withdrawal behavior.

If the roof panel is subjected to positive pressure, the nail is modeled using a linear spring with the stiffness equal to *AE*, where *E* (= 10.45 GPa) is the modulus of elasticity of timber, and *A* (=0.0052 m^2) represents the contact area of sheathing with the stud. This approximate modeling is unlikely to affect the uplift capacity of the panel because the uplift wind pressure is of concern. According to He et al. (2001), the initial stiffness can be used to approximate the loading and unloading for the force-deformation curve shown in Figure 3.3. The model does not include the degradation of nail withdrawal capacity due to cyclic dynamic loads.

The material properties of both the sheathing panel and nail withdrawal capacity are uncertain. Only uncertainty in the nail withdrawal behaviour is considered to assess the sheathing panel uplift capacity, as this work is focused on the effect of the nail withdrawal rather than the nail punching through failure model. The uncertainty in the nail withdrawal capacity, which is influenced by the nail installation method and the statistical inhomogeneity in timber or lumber, could be characterized by the uncertainties in f_m, f_p, d_m, and k_0, where their mean values, standard deviations and probabilistic models are also shown in Table 3.2 (Groom and Leichti 1993, Sutt 2000). Note that f_p can be characterized using the ratio γ, defined as $(f_m\text{-}f_p)/f_p$.

Given samples of f_m, k_0 and γ and the values of Q_0, Q_1, Q_2, and Q_3, because f_p and d_p can be calculated using

$$f_p = f_m/(1+\gamma), \tag{2a}$$

and

$$d_p = f_p / k_0, \tag{2b}$$

and a sample of the force-deformation curve for nail withdrawal is completely defined.

The nail withdrawal capacity for the nails within a panel is likely correlated as the nails serve under similar environment and are fastened to the same or similar timber specie. Unfortunately, statistical data that can be used to asses the correlation is scarce. For the parametric investigation of the impact of the correlation between the nail behaviour on the estimated panel uplift capacity, a simple multiplicative model is adopted. The model considers that a random variable Y_i of interest, such as f_m or k_0 or γ, for the i-th nail can be expressed as,

$$Y_i = Y_0 \times X_i,\ i = 1, \cdots, n, \tag{3}$$

where Y_0 represents a random variable that is common to all nails, X_i is "local" variable that only affects the i-th nail, and Y_0 and X_i are independently distributed. If Y_0 is lognormally distributed with a mean of m_{Y0} and a coefficient of variation (cov) of v_0, and X_i is lognormally distributed with a mean of 1.0 and a cov of v_X, it can be shown that Y_i is lognormally distributed, and the correlation coefficient between Y_i and Y_j for $i \neq j$, ρ_{ij}, is given by,

$$\rho_{ij} = \left(v_0 / v_Y\right)^2 \tag{4a}$$

and

$$v_Y = \sqrt{v_0^{\,2} v_X^{\,2} + v_0^{\,2} + v_X^2} \tag{4b}$$

where v_Y is the cov of Y_i. This shows that ρ_{ij} is controlled by the cov values of Y_0 and Y_i. In other words, given v_i, one can calculate the required v_0 to achieve a target ρ_{ij} using Eq. (4a), and the corresponding v_X is then evaluated by solving Eq. (4b). Therefore, for given v_Y, the degree of correlation can be easily controlled by changing the value of v_0. This model will be used to generate the correlated nail properties (i.e. f_m, k_0 and γ) for all nails

used to fasten the panel that are needed to evaluate the panel uplift capacity.

3.3 Modeling the spatially and temporarily varying wind pressure

The geometry and presence of surrounding buildings or houses, as well as the wind direction affect the wind pressure coefficient on roof panels (Surry and Stathopoulos 1978, Simiu and Stathopoulos 1997, Kopp et al. 2005). These coefficients can be measured from boundary layer wind tunnel experiments and results from the Boundary Layer Wind Tunnel at the University of Western Ontario for a test model are used as the basis to assign probabilistic model for wind pressure coefficient to be used in this study. The test model is shown in Figure 3.4. The time history of the pressure coefficient for the model scale is obtained for each pressure tap for 3 minutes, at a sampling frequency of 400Hz for open country terrain (z_0 = 0.01 m) and the reference mean wind speed of 13.7 m/s (45 ft/s). The ratio of the reference mean wind speed at the average roof height to the reference mean wind velocity equals 0.6984.

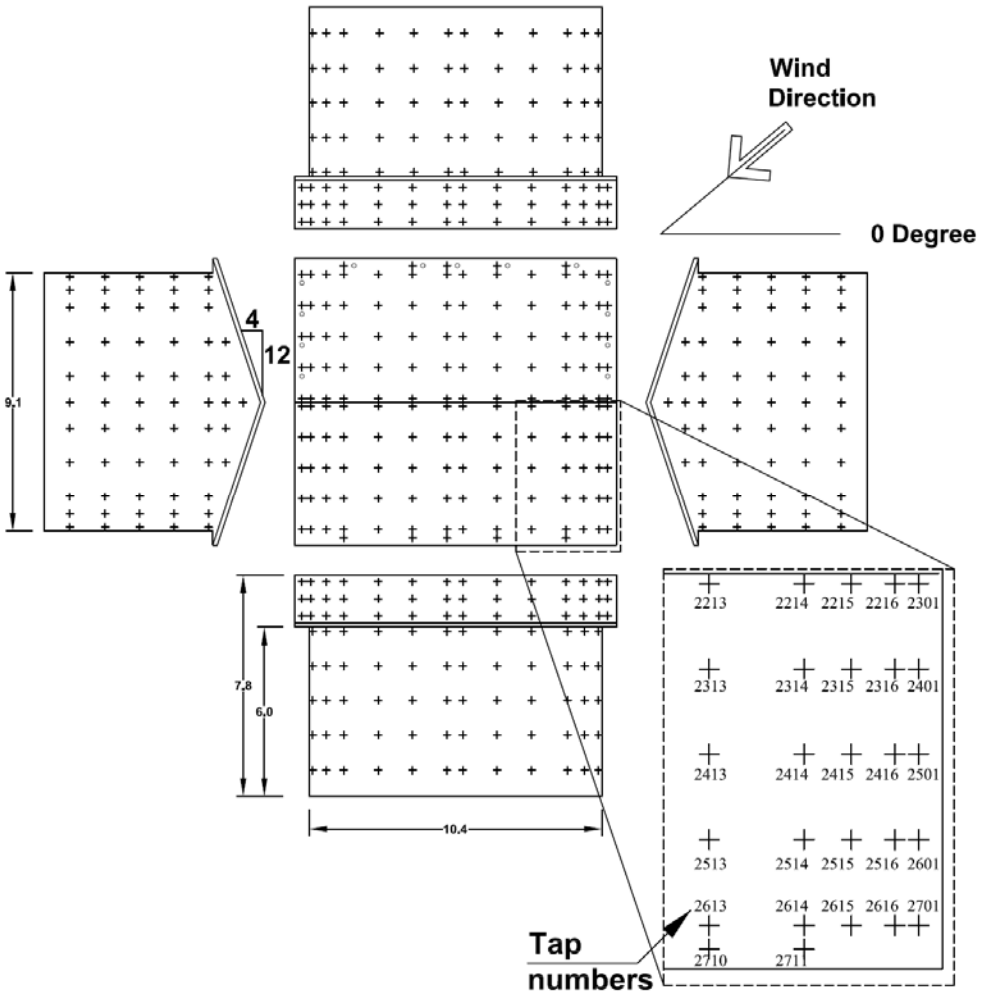

Figure 3.4 Locations of taps on the test model with the length scale of 1:50, representing a typical domestic dwelling with 4:12 gable roof, 8 m roof eave height (dimensions are in the plot is in inches).

To use the pressure coefficients for the full-scale, the relation between the sampling frequencies for the full-scale and the mode scale,

$$\left(\frac{fD}{U}\right)_{MS} = \left(\frac{fD}{U}\right)_{FS} \tag{5}$$

needs to be considered (Simiu and Scanlan 1996), where D is the length scale, f is the sampling frequency, U is the eave height mean wind speed, and the subscript FS and MS

denote the variables for the full-scale and model scale, respectively. For example, if the reference mean wind speed at the average roof height is 30 m/s, the full scale sampling frequency f_{FS} determined by using Eq. (5) equals 25.08 Hz (i.e., $f_{FS} = \frac{f_{MS} U_{FS}}{U_{MS}} \times \frac{D_{MS}}{D_{FS}} = \frac{400 \times 30}{13.7 \times 0.6984} \times \frac{1}{50}$). The total number of samples for each tap is 71871, which corresponds to about 45 minutes full-scale wind load history for a 30 m/s reference mean wind speed at the average roof height. The pressure time histories for the taps on the roof are calculated by multiplying C_p (obtained from the time histories) and the reference pressure.

Figure 3.4 identifies layout of the taps located on the roof of the test model. There are more taps placed near the roof corners and roof edges, because the spatial variation and magnitude of the wind pressure coefficients is greater in these locations (St. Pierre et al. 2005). The contour map of the instantaneous pressure coefficients is illustrated in Figure 3.5. The variation of pressure coefficients on the roof is reflected in the code recommended values (NBCC 2005), which considers three typical wind pressure regions: field, edge and corner regions.

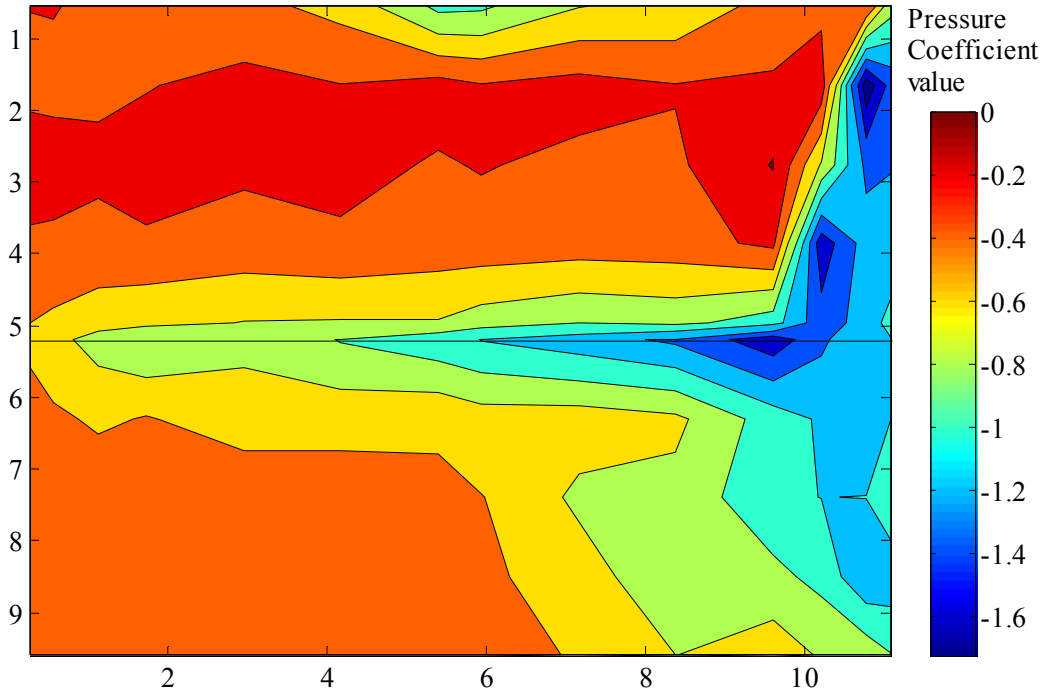

Figure 3.5 Illustration of the contour map of a point-in-time C_p value over the roof for a wind attack angle of 40^o.

To assess the spatial correlation coefficient of the wind pressure coefficients for roof panels located in the three pressure regions, records for the pressure taps on three panels labelled S34, S35, and S55 (shown in Figure 3.6a) are considered. The tributary area is indicated by the dashed lines for each tap in the figure, where the pressure coefficient within each tributary area is considered to be uniform. The time histories of the pressure coefficients for two pressure taps within S34 are illustrated in Figure 3.6b, indicating that they are not fully correlated or synchronized.

To assess the statistics of the wind pressure coefficient, C_p, the time histories of the pressure coefficient from the taps within each of the considered panels (i.e., S34, S35, and S55) are employed. The estimated mean and standard deviation values of C_p for each

tap are presented in Table 3.3. In general, the standard deviation of C_p for taps in the field wind pressure region is less than that in the edge and corner regions.

Table 3.3 Statistics and fitted probabilistic model of the wind pressure coefficient for taps located on the three panels shown in Figure 3.6a.

Tap number	Mean	Standard deviation	Probability distribution type
2412	-0.654	0.236	Gumbel (minimum)
2413	-0.749	0.293	Gumbel (minimum)
2414	-0.972	0.288	Longnormal*
2415	-1.320	0.392	Normal
2416	-1.303	0.432	Longnormal*
2501	-1.269	0.411	Longnormal*
2614	-1.011	0.311	Normal
2615	-1.052	0.318	Normal
2616	-1.010	0.344	Gumbel (minimum)
2701	-1.096	0.416	Gumbel (minimum)
2711	-0.883	0.257	Normal

* In these cases, the lognormal model is fitted to the negative values of the wind pressure coefficients.

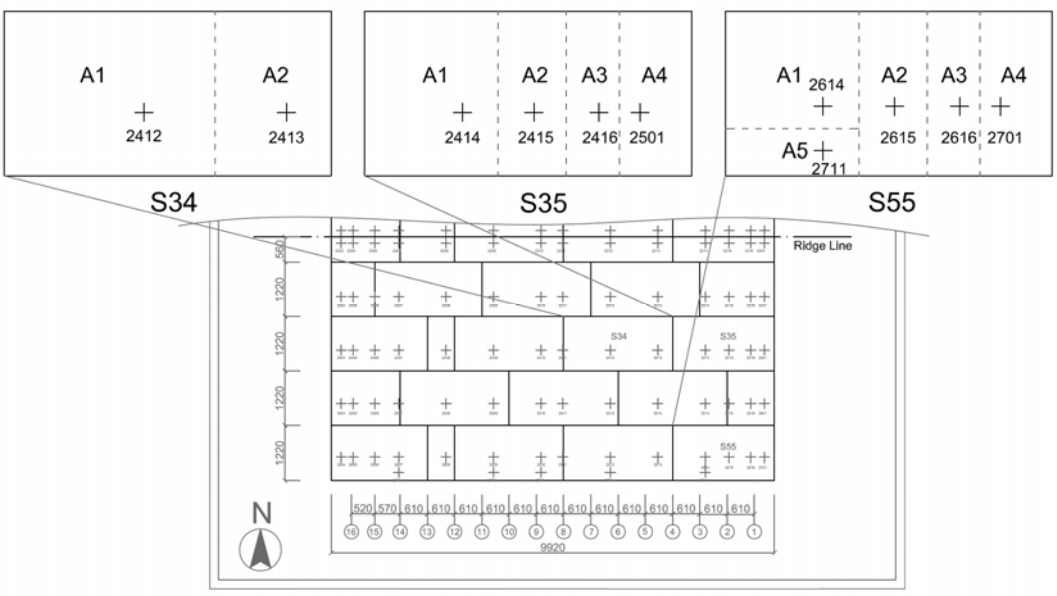

6a) Layout of three typical panels

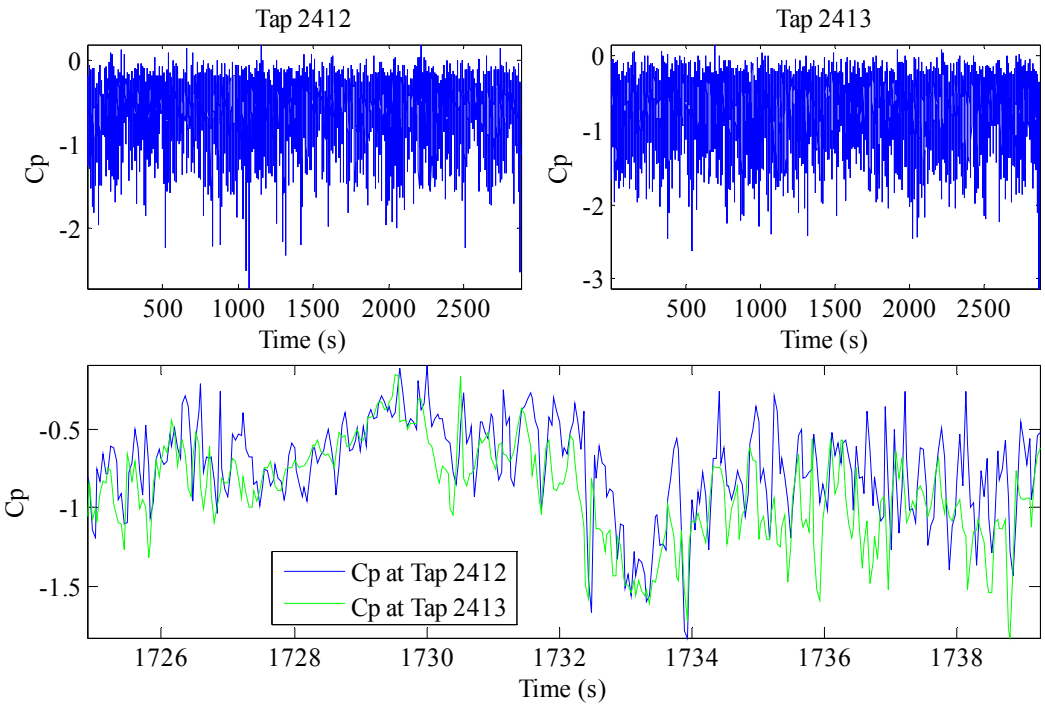

b) Illustration of pressure time histories at two locations for a wind attack angle of 40°.

Figure 3.6 Layout of three panels and illustration of pressure time histories at locations on panel S34 for 30m/s reference wind speed at the average roof height.

To assign the probability distribution of the wind pressure coefficient, we consider several commonly employed probabilistic models: Normal, Lognormal, Weibull, Gamma and Gumbel (maximum and minimum) distributions. We use these distributions to fit samples of the pressure coefficient from each tap shown in Figure 3.6a, and the best distribution type for each tap is shown in Table 3.3. The selection of the best fit distribution is based on the Kolmogorov-Smirnov goodness-of-fit test results (Benjamin and Cornell 1970) and using samples from one minute pressure coefficient time histories. In all cases, the best model could not be rejected at the 5% significance level. Figure 3.7 shows the fitted probabilistic models for different taps. The fitting shows that the probability distribution of pressure coefficient is not always Gaussian which is in agreement with that observed by Cope et al. (2005). For simplicity in the parametric investigation of the panel uplift capacity carried out in the following sections, the pressure coefficient is considered to be normally distributed for all cases.

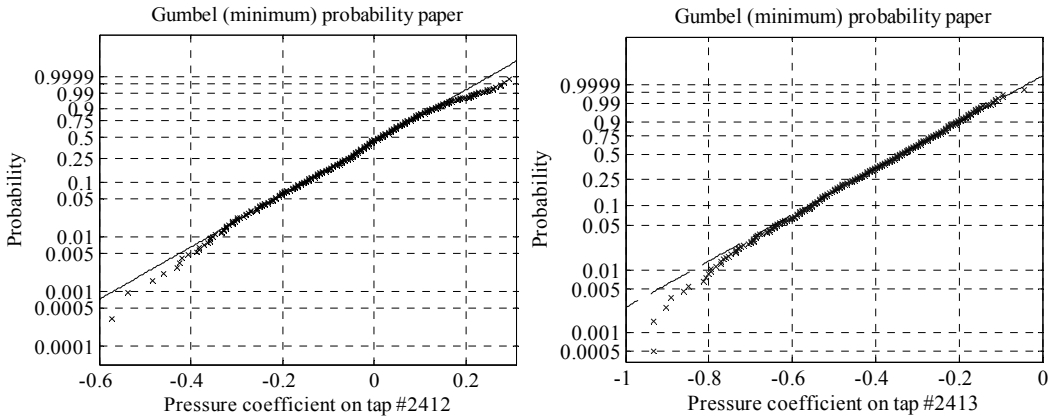

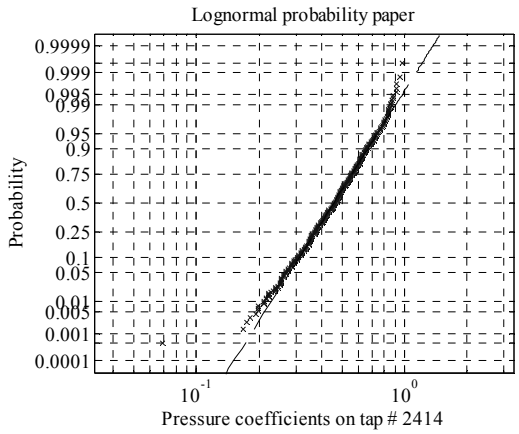
Lognormal probability paper
Probability
0.9999
0.999
0.995
0.99
0.95
0.9
0.75
0.5
0.25
0.1
0.05
0.01
0.005
0.001
0.0001
10^-1
10^0
Pressure coefficients on tap # 2414

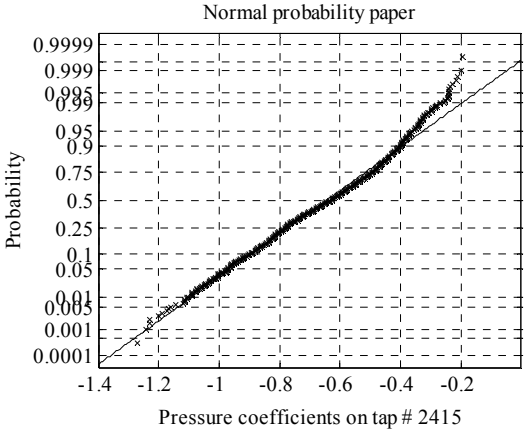
Normal probability paper
Probability
0.9999
0.999
0.995
0.99
0.95
0.9
0.75
0.5
0.25
0.1
0.05
0.01
0.005
0.001
0.0001
-1.4
-1.2
-1
-0.8
-0.6
-0.4
-0.2
Pressure coefficients on tap # 2415

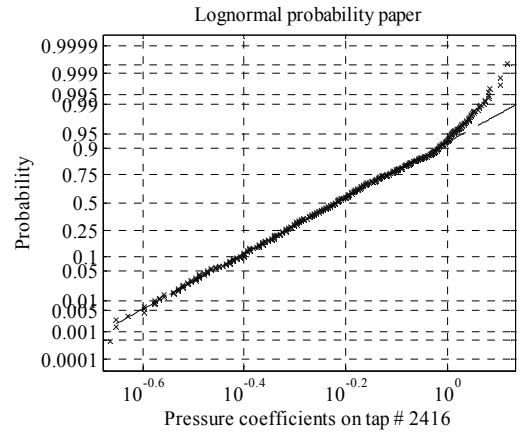
Lognormal probability paper
Probability
0.9999
0.999
0.995
0.99
0.95
0.9
0.75
0.5
0.25
0.1
0.05
0.01
0.005
0.001
0.0001
10^-0.6
10^-0.4
10^-0.2
10^0
Pressure coefficients on tap # 2416

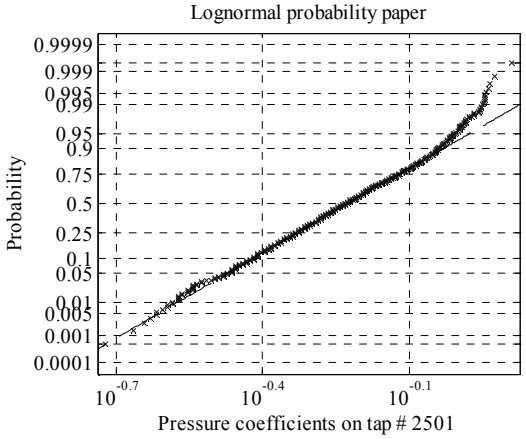
Lognormal probability paper
Probability
0.9999
0.999
0.995
0.99
0.95
0.9
0.75
0.5
0.25
0.1
0.05
0.01
0.005
0.001
0.0001
10^-0.7
10^-0.4
10^-0.1
Pressure coefficients on tap # 2501

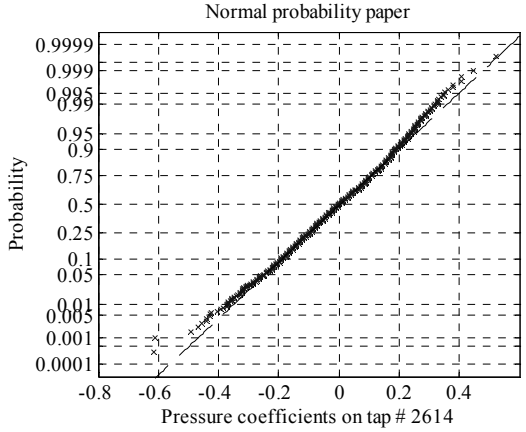
Normal probability paper
Probability
0.9999
0.999
0.995
0.99
0.95
0.9
0.75
0.5
0.25
0.1
0.05
0.01
0.005
0.001
0.0001
-0.8
-0.6
-0.4
-0.2
0
0.2
0.4
Pressure coefficients on tap # 2614

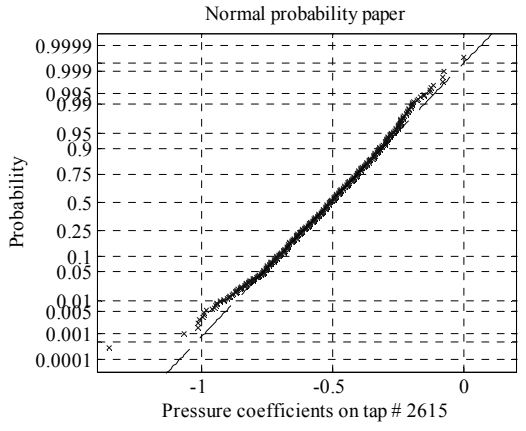
Normal probability paper
Probability
0.9999
0.999
0.995
0.99
0.95
0.9
0.75
0.5
0.25
0.1
0.05
0.01
0.005
0.001
0.0001
-1
-0.5
0
Pressure coefficients on tap # 2615

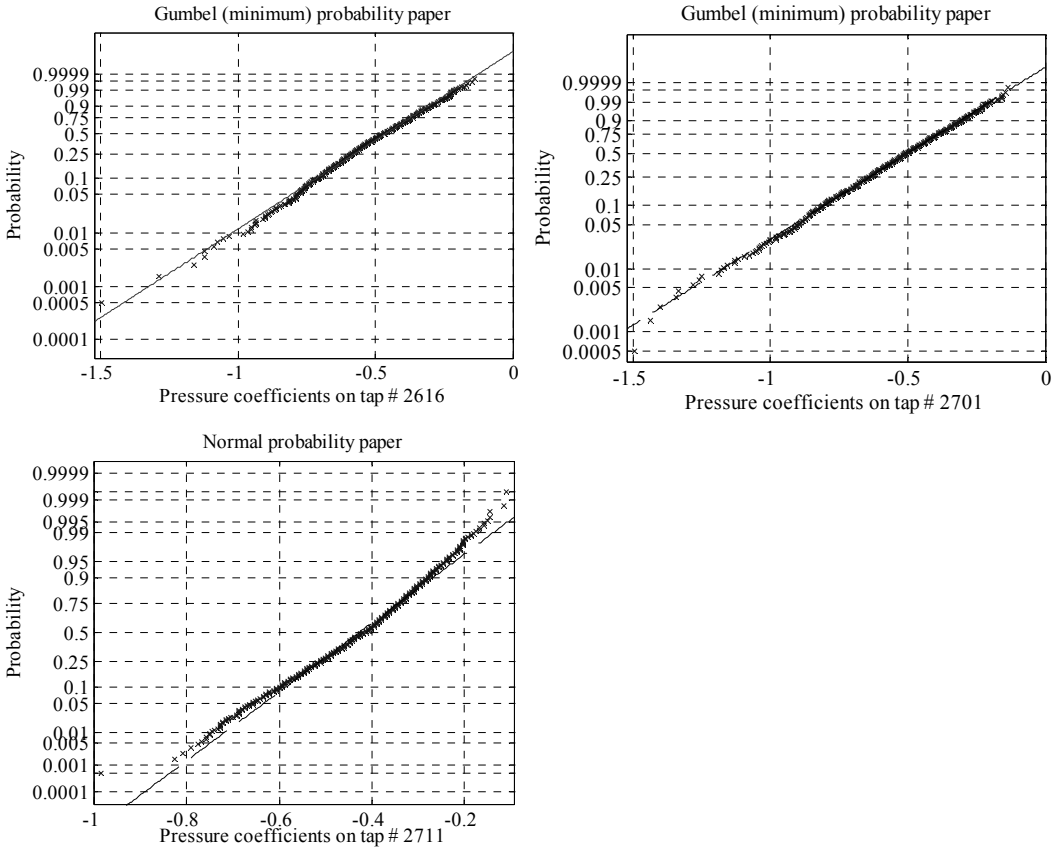

Figure 3.7 Samples of pressure coefficients presented on different probability papers.

The estimated correlation coefficients for C_p between any two pressure taps within each panel identified in Figure 3.6a are calculated and summarized in Table 3.4. The correlation coefficient matrix shown in the table for Panel S35 indicates that the value of an element in the matrix decreases as the element moves away from the diagonal. This suggests that the correlation decreases as the distance between the taps increases, which is expected. The observed trend is also found in the matrix for Panel S55 (e.g. for the instance where the correlation coefficient between the C_p values from Taps 2614 and 2711 is large, which is expected as the distance between these two taps is small). In all cases, the decrease in the correlation coefficient is not very drastic. It is interesting to

note that the degree of correlation for the taps in Panel S34 is no more significant than those for the taps in Panel S35 or in Panel S55.

Table 3.4 Correlation coefficients between wind pressure coefficients for different taps in the three considered panels shown in Figure 3.6a and for a wind direction of 40º illustrated in Figure 3.4.

Panel	Tap	2412	2413			
S34	2412	1	0.64			
	2413	symmetric	1			
Panel	Tap	2414	2415	2416	2501	
S35	2414	1	0.78	0.62	0.57	
	2415		1	0.87	0.81	
	2416	Symmetric		1	0.88	
	2501				1	
Panel	Tap	2614	2615	2616	2701	2711
S55	2614	1	0.78	0.52	0.51	0.85
	2615		1	0.74	0.70	0.68
	2616			1	0.84	0.48
	2701		symmetric		1	0.49
	2711					1

To better appreciate the spatial correlation of C_p, the values of the correlation coefficient, ρ_c, shown in Table 3.4 for Panels S34, S35, and S55 are plotted in Figure 3.8, where the abscissa represents the distance, d, between two taps used to evaluate ρ_c. The figure shows the typical exponential decay of the correlation coefficient versus distance found in the literature (Simiu and Scanlan 1996). By adopting the following mathematical model (Davenport 1961),

$$\rho_c = \exp(-d/\lambda) \tag{6}$$

and carrying out a nonlinear regression analysis, the obtained value of the correlation length λ equals 2.7 m for data associated with Panel 35, and 1.8 m for data associated with Panel 55. Furthermore, the predicted ρ_c values for λ equal to 1.45 and 3.7 m provide

the lower and upper bound to the samples of ρ_c shown in Figure 3.8, respectively. Therefore, it is deemed adequate that a value of λ within 1.5 and 3.0 is to be used in the following sections.

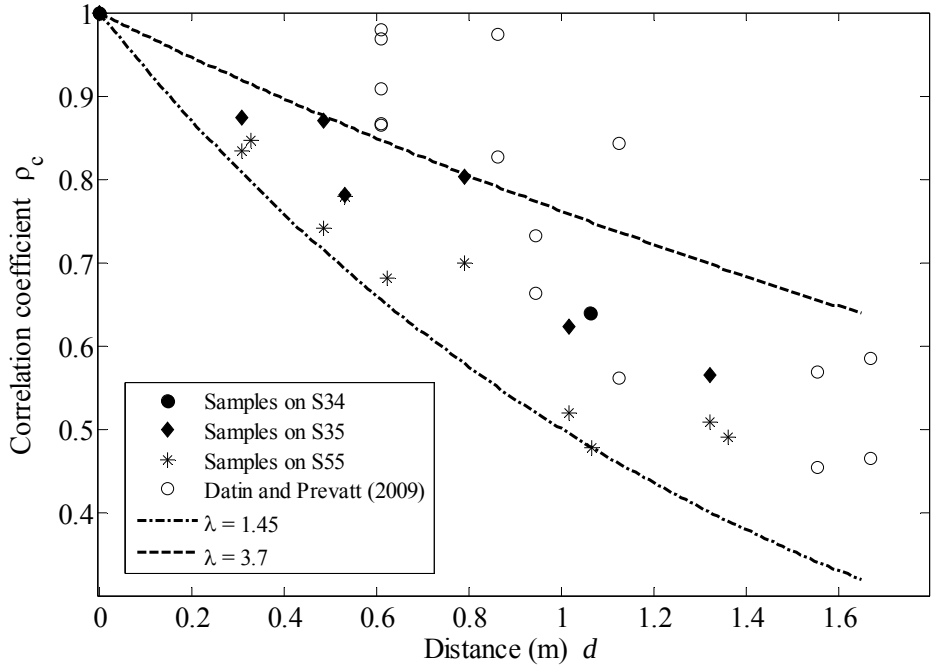

Figure 3.8 Correlation coefficients of the wind pressure coefficients.

Figure 3.8 also compares the afore-mentioned correlation coefficients to those reported by Datin and Prevatt (2009), which were obtained based on more dense arrays of pressure taps located in the corner region for an angle of attack of zero degrees. The figure shows that their values are higher than those found in this study for $d < 1$ m, and are in agreement with ρ_c reported in Table 3.4 for $d > 1$ m.

3.4 Uplift capacity evaluation procedure

To assess the impact of spatially varying load on the panel uplift capacity, the

capacity with the spatially varying C_p is estimated and compared with that estimated under uniform C_p. These are elaborated as follows.

Consider that the point-in-time pressure coefficient is available, as they could be time history measurements from experiments. If the panel with known properties of the fasteners is subjected to spatially uniformly/non-uniformly distributed wind pressure, its uplift capacity is estimated using the adopted nonlinear dynamic analysis with a ramp load (NDA-RL) (see Chapter 2). As mentioned in the introduction, the adoption of this method is justified since the method predicts the capacity that is close to that predicted by the incremental dynamic analysis (IDA) method; it demands much less computing effort as compared to the IDA method and avoids the non-convergence problem often associated with the nonlinear static pushover analysis. The NDA-RL considers a ramp load defined by spatially distributed pressure, whose magnitude increases linearly with time and proportional to pressure coefficients; the incipient failure uplift wind load that equals the ultimate total reaction force is obtained from the time history of the total reaction force. The rate of increase for the ramp load can be taken equal to the pressure associated with the yield capacity of the panel divided by twice of the first vibration period, where the yield capacity can be approximated by using the tributary method (Cunningham 1992, Murphy et al. 1996, Sutt 2000) as the obtained capacity curve is not very sensitive to the selected yield capacity.

For a panel with an area, A_T, under (spatially) uniformly distributed wind pressure with pressure coefficient C_p at a reference wind mean speed of U_r, the total applied force F_T for a reference wind mean speed of U_r (at the average roof height) is given by,

$$F_T = \frac{1}{2}\rho U_r^2 C_p A_T, \tag{7}$$

where ρ is the air density that is taken equal to 1.26 kg/m^3. Let F_{TF} denote the incipient failure uplift wind load predicted by the NDA-RL. This incipient failure wind load represents the uplift capacity of the panel, and corresponds to a critical reference mean wind speed at the average roof height U_{CR} ($U_{CR} = \sqrt{2F_{TF} / (\rho C_p A_T)}$). It must be emphasized that U_{CR} is associated with the point-in-time pressure coefficient rather than the gust pressure coefficient. If the gust pressure coefficient rather than the point-in-time pressure coefficient in the above calculation is used, U_{CR} will be decrease accordingly.

Now, consider that the panel is subjected to the spatially varying wind pressure for a given time that results in F_T,

$$F_T = \frac{1}{2}\rho U_r^2 \sum (C_i A_i) \tag{8}$$

where C_i is the pressure coefficient applicable to the i-th tributary area A_i. One can also carry out the NDA-RL to estimate the uplift capacity of the panel F_{TF}. Its corresponding U_{CR} can be calculated using,

$$F_{TF} = \frac{1}{2}\rho U_{CR}^2 \sum (C_i A_i) \tag{9}$$

Unfortunately, the calculated F_{TF} and its corresponding U_{CR} are not applicable for other combinations of C_i, because the values of C_i vary both spatially and temporally. That is, given a value of U_r, two combinations of C_i values can lead to the same F_T that is calculated using Eq. (8). However, one combination may not result in the failure of the panel, while the other does. This implies that the use of the total applied wind force (or reaction force) alone to characterize the uplift capacity of the panel may not be inadequate for the spatially and temporally varying wind load. In such a case, we could characterize the capacity of the panel directly based on the estimated U_{CR}. The use of

U_{CR} to characterize the uplift capacity can be advantageous since it could be used directly to represent the fragility curve.

We can define an equivalent uniform wind pressure coefficient C_E,

$$C_E = \left(\sum C_i A_i\right) / A_T \tag{10}$$

For the uniformly distributed wind pressure with pressure coefficient equal to C_E, as explained earlier, we evaluate the uplift capacity of the panel, denoted as $F_{TF,E}$. Its corresponding critical reference mean wind speed at the average roof height, denoted as $U_{CR,E}$, is calculated from

$$F_{TF,E} = \frac{1}{2}\rho U_{CR,E}^2 C_E A_T \,. \tag{11}$$

The difference between the uplift capacity of the panel under spatially varying wind pressure and uniform wind pressure can then be characterized using the ratio R_n, defined as,

$$R_n = F_{TF} / F_{TF,E} \tag{12}$$

which can be shown to be equal to $\left(U_{CR} / U_{CR,E}\right)^2$ by using Eqs. (9) and (11).

In the above discussion, it was considered that the pressure coefficients for all taps in a panel are available for a given instance. By considering the time-varying nature of the wind pressure coefficient, samples of the uplift capacity of the panel, critical reference mean wind speed at the average roof height (which is associated with the point-in-time rather than the gust pressure coefficient) and R_n can be obtained. Each sample of R_n is calculated for the sampled pressure coefficients from the taps at the same time. The statistics of the samples of R_n that take into account the uncertainty in wind pressure coefficients are used to characterize the uplifting capacity of the panel.

Furthermore, the above procedure can be repeated to incorporate the uncertainty in the nail withdrawal behaviour to statistically characterize F_{TF}, U_{CR} and/or R_n. This can be done, by repeatedly sampling the properties of the fasteners, and the pressure coefficients from the time histories, and carrying out the NDA-RL to evaluate F_{TF}, U_{CR} and/or R_n.

For the parametric analysis aimed at assessing the impact of the correlation of wind pressure on the estimated uplift capacity or R_n, rather than sampling the pressure coefficients from the time histories obtained from wind tunnel test, they are sampled from the probabilistic model discussed in Section 3.0 with the assigned correlation structure shown in Eq. (6). Note that if the pressure coefficients are considered to be correlated and non-normally distributed, their samples can be obtained using the Nataf transformation system (Der Kiureghian and Liu 1986). A flow chart outlining the above analysis procedure is given in Figure 3.9.

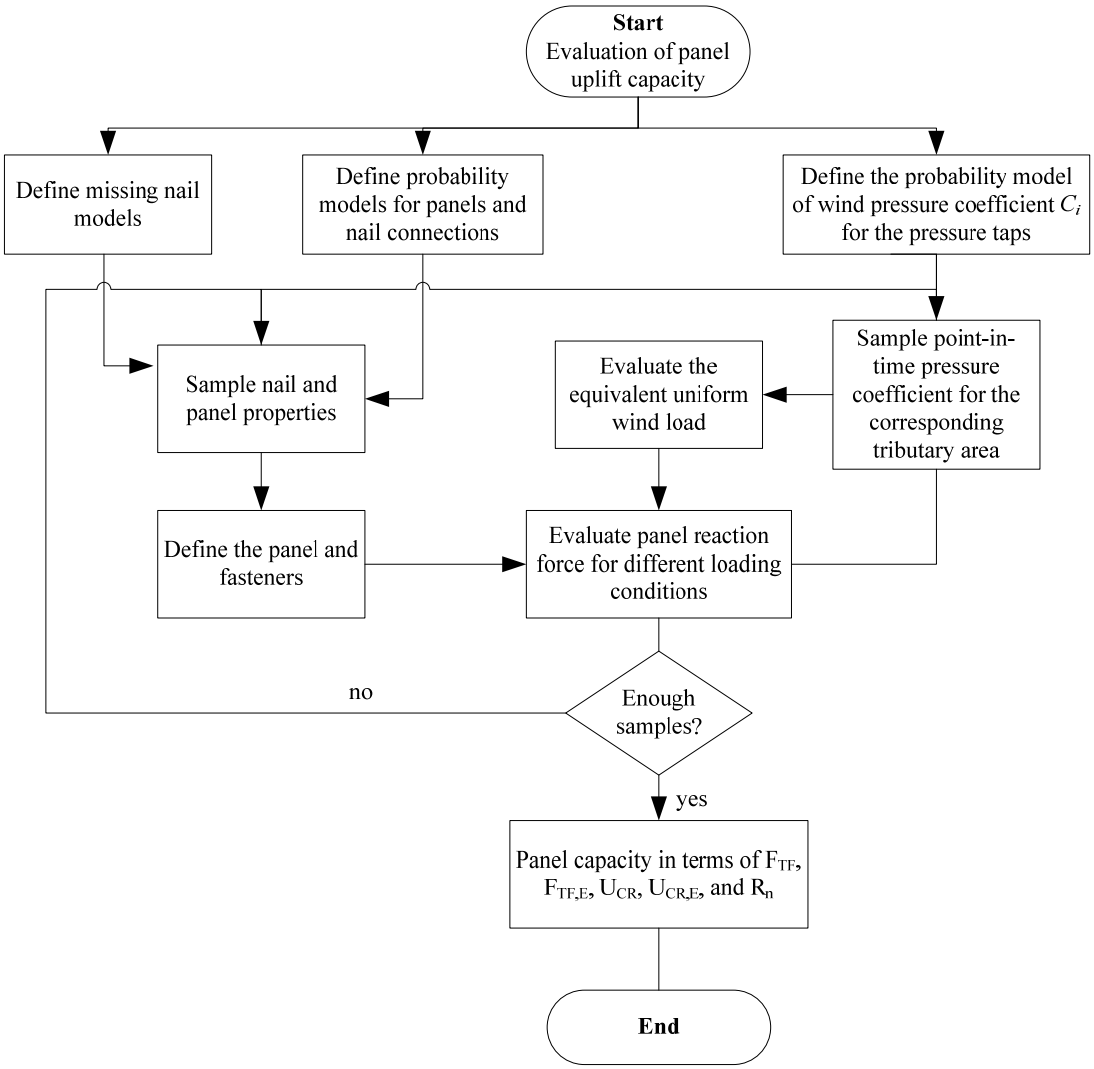

Figure 3.9 Flow chart for evaluation of panel capacity.

3.5 Characterizing the Panel Uplift Capacity

3.5.1 Uplift capacity of the panel

Before assessing the impact of the spatially and temporarily varying wind pressure on the uplift capacity of the panel, we mention that if the uncertainty in the nonlinear nail withdrawal behaviour is ignored and only the mean values of the model variables shown in Table 3.2 are used, F_{TF} equals 10418 N for the panel shown in Figure 3.1 subjected to

uniform wind pressure coefficient (see Chapter 2).

To investigate the impact of the spatially varying wind pressure on the estimated F_{TF}, first, we consider the three panels: S34, S35, and S55, and ignore the uncertainty in the nail withdrawal behaviour. For each panel, we directly use the samples of the wind pressure coefficients from the time histories obtained from the wind tunnel test, and evaluate F_{TF}, U_{CR}, $F_{TF,E}$, $U_{CR,E}$, and R_n following the simulation procedure described in the previous section and outlined in Figure 3.9. For each calculation, the point-in-time wind pressure coefficients from the taps are employed. For this and the remaining analyses, a simulation cycle of 500 is considered, which represents about 20 seconds of full scale pressure coefficients time history with a reference mean wind speed of 30 m/s. The statistics of F_{TF}, U_{CR}, $F_{TF,E}$, $U_{CR,E}$, and R_n calculated from the samples are shown in Table 3.5. The table indicates that the mean and cov of F_{TF} do not differ significantly for different panels, and that the cov values are about 5%. This implies that the statistics of the uplift capacity of the panel in terms of F_{TF} are insensitive to the spatially varying wind pressure coefficient if the uncertainty in nail withdrawal behaviour is negligible. The table shows that $F_{TF,E}$ is identical and equal to the value mentioned in the previous paragraph. This is expected as the uncertainty in nail withdrawal behaviour is ignored and the wind pressure is considered to be uniform. However, as the pressure coefficients at the taps vary spatially and temporally, the uplift capacity of the panel in terms of U_{CR} or $U_{CR,E}$ is significantly uncertain with a cov of up to 17.1%. The large cov is caused by the temporally varying wind pressure coefficients. It must be noted that as the evaluation of U_{CR} or $U_{CR,E}$ is based on the point-in-time pressure coefficients, U_{CR} or $U_{CR,E}$ represent the panel uplift capacity associated with the point-in-time pressure coefficients and do not

include the gust effect. The fact that the mean of R_n shown in Table 3.5 is close to 1 and the cov of R_n is small indicates that the use of the equivalent uniformly distributed wind loading with the pressure coefficient of C_E to evaluate the uplift capacity of panel is adequate if the uncertainty in the nail withdrawal behaviour can be ignored. No attempt is made in finding the best fit probability distributions to the samples of F_{TF}, U_{CR}, $U_{CR,E}$, and R_n because the inherent uncertainty in the nail withdrawal behaviour, which must be considered in assessing the uplift capacity of the panel was not incorporated in this case.

Table 3.5 Statistics of panel uplift capacity determined by using samples of wind pressure coefficients determined from wind tunnel test and ignoring the uncertainty in nail withdrawal behaviour.

Parameter and statistics		Panel S34	Panel S35	Panel S55
F_{TF}	Mean (N)	10215	10264	10238
	Cov	0.052	0.054	0.052
$F_{TF,E}$	Mean (N)	10422	10422	10422
	Cov	-	-	-
U_{CR}	Mean (m/s)	97.4	73.1	80.1
	Cov	0.167	0.155	0.151
$U_{CR,E}$	Mean (m/s)	100.8	75.1	82.8
	Cov	0.171	0.154	0.148
R_n	Mean	0.978	0.983	0.982
	Cov	0.052	0.054	0.052

Note: U_{CR} and $U_{CR,E}$ are associated with the point-in-time pressure coefficient rather than the gust pressure coefficient. If the gust pressure coefficient rather than the point-in-time pressure coefficient is used, U_{CR} and $U_{CR,E}$ will be decreased accordingly.

If we repeat the above analysis but considering that the nail withdrawal behaviour for the nails are independent ($\rho_{ij} = 0$) or fully correlated ($\rho_{ij} = 1$), the obtained statistics of F_{TF}, U_{CR}, $F_{TF,E}$, $U_{CR,E}$ and R_n are summarized in Table 3.6.

Table 3.6 Statistics of the uplift capacity of the panel by considering the uncertainty in the nail withdrawal behaviour.

Case	Parameter	Statistics	Panel S34	Panel S35	Panel S55
$\rho_{ij} = 0$	F_{TF}	Mean (N)	9991	9890	9886
		cov	0.081	0.081	0.083
	$F_{TF,E}$	Mean (N)	10138	10137	10138
		cov	0.074	0.076	0.074
	U_{CR}	Mean (m/s)	94.1	71.4	78.6
		cov	0.195	0.164	0.150
	$U_{CR,E}$	Mean (m/s)	94.8	72.2	79.7
		cov	0.197	0.164	0.151
	R_n	Mean	0.987	0.980	0.976
		Cov	0.061	0.056	0.063
$\rho_{ij} = 1$	F_{TF}	Mean (N)	10216	10329	10261
		cov	0.179	0.170	0.177
	$F_{TF,E}$	Mean (N)	10833	10833	10833
		cov	0.154	0.154	0.154
	U_{CR}	Mean (m/s)	97.2	72.8	79.9
		cov	0.198	0.184	0.174
	$U_{CR,E}$	Mean (m/s)	100.2	74.7	82.2
		cov	0.193	0.179	0.168
	R_n	Mean	0.941	0.952	0.945
		cov	0.063	0.055	0.056

The results show in the table indicate that the mean and cov of F_{TF} for the case with $\rho_{ij} = 0$ are smaller than those for the case with $\rho_{ij} = 1$. The difference between the mean of F_{TF} for the case with $\rho_{ij} = 0$ is less than 5%, while the cov of F_{TF} for the case with $\rho_{ij} = 0$ is about 50% of that for the case with $\rho_{ij} = 1$, which is very significant. The same trend was observed for U_{CR}, $F_{TF,E}$ and $U_{CR,E}$, although the differences between the cov values of U_{CR} and $U_{CR,E}$ for the cases with $\rho_{ij} = 0$ and $\rho_{ij} = 1$ are much smaller. The latter can be explained by noting that the uncertainty in the nail withdrawal behaviour significantly contributes to the uncertainty in the F_{TF} and $F_{TF,E}$, while the variability in both the nail withdrawal behaviour and the pressure coefficients adds to the variability of U_{CR} and $U_{CR,E}$. In all cases, the mean of R_n shown in Table 3.6 is near unity and the cov of R_n is

small compared to those of F_{TF}, U_{CR}, $F_{TF,E}$ and $U_{CR,E}$. This suggests again that the use of the equivalent uniformly distributed wind loading with the pressure coefficient of C_E to evaluate the panel uplift capacity is adequate. Furthermore, comparison of the results shown in Tables 3.5 and 3.6 indicates that the incorporation of the uncertainty in the nail withdrawal capacity behaviour resulted in a significant increase in the cov of the panel uplift capacity. Therefore, such an uncertainty must be considered in characterizing the uplift capacity of the panel.

An exercise of fitting probability distributions to the samples of F_{TF}, U_{CR}, $F_{TF,E}$, $U_{CR,E}$ and R_n is carried out using commonly employed probabilistic models: Normal, Lognormal, Weibull, and Gamma. It is concluded that F_{TF}, U_{CR}, $F_{TF,E}$, and $U_{CR,E}$ could be adequately modeled as lognormal variates. In fact, the Kolmogorov-Smirnov goodness-of-fit test results (Benjamin and Cornell 1970) indicate that the lognormal model could not be rejected at the 5% significance level. The samples and fitted distributions are presented in Figure 3.10 for Panel S35. Samples and fitted distributions for other panels are not shown, as they exhibit similar fits. It can be observed that $F_{TF,E}$ can be modeled as a lognormal variate. However, none of the considered models exhibit good fits for the samples of R_n. As the cov of R_n is much smaller than those of F_{TF}, U_{CR}, $F_{TF,E}$, and $U_{CR,E}$ (see Table 3.6) and the mean of R_n is near unity, it is suggested that R_n could be assumed to be lognormally distributed for practical applications.

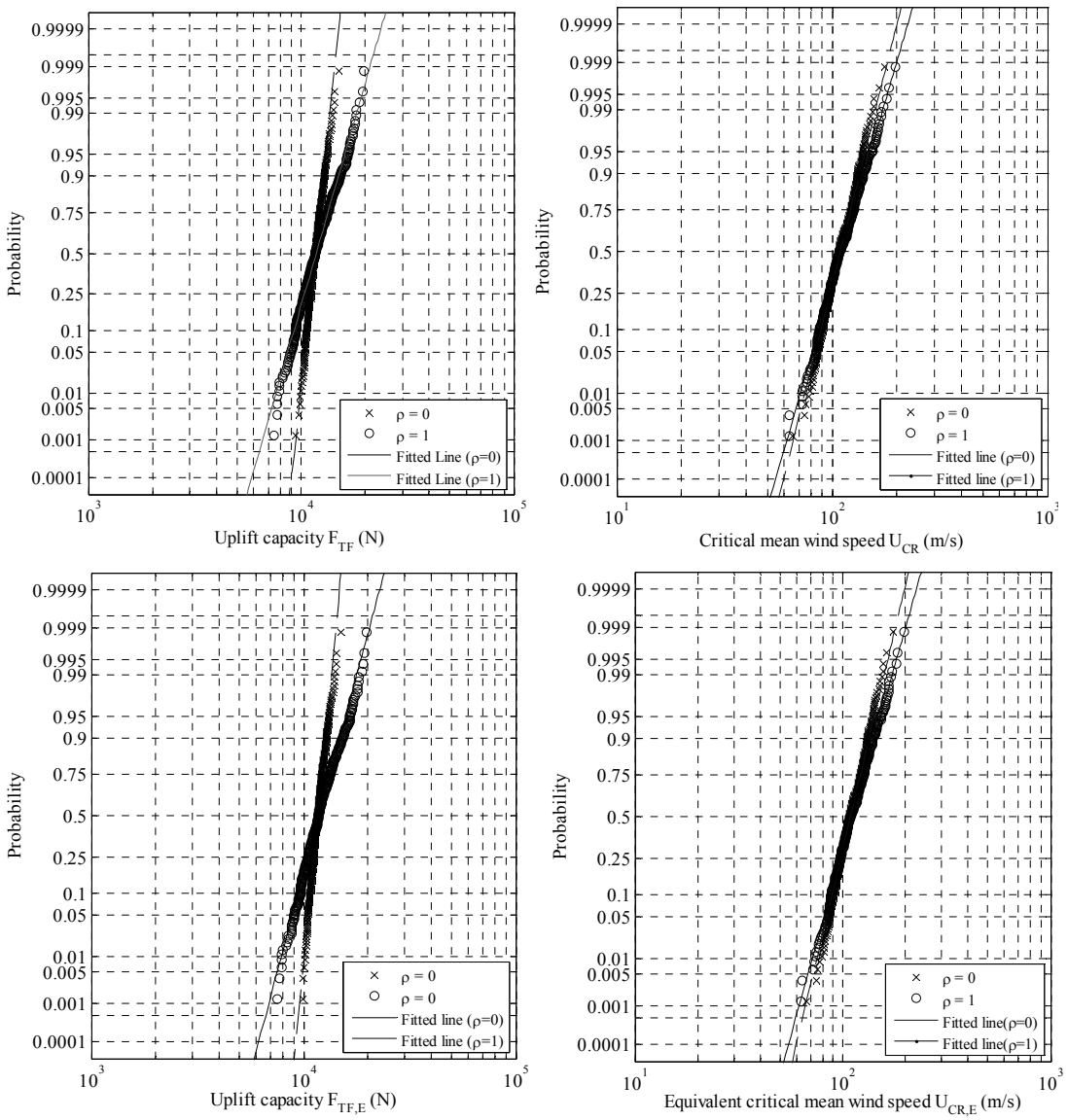

Figure 3.10 Samples of F_{TF}, U_{CR}, $F_{TF,E}$ and $U_{CR,E}$ plotted on lognormal probability paper for $\rho_{ij} = 0$ and for $\rho_{ij} = 1$.

The nail withdrawal behaviour for nails used to fasten a panel could be partially correlated because they are constructed and serve under similar environment. To see the effect of the partial correlation on the panel uplift capacity of the panel, the analysis for the fully correlated case is repeated but considering ρ_{ij} equal to 0.5 or 0.8 or 0.9. The obtained statistics of the F_{TF}, U_{CR}, $F_{TF,E}$, $U_{TF,E}$, and R_n are summarized in Table 3.7.

Table 3.7 Statistics of the uplift capacity of the panel by considering the partially correlated nail withdrawal behaviour.

Case	Parameter	Statistics	Panel S34	Panel S35	Panel S55
$\rho_{ij} = 0.5$	F_{TF}	Mean (N)	10049	9966	9962
		Cov	0.153	0.151	0.153
	$F_{TF,E}$	Mean (N)	10350	10350	10350
		Cov	0.132	0.132	0.132
	U_{CR}	Mean (m/s)	94.0	71.4	76.9
		Cov	0.199	0.175	0.157
	$U_{CR,E}$	Mean (m/s)	95.5	72.8	78.4
		Cov	0.198	0.168	0.156
	R_n	Mean	0.970	0.962	0.962
		Cov	0.063	0.064	0.059
$\rho_{ij} = 0.8$	F_{TF}	Mean (N)	10087	10130	10071
		Cov	0.181	0.171	0.173
	$F_{TF,E}$	Mean (N)	10575	10575	10575
		Cov	0.147	0.147	0.147
	U_{CR}	Mean (m/s)	97.3	72.2	77.7
		Cov	0.256	0.179	0.179
	$U_{CR,E}$	Mean (m/s)	99.9	73.9	79.7
		Cov	0.244	0.174	0.175
	R_n	Mean	0.951	0.956	0.950
		Cov	0.069	0.066	0.061
$\rho_{ij} = 0.9$	F_{TF}	Mean (N)	10222	10183	10174
		Cov	0.183	0.172	0.177
	$F_{TF,E}$	Mean (N)	10691	10691	10691
		Cov	0.151	0.151	0.151
	U_{CR}	Mean (m/s)	94.6	71.9	77.5
		Cov	0.198	0.178	0.157
	$U_{CR,E}$	Mean (m/s)	96.9	74.0	79.6
		Cov	0.197	0.174	0.155
	R_n	Mean	0.953	0.951	0.950
		Cov	0.061	0.059	0.059

Comparison of the results shown in Table 3.7 to those in Table 3.6 indicate that the statistics of the uplift capacity of the panel for partially correlated cases are within those for the fully correlated case and independent case. The cov values of F_{TF} and of $F_{TF,E}$ for ρ_{ij} equal to 0.5 are about twice of those for ρ_{ij} equal to 0.0. The variation of ρ_{ij} does not affect significantly the cov of U_{CR} and $U_{CR,E}$ for each of the considered panels. This

again indicates that the degree of uncertainty in U_{CR} and $U_{CR,E}$ is significantly influenced by the uncertainty in the point-in-time wind pressure coefficients.

3.5.2 Parametric investigation for panel uplift capacity

The use of the pressure coefficients from the time histories obtained from wind tunnel test allowed us to assess the impact of the spatial variability of the wind pressure on the uplift capacity of the panel. The assessment is specific to the considered panel and the wind direction used to obtain the time histories of the pressure coefficients. To further investigate the effect of the correlated pressure on the uplift capacity of the panel, rather than using the time histories of the pressure coefficients from the wind tunnel test, we sample the pressure coefficients for the taps shown in Figure 3.6. To generate samples of pressure coefficients, it is assumed that the statistics of the pressure coefficient shown in Table 3.3 are applicable and they can be considered to be normally distributed. Furthermore, the pressure coefficients are considered to be spatially correlated with the correlation coefficient ρ_c defined by Eq. (6).

The results for the cases where λ equal to 1.5, 2.0 and 3.0 m and having a ρ_{ij} equal to 0.5 are shown in Table 3.8. Comparison of the results shown in Table 3.8 to those depicted in Tables 3.6 and 3.7 indicates that in general the observations drawn from Tables 3.6 and 3.7 are also applicable to Table 3.8.

Table 3.8 Statistics of the uplift capacity of the panel using the simulated spatially correlated wind pressure coefficients and considering uncertainty in the nail withdrawal behaviour.

Case	Parameter	Statistics	Panel S34	Panel S35	Panel S55
λ = 1.5	F_{TF}	Mean (N)	9963	9832	9830
		Cov	0.160	0.156	0.165
	U_{CR}	Mean (m/s)	97.6	70.9	77.7
		Cov	0.232	0.192	0.241
	$U_{CR,E}$	Mean (m/s)	99.7	72.8	81.0
		Cov	0.241	0.193	0.223
	R_n	Mean	0.962	0.949	0.949
		Cov	0.076	0.069	0.089
λ = 2.0	F_{TF}	Mean (N)	9975	9973	9915
		Cov	0.159	0.157	0.154
	U_{CR}	Mean (m/s)	95.1	70.7	78.0
		Cov	0.228	0.196	0.183
	$U_{CR,E}$	Mean (m/s)	97.1	72.1	79.8
		cov	0.233	0.190	0.182
	R_n	Mean	0.962	0.962	0.957
		cov	0.068	0.068	0.070
λ = 3.0	F_{TF}	Mean (N)	10010	10014	9966
		cov	0.159	0.152	0.159
	U_{CR}	Mean (m/s)	95.7	72.7	79.6
		cov	0.242	0.198	0.202
	$U_{CR,E}$	Mean (m/s)	97.6	74.0	81.3
		cov	0.247	0.194	0.203
	R_n	Mean	0.965	0.967	0.962
		cov	0.066	0.063	0.068

Note: Since in all cases the mean and cov of $F_{TF,E}$ are equal to 11942 (N) and 0.141, respectively, they are not shown in the table.

It is often observed that nails may not be fastened properly or simply missing. To illustrate the effect of the missing nail on the panel uplift capacity, it is considered that Nail 11, or Nails 11 and 13 shown in Figure 3.1 are missing and that the nail withdrawal behaviour is uncorrelated (i.e., $\rho_{ij} = 0$), although it is acknowledged in construction practice the pattern of the missing nails are random. Note that Nail 11 (or Nail 13, or 21 or 23) is the most critical nail for the panel uplift capacity. After repeating the analysis that was carried out for the results presented in Table 3.6, for $\rho_{ij} = 0$ but considering the

mentioned missing nails, the obtained statistics of the panel uplift capacity are shown in Table 3.9. The results shown in the table again indicates that the mean of R_n is near unity and its cov is small as compared to that of F_{TF}. Comparison of the results shown in Tables 3.9 and 3.6 indicates that missing the single critical nail (i.e., Nail 11) could reduce the mean of the panel uplift capacity by about 7% whether the comparison is based on F_{TF} or $F_{TF,E}$. For the case with two missing nails, the reduction in the mean of the panel uplift capacity is 13%. In all cases, the increase in the cov of F_{TF} is not significant.

Table 3.9 Statistics of the panel uplift capacity considering the partially correlated wind load and missing nail effects.

Case	Parameter	Statistics	Panel S34	Panel S35	Panel S55
Missing Nail 11	F_{TF}	Mean (N)	9067	9315	9347
		cov	0.089	0.083	0.083
	$F_{TF,E}$	Mean (N)	9392	9392	9392
		cov	0.080	0.080	0.080
	U_{CR}	Mean (m/s)	90.4	68.6	75.1
		cov	0.175	0.162	0.156
	$U_{CR,E}$	Mean (m/s)	91.2	68.9	75.3
		cov	0.176	0.159	0.154
	R_n	Mean	0.968	0.993	0.996
		cov	0.059	0.056	0.055
Missing Nail 11 and 13	F_{TF}	Mean (N)	8846	8986	9016
		cov	0.088	0.095	0.097
	$F_{TF,E}$	Mean (N)	9062	9062	9062
		cov	0.091	0.091	0.091
	U_{CR}	Mean (m/s)	89.1	67.5	74.0
		cov	0.192	0.153	0.145
	$U_{CR,E}$	Mean (m/s)	90.1	67.7	74.2
		cov	0.197	0.152	0.146
	R_n	Mean	0.977	0.993	0.997
		cov	0.060	0.056	0.064

3.6 Conclusions

The numerical results presented in this study are focused on the assessment of the uplift capacity of the roof panel under spatio-temporally varying wind pressure. The analysis considers the nonlinear nail withdrawal behaviour, and uncertainty in pressure coefficients and the nail withdrawal capacity. The results indicate that the statistics of the panel uplift capacity in terms of the (ultimate) total reaction force are not sensitive to the spatially varying wind, but are significantly influenced by the adopted probabilistic model and correlation of nail withdrawal behaviour. This is especially true for the coefficient of variation (cov) of the total reaction force. Results also indicate that the use of the equivalent uniformly distributed wind loading, with the pressure coefficient equal to the weighted average wind pressure coefficient, provides sufficiently accurate estimates of the statistics of the uplift capacity of panel. This approximate approach is therefore recommended for assessing the panel uplift capacity as it simplifies the analysis. The approximation introduces a modeling error with a bias close to unity and a cov of only 4% which is much smaller than those associated of the ultimate total reaction force ranging from 7% to 20%. In all cases, the ultimate total reaction force of the panel could be modeled as lognormal variate. The investigation of the effect of missing nail on the uplift capacity indicates that missing a single critical nail could reduce the mean of the panel uplift capacity by 8%.

The panel uplift capacity is also characterized by using the critical reference mean wind speed at the average roof height. As expected, the statistics of the critical mean wind speed depend on the location of the roof panel because the magnitude of and uncertainty in the pressure coefficients are location dependent. It must be noted that the

critical wind speed used to represent the uplift capacity of the panel is associated with the point-in-time pressure coefficients, and they do not incorporate the gust effect or exposure factor. Also, statistical analysis shows that the spatial correlation can be modeled using an exponential model with correlation length within 1.5 m to 3.0 m.

References

ANSYS Inc. (2005), ANSYS User's Manual, Version 10.0, Canonsburg, PA.

APA – The Engineered Wood Association. (1995). Design capacities of APA performance rated structural use panels, Technical Note #N375B, Tacoma, WA.

Bartlett F.M., Galsworthy, J.K., Henderson, D., Hong, H.P., Iizumi, E., Inculet, D.R., Kopp, G.A., Morrison, M.J., Savory, E., Sabarinathan, J., Sauer, A., Scott, J., St. Pierre, L.M., Surry, D. (2007). The Three Little Pigs Project: A New Test Facility for Full-Scale Small Buildings. In: International Conference on Wind Engineering, Cairns.

Benjamin, J.R. and Cornell, C.A. (1970). Probability, Statistics and Decision for Civil Engineers, McGraw-Hill, New York.

Canadian Plywood Association (2005). Plywood Design Fundamentals, www.canply.org

Chui, Y.H., Ni, C., and Jiang, L. (1998). Finite element model for nailed wood joints under reversed cyclic load, Journal of Structural Engineering, ASCE, 124(1), pp 96-103.

Cope, A.D., Gurley, K.R., Gioffre, M. and Reinhold, T.A. (2005). Low-rise gable roof wind loads: Characterization and stochastic simulation, Journal of Wind Engineering and Industrial Aerodynamics, 93(9):719-738.

Cunningham, T.P. (1992). Roof Sheathing Fastening Schedules for Wind Uplift, APA Report T92-28, American Plywood Association, Tacoma, WA.

Dao, T.N. and van de Lindt, J.W. (2009). New Nonlinear Roof Sheathing Fastener Model for Use in Finite-Element Wind Load Applications, Journal of Structural Engineering, ASCE, 134(10): 1668-1674.

Datin, P.L. and Prevatt, D.O. (2009). Equivalent roof panel wind loading for full scale sheathing testing, 11th Americas Conference on Wind Engineering.

Davenport, A.G. (1961). The spectrum of horizontal gustiness near the ground in high winds, J. Royal Meteorol. Soc., 87, 194-211.

Der Kiureghian, A. and Liu, P. (1986). Structural reliability under incomplete probability information, Journal of Engineering Mechanics, 112 (1), pp. 85-104.

Florida Building Code (2007). Florida Building Code -- Residential, International Code Council, Inc., FL.

Forest Products Laboratory (1999). Wood handbook—Wood as an engineering material. Gen. Tech. Rep. FPL–GTR–113. Madison, WI: U.S. Department of Agriculture, Forest Service.

Foschi, R.O. (2000). Modeling the hysteretic response of mechanical connections for wood structures, Proc., World Conf. on Timber Engrg., Dept. of Wood Sci., ed., University of British Columbia, Vancouver.

Groom, K.M. and Leichti, R.J. (1993). Load withdrawal displacement characteristics of nails, Forest Products Journal, 43(1), pp. 51-54.

Gurley K., Davis Jr. R.H., Ferrera S.P., Burton J., Masters F., Reinhold T., Abdullah M. (2006), Post 2004 Hurricane field survey - An evaluation of the relative performance of the standard building code and the Florida building code, Proceedings of the Structures Congress and Exposition, pp.8.

He, M., Lam, F. and Foschi, R.O. (2001). Modeling three-dimensional timber light-frame buildings, Journal of Structural Engineering, ASCE, 127(8), pp.901-913

Hill, K., Datin, P., Prevatt, D.O., Gurley, K. and Kopp, G.A. (2009). A Case for Standardized Dynamic Wind Uplift Pressure Test for Wood Roof Structural Systems, 11th Americas Conference on Wind Engineering, San Juan, Puerto Rico, June, 2009

Kopp, G.A., Morrison, M.J., Gavanski, E., Henderson, D. and Hong, H.P. (2010). The "Three Little Pigs" Project: Hurricane Risk Mitigation by Integrated Wind Tunnel and Full-Scale Laboratory Tests, Natural Hazards Review, http://dx.doi.org/10.1061/(ASCE) NH.1527-6996.0000019.

Kopp, G.A., Surry, S. and Mans, C. (2005). Wind effects of parapets on low buildings: Part 1. Basic aerodynamics and local loads, Journal of Wind Engineering and Industrial Aerodynamics, 93: 817-841.

Mizzell, D.P. (1994). Wind Resistance of Sheathing for Residential Roofs, Civil Engineering Department, MS Thesis Clemson, Clemson University.

Murphy, S., Schiff, S., Rosowsky, D. and Pye, S. (1996). System effects and uplift capacity of roof sheathing fasteners, Building an International Community of Structural Engineers, New York, NY, USA, p765-770.

NBCC. 2005. National Building Code of Canada 1995. Institute for Research in Construction, National Research Council of Canada, Ottawa, Ont.

Ontario Ministry of Municipal Affairs and Housing, (2006), 2006 Building Code. Government of Ontario, Queen's Printer for Ontario, Toronto, ON.

Rosowsky, D.V. and Schiff, S.D. (1996). Probabilistic modeling of roof sheathing uplif capacity, Probabilistic Mechanics and Structural and Geotechnical Reliability, Proceedings of the Specialty Conference, pp.334-337.

Simiu, E. and Scanlan R.H. (1996). Wind Effects on Structures, Fundamentals and Application to Design, New York: John Wiley.

Simiu, E. and Stathopoulos. T. (1997). Codification of wind loads on buildings using bluff body aerodynamics and climatological data bases. Journal of Wind Engineering and Industrial Aerodynamics, v69-71: 497-506.

Smith T.L. (2005). Hurricanes: an overview by FEMA – Findings and recommendations for roof system performance, Nations Roof, Vol. 2, No. 09.

St. Pierre, L.M., Kopp, G.A., Surry, D. and Ho, T.C.E. (2005). The UWO contribution to the NIST aerodynamic database for wind loads on low buildings: Part 2. Comparison of data with wind load provisions, Journal of Wind Engineering and Industrial Aerodynamics, 93 (1): 31-59.

Surry, D. and Stathopoulos, T. (1978). An experimental approach to the economical measurement of spatially - Averaged Wind Loads, Journal of Ind. Aerodynamics, Vol. 2: 385-397.

Surry, D., Kopp, G.A., and Bartlett, F.M. (2005). Wind load testing of low buildings to failure at model and full scale, ASCE Natural Hazards Review, vol. 6: 121-128.

Sutt, E.G. (2000). The Effect of Combined Shear and Uplift Forces on Roof Sheathing Panels, PhD thesis, Dept. of Civil Engineering, Clemson University, Clemson, S. C.

CHAPTER 4

THE EFFECTS OF MISSING NAILS ON THE PANEL UPLIFT CAPACITY AND RELIABILITY OF ROOF PANELS UNDER WIND LOAD

4.1. Introduction

The damage to and insured losses of light frame wood houses caused by windstorms are rising. This trend is partly due to increased population and construction in the coastal areas, and possibly caused by increased number of high wind events. The failure of a single roof panel has the potential to increase insured losses dramatically due to water penetration during wind storms (Sparks et al. 1994). This problem is compounded by the fact that wind-induced failure is frequent and often initiates at roof sheathing panels. This is true even for newer homes built to more recent and stringent building codes (Gurley et al. 2006).

Numerical and experimental investigations have been conducted to investigate the uplift capacity of typical roof sheathing panels, considering that the wind pressure can be treated as a time-invariante or static uniform pressure (Mizzell 1994, Rosowsky and Schiff 1996, Sutt 2000). The Insurance Research Lab for Better Homes (IRLBH) at the University of Western Ontario, a state-of-the-art test facility, is equipped with pressure loading actuators, which allows the investigation of the performance of houses under environmental actions, including full-scale wood frame houses under wind loading.

An inspection of the results from damage surveys (Allen 1986a) and details of newly constructed houses indicates that, similar to any other construction or manufacturing process, some of the nails used to fasten the roof panels to the roof trusses may be

missing or improperly installed. The missing or improperly fastened nails are likely to affect the panel uplift capacity and its reliability under wind load.

The influence of construction quality on the reliability of structures is a well-known problem. Ellingwood (1987) indicated that it is not surprising that structural failures rarely occur because of high loads and low strengths, since design codes are developed to cope with the uncertainty in loads and structural resistance. The proportion of failures attributed to human error varies from about 75% to 90% (Matousek 1982, Madsen et al. 1986, Melchers 1989, Stewart 1993). However, error in construction is difficult to quantify. This is partially due to limited accessibility to construction sites to carry out detailed inspection, as well as the fact that failures attributed to poor construction quality or human error are not an integral part of design code calibration. The subject of human error and structural practice was also discussed by Allen (1986b) in terms of how mistakes are made and discovered. As the building process involves a wide variety of tasks carried out by humans, research focused on human error needs a multidisciplinary approach with expertise from psychology, forensic engineering, sociology and quality management (Atkinson 1998). This range of consideration is valuable, but is beyond the scope of this study. Rather, we take the advantage of having complete access to the house during the construction process of the two-story full-scale wood frame test house at the IRLBH facility for the purpose of quality inspection. More specifically, we inspected and surveyed the fastening of the roof panel, nail-by-nail, for the full-scale two-story test house, which was constructed at the IRLBH facility (Surry et al., 2005; Bartlett et al., 2007; Kopp et al., 2010) by students from Fanshawe College in London, Ontario, Canada. The quality of the construction, according to more than 20 local building inspectors, was

representative of average construction quality.

The collected information on the quality of fastening was employed in this study to assess the frequency of missing or improperly installed nails used to fasten the plywood roof panels. This frequency is incorporated in assessing the roof panel uplift capacity. For the assessment of the statistics of the panel uplift capacity, a spatio-temporally varying wind pressure was considered, a finite element model is used to represent the panel and fasteners and a nonlinear dynamic analysis with ramp load (NDA-RL) is employed. The use of the NDA-RL is justified because it provides sufficient accurate estimates of the panel uplift capacity (see Chapter 2) as compared to those obtained based on the nonlinear incremental dynamic results. Parametric investigation of the uplift capacity of the panel is carried out by considering nonlinear force-displacement behaviour of fasteners. A comparison of the statistics of the uplift capacity with and without the missing or improperly fastened nails is carried out. Also, the impact of considering and ignoring the missing or improperly fastened nails on the estimated reliability of roof panel under wind loading is presented.

4.2. Construction error: the case of improper fastening of roof panels

One of the major contributing factors to structural failure is human error or construction error, which may be defined as "significant departure from standard practice" (Nowak and Collins 2000). However, the quantification of the human error in practice is a complex task. In this section, the assessment of the human error in construction is very specific in that it focuses on the quality of the fastening of the plywood roof panel to the roof trusses. Missing nails (i.e., nails at specific locations are

required but missing) and improperly fastened nails (i.e., nails that have penetrated to the roof panels but missed the roof trusses) are considered to be caused by human error.

a) Full scale test house during construction (Modification has been made to avoid commercial issue.).

b) Full scale house after installing brick veneer walls.

Figure 4.1 Photos of the two story test house.

The assessment of the statistics of the missing or improperly installed nails is carried out based on the information gathered from the construction of the full-scale two-story test house at the IRLBH (Bartlett et al., 2007; Kopp et al., 2010). The testing structure is a full-scale two-story wood frame house, shown in Figure 4.1, with brick veneer which was built with standard building technology and normal construction procedure. The quality of construction, according to more than 20 local building inspectors, was representative of current industry standard. In other words, the quality of the construction of this "as-built" house is no better or no worse than that of a typical Canadian residential house. This two-story test house has plane dimension of 9.3 m × 9.3 m, an eave height of 5.2 m and a gable roof slope of 4:12. The ½ inch (nominal thickness 11.5 mm) plywood panels were used as roof panels; 8d common nails (with 63 mm (2.5″) length and 3.4 mm (0.133″) diameter) were installed using nail guns to fasten the panels to the roof trusses constructed of 2″×4″ lumber. The fastening schedule for the roof panels used is based on that recommended by the NBCC (2005), which considers a nail spacing of 150 mm along the edge supports and 300 mm along the intermediate supports. Illustrations of the roof panel connection tolerance can be found in (NAHB Research Center 2003).

The inspection and survey of the fastening for the roof were carried out immediately after the completion of the construction of roof panels and before the installation of shingles. Extensive photos of the roof top were taken, and the location of the nails along each roof truss was measured. Also, a survey of the adequacy of the fastening was conducted in the attic to see whether a nail appearing on the top of the roof panel had missed the roof truss. Nails that were not properly installed were identified by pairing the

locations of nail heads and nails that missed the indented frame.The information on the fastening obtained from the survey is shown in Figure 4.2 and Table 4.1.

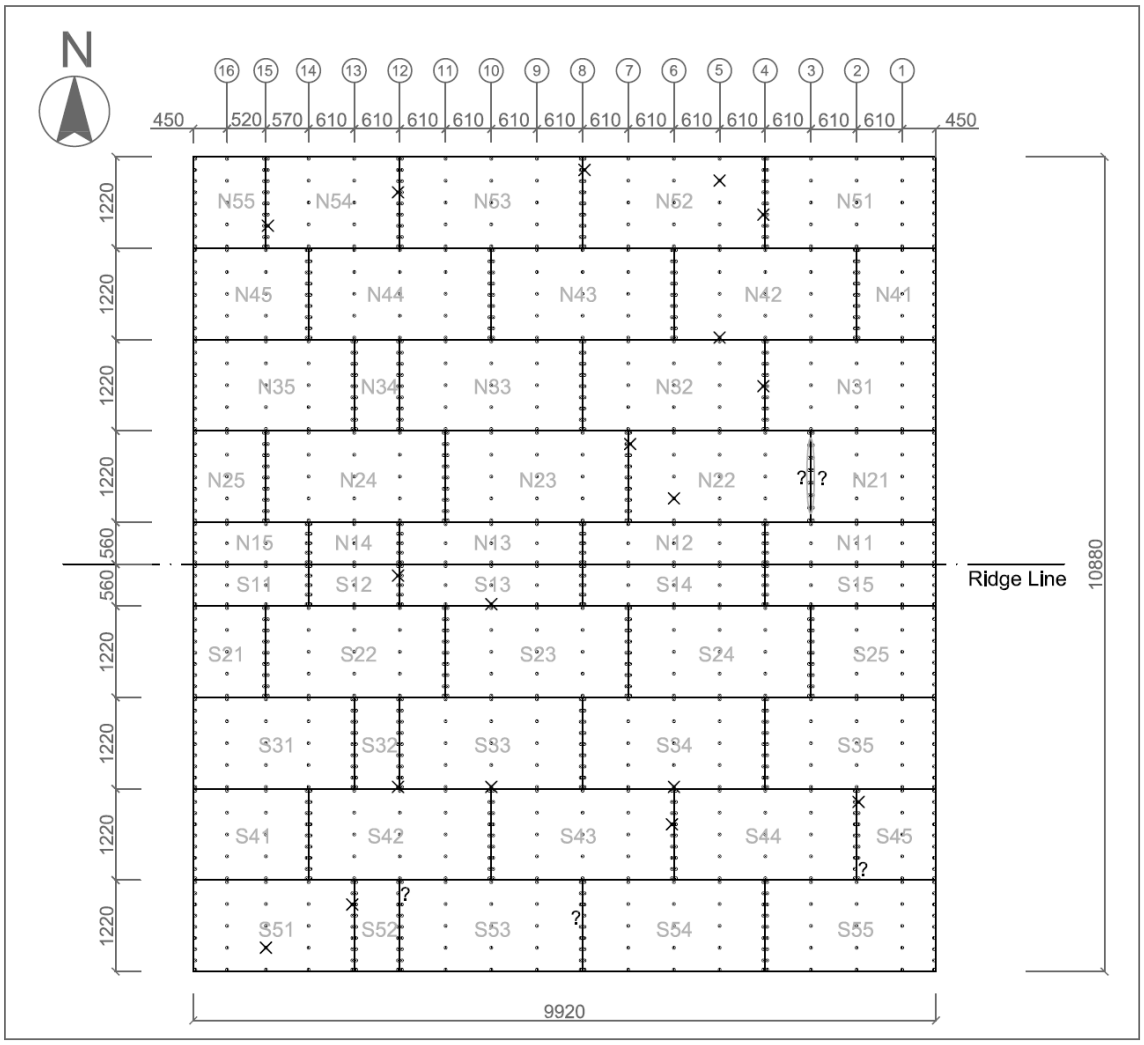

a) Surveying information on the nails (nail locations are shown in dots; improperly installed nails are marked as '×', and missing nails are marked with '?').

b) The typical improperly installed nail

Figure 4.2 Surveying information on the fasteners and roof panel layout.

Figure 4.2 shows the locations of the properly installed nails as well as the improperly installed nails. It also shows the locations where nails are required but are missing. Note that if no human error is involved and the recommended fastening schedule in the NBCC (2005) is followed, the number of the properly installed nails to fasten the roof panels is equal to 33 for a standard roof panel. There are 1467 nails that are properly installed to fasten the roof panels; there are 18 improperly installed nails as they missed the roof trusses, and 5 missing nails as the actual nail spacing for the nails along the direction of the roof truss used to fasten the panel is greater than 1.5 times of the specified nail spacing. The panel numbering is also shown in Figure 4.2, where “N” and “S” are used to identify whether the panels are on the north or south sides of the roof ridge.

Table 4.1 Survey information on missing nails.

Panel label		n_f	P_f	$p(n_f)$
Typical	Non-typical			
N22, N52	-	3	0.074	0.011
S51, S53	N54, S45	2	0.074	0.074
N32, N42, S33, S34, S43	N21, S12, S13, S32	1	0.185	0.305
N53, N51, N44, N43, N35, N33, N31, N24, N23, S22, S23, S24, S31, S35, S42, S44, S54, S55	other panels	0	0.667	0.607

Note: n_f = Number of missing or improperly installed nails; P_f = frequency that a typical panel has n_f missing or improperly installed nails (from observation); $p(n_f)$ is calculated using Eq. (1) considering n_f missing nails in a typical panel that requires 33 nails.

For simplicity, the missing or improperly installed nail will be referred to as "missing nail" in the following. Based on the information listed in Table 4.1, it can be observed that there are 15 panels with at least one missing nail, and there are 2 panels with up to 3 missing nails, one of which is located at the north edge of the roof that is likely to experience high wind pressure. Although most of the observed missing nails are located on the panel edge supports, there is no evidence that the missing nail only occurs on such locations as the required number of fasteners for the edge support is greater than that for the intermediate support. It is noted that the missing nail statistics listed here are based on a single typical "as-built" Canadian residential house.

If the occurrence of the missing nail is assumed to be spatially homogeneous as there is no strong evidence to suggest otherwise, the rate of missing nail calculated using the information obtained from surveying equals 1.5% (=(18+5)/(1467+18+5)). By considering that the occurrence of the missing nail follows the binomial process with the probability of an intended nail fastening being missing, p, equal to 1.5%, the probability that there are k missing nails for panel that requires n fasteners, $p(k)$, is given by,

$$p(k) = \frac{n!}{k!(n-k)!} p^k (1-p)^{n-k} \tag{1}$$

The calculated $p(k)$ for a typical roof panel with fastening schedule recommended by the NBCC code (see Figure 4.3), is shown in Table 4.1. Comparison of the calculated probabilities with those obtained directly from the survey indicates that the model could be considered adequate. Note that we did not scrutinize possible splitting of the lumber in the roof panel due to nail installation, as visual inspection indicates that this is not a problem for this test roof.

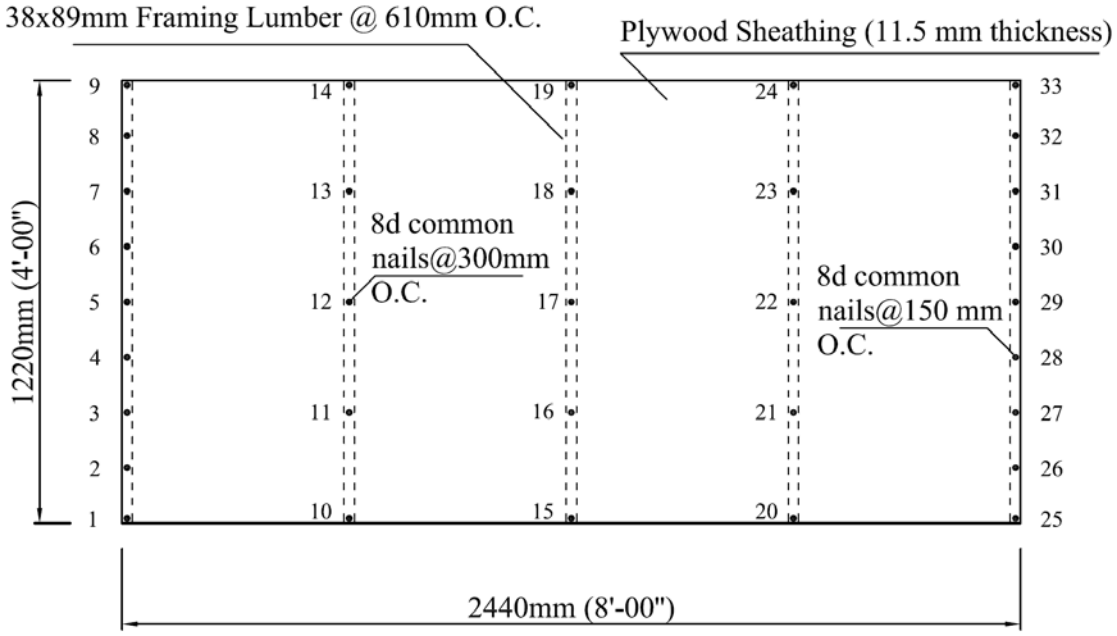

Figure 4.3 Nail schedule recommended by NBCC (2005) for typical roof panel.

4.3. Modeling and procedure for evaluating the uplift capacity

The typical plywood roof sheathing panel shown in Figure 4.3 is modeled using 4–node shell element with 6 degrees of freedom at each node implemented in ANSYS (ANSYS Inc 2005), considering both bending and membrane stiffness to allow large deflection capability. As the Douglas-fir is the common wood species used to manufacture plywood panels (Canadian Plywood Association 2005), it is assumed that the modulus of elasticity of the plywood roof panel, E, equals that of Douglas-fir along the longitudinal grain, which is listed in Table 4.2.

A nonlinear force-displacement relation with the statistics of model parameters summarized in Table 4.2 is adopted to represent nail withdrawal behaviour. The model is based on studies by Groom and Leichti (1993) and Foschi (2000), and is discussed in Chapter 2. The model does not incorporates the effects of shear (Sutt 2000) or the edge bending moment effect (Dao and van de Lindt 2009), since these effects are considered to be negligible for the uplift capacity of panel under uplift wind pressure with the fastening schedule shown in Figure 4.3. Although the nonlinear spring is unlikely to sustain compression under uplift wind pressure, for completeness, the nail is modeled using a linear spring with the stiffness equal to AE if the nonlinear spring is under compression, where A (=0.0052 m^2) represents the contact area of sheathing with the 2″×4″ stud.

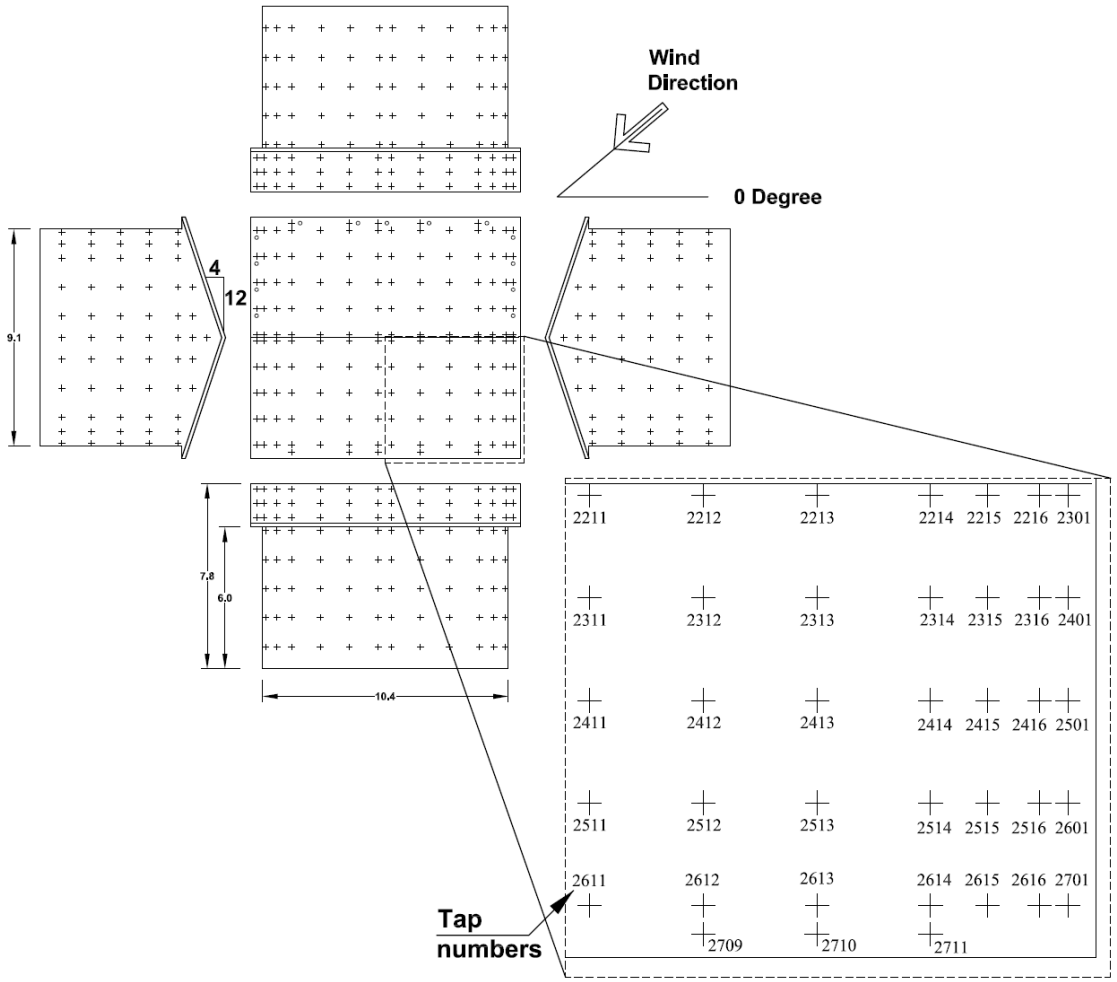

a) Distribution of pressure taps for model test

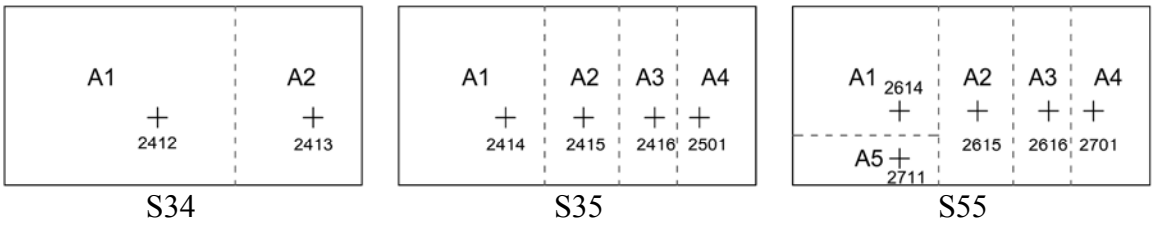

b) Pressure taps locations for the selected panels

Figure 4.4 Locations of pressure taps and the selected panels ('+' is used to mark the tap location, and dashed lines are used to define the tributary area for the pressure taps).

Table 4.2 Summary of the models used to represent the roof panel, the withdrawal behaviour of the nails and their correlation, and the characteristics of the wind pressure coefficients.

Model	Parameter	Value
Roof panel modeled as linear elastic	Modulus of elasticity, E	10.45 GPa
Nail withdrawal model: The relation between the force, F, and displacement along the nail shank, D $F = \begin{cases} k_0 D, & \text{for } D \le d_p \\ f_p + (Q_0 + Q_1 d)\left(1 + \exp\left(-\frac{k_0 d}{Q_0}\right)\right), & \text{for } d_p < D \le d_m \\ f_m \exp\left(Q_4 (D - d_m)^2\right), & \text{for } D > d_m \end{cases}$	$d = D - d_p$, $Q_4 = \ln(Q_2)/[d_m(Q_3 - 1)]^2$, $f_p = f_m/(1+\gamma)$ (Q_0, Q_1, Q_2, Q_3) are model parameters for 8d common nail; the displacement d_m is evaluated from the second equation for $F = f_m$.	$Q_0 = 121$ $Q_1 = 1\times10^5$ $Q_2 = 0.9$ $Q_3 = 2.6$
Nail under compression: The nail is modeled using a linear spring with the stiffness equal to AE.	A = the contact area of panel with the 2″×4″ stud	$A = 0.0052$ m^2
Multiplicative model for correlated nails: a random variable Y_i, representing f_m or k_0 or γ, for the i-th nail is expressed as, $Y_i = Y_0 \times X_i$, $i = 1, \cdots, n$. The correlation coefficient between Y_i and Y_j for $i \ne j$, ρ_{ij}, equals $\left(v_0 / \sqrt{v_0^2 v_X^2 + v_0^2 + v_X^2}\right)^2$	$Y_0 \in$ LN(m_{Y0}, v_0) and $X_i \in$ LN(1.0, v_X), where LN(m,v) denote a lognormally distributed random variable with mean of m and coefficient of variation of v.	Variable — Mean — cov K_0 (N/m) — 4171521.2 — 0.39 f_p (N) — 680.6 — 0.20 f_m (N) — 805.1 — 0.17 d_m (mm) — 0.254 — 0.38
Model for wind pressure coefficient C_i: For the parametric investigation, C_i is considered to be normally distributed, although it is acknowledged that in some cases other probability models could be assigned (see Chapter 2). The spatial correlation ρ_c between C_i for different taps is considered to be given by $\rho_c = \exp(-d/\lambda)$, where d is distance between two taps and the correlation length λ takes a value within [1.5, 3.0].	Tap number, mean of C_i and coefficient of variation (cov) of C_i for the taps shown in Figure 4.4 for the selected panels	Tap # — Mean — cov 2412 — 0.289 — 0.112 2413 — 0.362 — 0.142 2414 — 0.513 — 0.166 2415 — 0.570 — 0.185 2416 — 0.582 — 0.195 2501 — 0.574 — 0.194 2614 — 0.442 — 0.141 2615 — 0.462 — 0.151 2616 — 0.479 — 0.171 2701 — 0.476 — 0.184 2711 — 0.422 — 0.143

Note: C_i is used to represent the absolute value of the negative wind pressure coefficient.

The nail withdrawal behaviour in a roof panel is likely to be correlated as the nails serve under similar environment and are fastened to the same, or similar, timber species. Because statistical data for assessing this correlation is lacking, a multiplicative model for each model parameter used to represent the nail behaviour (see Table 4.2) is adopted for the parametric investigation.

The pressure coefficients on the roof panels are affected by the geometry of surrounding structures, and the wind direction (Surry and Stathopoulos 1978, Simiu and Stathopoulos 1997, Kopp et al. 2005). The pressure coefficients are taken from measurements obtained from the boundary layer wind tunnel of a test model with a scale of 1:50, representing the full-scale wood frame test house with distribution of the pressure taps shown in Figure 4.4a. The obtained statistics of the point-in-time pressure coefficients are listed in Table 4.2 for a few selected pressure taps located on Panels S34, S35, and S55 shown in Figure 4.4b. The statistics are obtained from 71871 samples for each tap, representing about 3 minutes time history for the model scale for a reference mean wind speed of 13.7 m/s (or about 45 minutes full-scale pressure history for a 30 m/s mean wind speed at the average roof height). Furthermore, based on the Kolmogorov-Smirnov goodness-of-fit and statistical analysis, it was observed that in most cases, the point-in-time wind pressure coefficients could be modeled as a normal variate (see Chapter 2); and that the spatial correlation of the point-in-time pressure coefficients can be modeled using an exponential model depicted in Table 4.2 with a correlation length λ between 1.5 m and 3.0 m.

To assess the panel uplift capacity, including the effect of human error, we use the nonlinear dynamic analysis with ramp load (NDA-RL) since it provides sufficient

accurate estimates of the panel uplift capacity as compared to that obtained from the nonlinear time history dynamic analysis considering the wind pressure time histories (see Chapter 2). For a panel subjected to the spatially varying wind pressure for a given set of point-in-time pressure coefficients, C_i, applicable to the *i*-th tributary area A_i, within the panel, the NDA-RL is used to estimate the uplift capacity of the panel F_{TF}, which equals the maximum reacting force that the panel can sustain. Its corresponding critical mean wind speed U_{CR} (for the same reference height used to evaluate C_i, say at the average roof height) can be calculated using,

$$F_{TF} = \frac{1}{2}\rho U_{CR}^2 \sum (C_i A_i) \tag{2}$$

where ρ is the air density that is taken equal to 1.26 kg/m^3. Note that in this equation as U_{CR} is associated with the point-in-time pressure coefficient rather than the gust pressure coefficient, U_{CR} will be reduced if the gust pressure coefficient is used in this calculation. Since the calculated F_{TF} and U_{CR} vary with different combinations of C_i values, to possibly simplify the characterization and assessment of the panel uplift capacity, we evaluate it by considering that the panel is under an equivalent spatially uniform pressure, C_E,

$$C_E = \left(\sum C_i A_i\right) / A_T \tag{3}$$

The estimated capacity under the equivalent uniform pressure, denoted by $F_{TF,E}$, and its corresponding critical reference mean wind speed, denoted as $U_{CR,E}$, is calculated from,

$$F_{TF,E} = \frac{1}{2}\rho U_{CR,E}^2 C_E A_T \tag{4}$$

In the above equation and throughout this study, it is understood that the negative pressure, or suction, is of interest, and C_i is used to represent the absolute value of the

negative pressure coefficient. The ratio between F_{TF} and $F_{TF,E}$, denoted by R_n, which can be shown to be equal to $\left(U_{CR}/U_{CR,E}\right)^2$, can be used to characterize the adequacy of using $F_{TF,E}$, and $U_{CR,E}$ to approximate F_{TF} and U_{CR}. A flow chart that outlines the analysis procedure based on the simulation technique (Rubinstein and Kroese 2007) for evaluation of the panel uplift capacity by including or excluding the human error is presented in Figure 4.5.

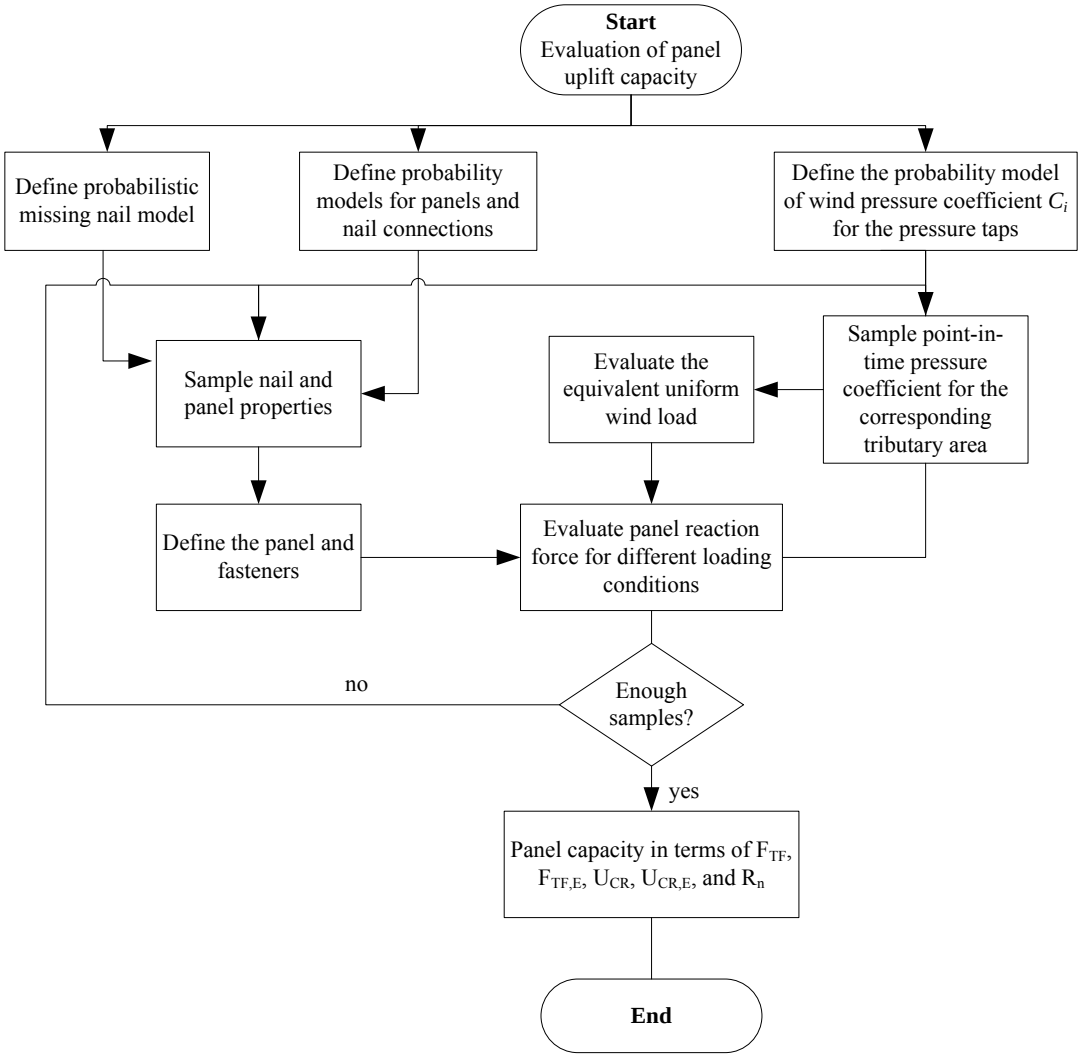

Figure 4.5 Flow chart for evaluation of the roof panel uplift capacity.

4.4. Analysis results

4.4.1 Spatially uniform wind pressure coefficient

In this section, investigation of the panel uplift capacity under spatially uniform pressure is carried out by considering the uncertainty in nail withdrawal behaviour and by including construction error modeled as a binomial process with p = 1.5%. The calculated statistics of F_{TF} from 500 samples obtained following the procedure presented in Figure 4.5 are summarized in Table 4.3 for ρ_{ij} equal to 0, 0.5, 0.8, 0.9, and 1.0. Also, the corresponding statistics resulting from neglecting the construction error are estimated and compared in Table 4.3. The comparison indicates that the mean of the predicted panel uplift capacity by considering the construction error with p = 1.5% is 6% lower than that without construction error. Also, the cov value of F_{TF} for the case with construction error is consistently higher than that without construction error. The samples of F_{TF} for the case with construction error are plotted on lognormal probability paper in Figure 4.6, indicating that the roof uplift capacity can be modeled as a lognormal variate. Similar analysis shows that F_{TF} can be adequately modeled as a lognormal variate if there is no construction error.

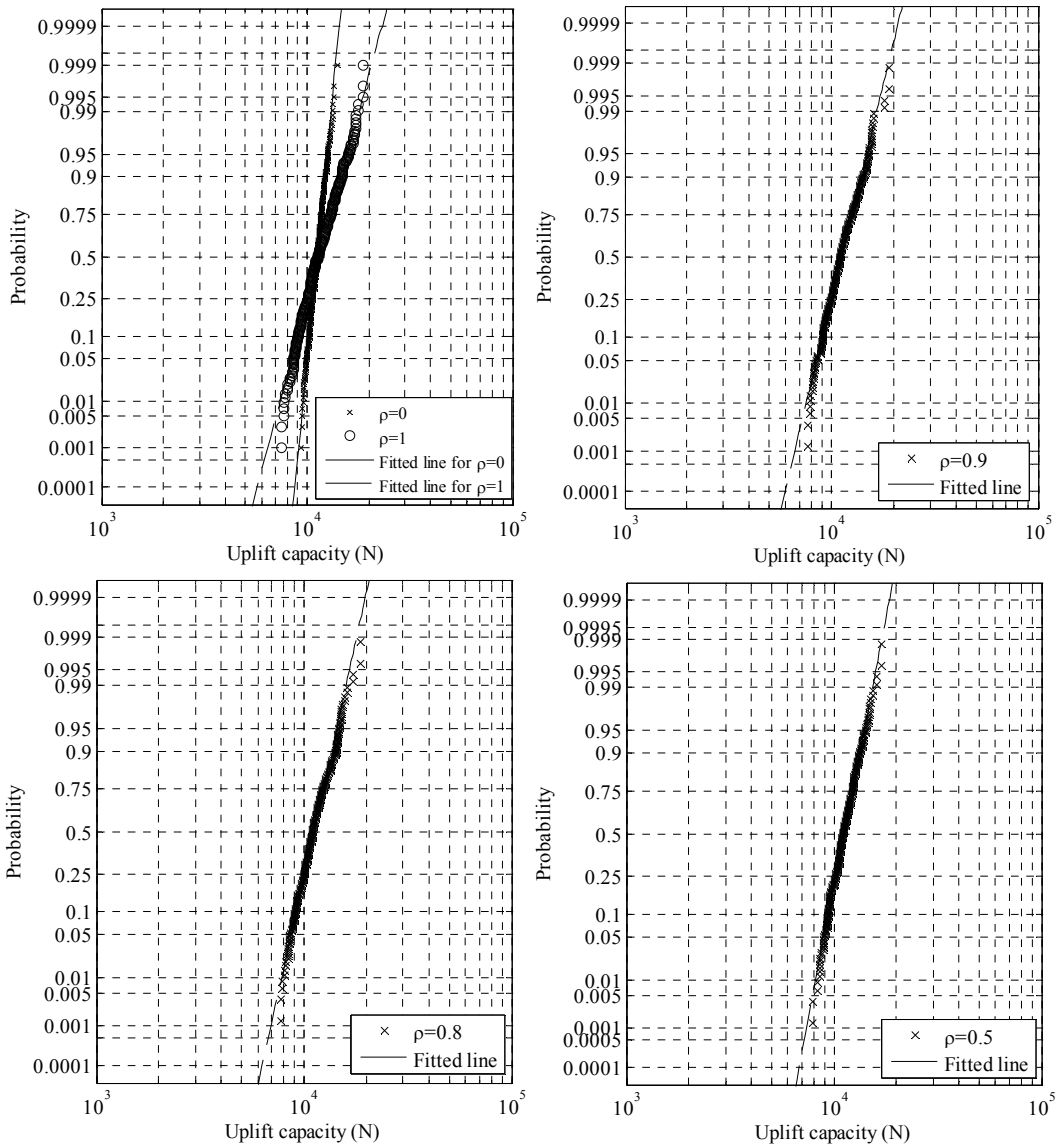

Figure 4.6 Empirical probability distribution of the uplift capacity considering construction error with p = 1.5%.

Table 4.3 Estimated statistics of uplift capacity with and without construction error.

Condition & value of ρ_{ij}		Without construction error		With construction error, p = 1.5%	
		Mean (N)	Coefficient of variation	Mean (N)	Coefficient of variation
Fully correlated	1	10893	0.154	10502	0.179
Partially correlated	0.9	10691	0.151	10412	0.168
	0.8	10575	0.147	10270	0.171
	0.5	10350	0.132	10079	0.151
Independent	0	10138	0.074	9936	0.081

4.4.2 Spatially varying pressure coefficients

Rather than assuming that the wind pressure coefficient is spatially uniform, consider that the wind pressure coefficients are spatially varying. In particular, we consider the three panels S34, S35 and S55 shown in Figure 4.4b. For each panel, we directly use the samples of the point-in-time wind pressure coefficients from the time histories obtained for the pressure taps located on the panels, the tributary area for each tap is also shown in Figure 4.4 for the considered panels.

By carrying out the simulation analysis with and without considering the construction error, the statistics of the uplift capacity in terms of F_{TF}, U_{CR}, $F_{TF,E}$, $U_{CR,E}$, and R_n calculated from 500 samples (for each case) are shown in Table 4.4 for ρ_{ij} equal to 0 and 1.0. The results shown in the table indicate that the observed trends for the results shown in Table 4.3 are equally applicable to this case, except that in this case the decrease in the mean of F_{TF} is only up to 2%. Given a value of ρ_{ij}, the differences between the statistics of $F_{TF,E}$ and of F_{TF} are not very significant. This implies that the roof uplift capacity can

be adequately approximated by that estimated using the equivalent uniformly distributed wind loading. This view is further supported by the fact that the mean of R_n shown in Table 4.4 is almost identical to unity, and the cov of R_n is less than 4%. Since the cov of R_n is much smaller than that of $F_{TF,E}$ or F_{TF}, R_n could be treated as a deterministic quantity.

As the wind pressure coefficients at the taps vary temporally, the uplift capacity of the panel in terms of U_{CR} or $U_{CR,E}$ is significantly uncertain with a cov of up to 20%. The large cov is caused by the temporally varying wind pressure coefficients. It must be emphasized that as the evaluation of U_{CR} or $U_{CR,E}$ is based on the point-in-time wind pressure coefficients, U_{CR} or $U_{CR,E}$ represent the panel uplift capacity associated with the point-in-time wind pressure coefficients and do not include gust effects. The implication of this in reliability analysis will be discussed shortly.

An exercise of fitting probability distributions to the samples of F_{TF}, U_{CR}, $F_{TF,E}$, and $U_{CR,E}$ is carried out using commonly employed probabilistic models: Normal, Lognormal, and Gamma. It is concluded that these variables could be modeled as lognormal variates as the Kolmogorov-Smirnov goodness-of-fit test results (Benjamin and Cornell 1970) indicate that the lognormal model could not be rejected at the 5% significance level.

Table 4.4 Statistics of the uplift capacity of three selected panels by considering and ignoring construction error.

	Case	Parameter	Statistics	Panel S34	Panel S35	Panel S55
Without construction error	$\rho_{ij} = 0$	F_{TF}	Mean (N)	9991	9890	9886
			cov	0.081	0.081	0.083
		$F_{TF,E}$	Mean (N)	10138	10137	10138
			cov	0.074	0.076	0.074
		U_{CR}	Mean (m/s)	94.1	71.4	78.6
			cov	0.195	0.164	0.150
		$U_{CR,E}$	Mean (m/s)	94.8	72.2	79.7
			cov	0.197	0.164	0.151
		R_n	Mean	0.987	0.980	0.976
			Cov	0.061	0.056	0.063
	$\rho_{ij} = 1$	F_{TF}	Mean (N)	10216	10329	10261
			cov	0.179	0.170	0.177
		$F_{TF,E}$	Mean (N)	10833	10833	10833
			cov	0.154	0.154	0.154
		U_{CR}	Mean (m/s)	97.2	72.8	79.9
			cov	0.198	0.184	0.174
		$U_{CR,E}$	Mean (m/s)	100.2	74.7	82.2
			cov	0.193	0.179	0.168
		R_n	Mean	0.941	0.952	0.945
			cov	0.063	0.055	0.056
With construction error for p =1.5%	$\rho_{ij} = 0$	F_{TF}	Mean (N)	9862	9701	9695
			cov	0.093	0.089	0.094
		$F_{TF,E}$	Mean (N)	9911	9911	9911
			cov	0.084	0.084	0.084
		U_{CR}	Mean (m/s)	94.4	70.6	76.9
			cov	0.196	0.166	0.165
		$U_{CR,E}$	Mean (m/s)	94.7	71.4	78.1
			cov	0.197	0.164	0.163
		R_n	Mean	0.997	0.980	0.974
			Cov	0.071	0.065	0.059
	$\rho_{ij} = 1$	F_{TF}	Mean (N)	10119	10133	10003
			cov	0.185	0.185	0.186
		$F_{TF,E}$	Mean (N)	10532	10532	10532
			cov	0.168	0.168	0.168
		U_{CR}	Mean (m/s)	94.4	71.2	76.6
			cov	0.209	0.185	0.183
		$U_{CR,E}$	Mean (m/s)	96.4	72.6	78.8
			cov	0.206	0.179	0.181
		R_n	Mean	0.960	0.961	0.949
			cov	0.060	0.058	0.061

4.4.3 Parametric analysis

The assessment of the statistics of roof panel uplift capacity in the previous section considered the construction error and the spatially and temporally varying wind pressure. It is specific to the considered panel and the wind direction used to obtain the time histories of the pressure coefficients. To further investigate the effect of the correlated pressure coefficients on F_{TF}, U_{CR}, $F_{TF,E}$, $U_{CR,E}$ and R_n, samples of correlated pressure coefficients for the taps shown in Figure 4.4 are generated based on their probabilistic models listed in Table 4.2. The calculated mean and cov of F_{TF}, U_{CR}, $U_{CR,E}$ and R_n are shown in Table 4.5. The mean and cov of $F_{TF,E}$ are not shown in the table as they are the same as those shown in Table 4.4 for the case with $\rho_{ij} = 0$, since $F_{TF,E}$ is independent of spatially varying wind pressure coefficients. The results presented in the table indicate that the mean and cov of F_{TF} varies only slightly for different λ.

As more stringent fastening requirements for geographic regions with significant wind hazard are needed, the analysis carried out for a typical panel considering 1.5% construction error (see Table 4.3) is repeated by considering a nail spacing of 150 mm for both edge and intermediate supports. The estimated statistics of F_{TF} are shown in Table 4.6. Comparison of the results shown in Tables 4.3 and 6 indicates that the reduction in the nail spacing from 300 mm to 150 mm resulted in doubling the mean of F_{TF}. Such an increase in the roof panel uplift capacity is very significant and can be a cost-effective means to reduce the wind risk for wood frame houses.

Table 4.5 Statistics of the uplift capacity by considering $\rho_{ij} = 0$, construction error with p = 1.5% and correlated wind pressure coefficients with correlation length within 1.5 to 3.0.

Case	Parameter	Statistics	Panel S34	Panel S35	Panel S55
$\lambda = 1.5$	F_{TF}	Mean (N)	9748	9715	9688
		cov	0.102	0.094	0.095
	U_{CR}	Mean (m/s)	95.8	72.8	76.2
		cov	0.202	0.158	0.162
	$U_{CR,E}$	Mean (m/s)	97.6	74.4	77.4
		cov	0.215	0.164	0.167
	R_n	Mean	0.975	0.974	0.971
		cov	0.082	0.067	0.069
$\lambda = 2.0$	F_{TF}	Mean (N)	9792	9674	9629
		cov	0.091	0.092	0.099
	U_{CR}	Mean (m/s)	94.1	71.6	77.2
		cov	0.214	0.175	0.199
	$U_{CR,E}$	Mean (m/s)	95.1	72.1	78.8
		cov	0.226	0.193	0.202
	R_n	Mean	0.977	0.972	0.967
		cov	0.063	0.070	0.072
$\lambda = 3.0$	F_{TF}	Mean (N)	9760	9652	9618
		cov	0.105	0.095	0.098
	U_{CR}	Mean (m/s)	97.0	73.8	77.9
		cov	0.274	0.183	0.198
	$U_{CR,E}$	Mean (m/s)	99.0	74.9	79.5
		cov	0.288	0.199	0.212
	R_n	Mean	0.981	0.969	0.965
		cov	0.085	0.072	0.075

To show the impact of the different fastening schedules in combination with different construction error rate on the panel uplift capacity, the analysis carried out for Table 4.3 is repeated but only for ρ_{ij} = 0 and 1, and considering p = 1% and 3% and two fastening schedules. The calculated statistics of F_{TF} are depicted in Table 4.7, indicating again that the roof panel uplift capacity is most significantly affected by the fastening schedule and that the increase in the construction error rate reduces the mean of F_{TF}, and slightly increases the cov of F_{TF}.

Table 4.6 Estimated statistics of panel uplift capacity considering construction error with p = 1.5% and a more stringent fastener requirement with a spacing of 150 mm for the edges and intermediate supports.

Condition & value of ρ_{ij}			Without construction error		With construction error, p = 1.5%	
			Mean (N)	Coefficient of variation	Mean (N)	Coefficient of variation
Fully correlated		1	22156	0.154	19630	0.243
Partially correlated		0.9	21623	0.152	19475	0.235
		0.8	21309	0.148	19389	0.224
		0.5	20710	0.127	19264	0.186
Independent		0	19683	0.063	18684	0.070

Table 4.7 Estimated statistics of panel uplift capacity, F_{TF}, by considering different fastening schedule and different construction error rate.

Fastening schedule	p	ρ_{ij}	Mean (N)	Coefficient of variation
Fastening schedule shown in Figure 4.3	1%	1	10577	0.171
		0	9985	0.082
	3%	1	10362	0.189
		0	9792	0.090
The fastening Spacing of 150 mm for the edges and intermediate supports	1%	1	21962	0.154
		0	19544	0.059
	3%	1	18153	0.245
		0	17443	0.084

4.5. Implication on reliability and codification

Although the reliability of light-frame wood construction under wind load has been presented in the literature (Rosowsky and Cheng 1999, Ellingwood et al. 2004, Lee and Rosowsky 2005, Shanmugam et al. 2009), these studies do not included the effect of the construction error, nor do they incorporate the nonlinear structural responses and/or temporal variation of pressure coefficients directly. Since the effect of construction error on the roof panel has been incorporated in probabilistically characterizing the panel uplift capacity in the previous sections, the reliability analysis including the effect of construction error is largely simplified as shown below.

Consider that failure of roof panel under suction occurs if the panel uplift capacity F_{TF} is less than the applied uplifting wind load F_A. In such a case and the equivalent uniform pressure discussed in the previous sections, the limit state function g can be expressed as,

$$g = R_n F_{TF,E} - \frac{1}{2}\rho U^2 C_E A_T \tag{5}$$

where R_n, ρ, C_E and A_T are defined previously, and U is the mean wind speed at the average roof height. If C_E is evaluated from the point-in-time pressure coefficients C_i, the estimated failure probability (i.e., probability of $g \leq 0$), P_f, does not consider the gust effect. To take into account the gust effect, the probability distribution of extreme value of C_E needs to be used in estimating P_f.

If the point-in-time wind pressure coefficients C_i are normally distributed, the point-in-time values of C_E can also be modeled as a normal variate with the mean and standard deviation denoted by m_{cm} and σ_{cm}. Given the attack angle of the wind being of 40 degree in the present study, the m_{cm} and σ_{cm} calculated based on Eq. (3) for the wind pressure

time histories obtained from the wind tunnel test are 0.646 and 0.230 for Panel S34, 1.124 and 0.330 for Panel S35, and 0.935 and 0.275 for Panel 55.

The maximum of n (point-in-time) values of C_E, $\hat{C}_m$ is Gumbel distributed with the probability distribution function $F(\hat{c}_m)$ given by (Jordaan 2005),

$$F(\hat{c}_m) = \exp(-\exp(-\alpha_n(\hat{c}_m - a_n))) \tag{6}$$

where

$$a_n = m_{cm} + \sigma_{cm}\left(\sqrt{2\ln n} - \frac{\ln(\ln n) + \ln(4\pi)}{2\sqrt{2\ln n}}\right) \tag{7}$$

and,

$$\alpha_n = \sqrt{2\ln n} / \sigma_{cm} \tag{8}$$

To select the value of n, it is noted that C_i used in this study is obtained from the boundary layer wind tunnel at the University of Western Ontario for the test model with the length scale of 1:50, sampling frequency of 400Hz, the wind tunnel reference mean wind speed of 13.7 m/s, and the ratio of the reference mean wind speed at the average roof height to the reference mean wind speed equal to 0.6984. The sampling rate for the full-scale with a mean wind speed of U (m/s) at the average roof height can be calculated using a similarity relation (Simiu and Scanlan 1996) resulting in,

$$f = \left(\frac{fD}{U}\right)_{MS} / \left(\frac{D}{U}\right) = \frac{400U}{50 \times 13.7 \times 0.6984} \tag{9}$$

where D is the length scale, f is the sampling frequency, U is the mean wind speed, the subscript MS denotes the quantities associated with model scale, and symbols without subscript denote those associated with full-scale. This equation indicates that the number of point-in-time readings, n, for the duration of one hour and the mean wind speed at the

average roof height U can be calculated from,

$$n = 3600 f = 3010U \tag{10}$$

Use of Eq. (10) and the values of m_{cm} and σ_{cm} in Eqs. (6) to (8) completely characterises the statistics of $\hat{C}_m$.

However, it is known that the use of this approach (i.e., the parent distribution approach) is insensitive to the extreme observations. Therefore rather than applying the parent distribution approach, we fit directly the probability distribution to the extreme observations in the following. For each tap, we divide the wind tunnel pressure time history in non-overlapping segments, each segment with 5989 samples representing about 15 seconds time history for the model scale that corresponds to about four minutes full-scale pressure history for the mean wind speed at the average roof height of 30 m/s. The statistics of the absolute value of the peak negative pressure coefficients are shown in Table 4.8. By considering that the Gumbel probability model can be used to represent the peak pressure coefficient and based on the extreme value analysis, the parameters of the probability model for a period of one hour and the reference wind speed U at the average roof height is calculated and shown in Table 4.8. Also shown in the table are the calculated mean and cov of $\hat{C}_m$. From the table, it can be observed that the values of the estimated mean of $\hat{C}_m$ are within the range of the values of the pressure-gust coefficients (i.e., C_pC_g) for primary structural actions arising from wind load acting simultaneously on all surfaces recommended by the NBCC (2005). However, they are much smaller than the C_pC_g values for the design of structural components and cladding suggested by the same code. This is expected as the code value represents the maximum wind pressure from different wind directions. The implication that the (absolute) C_pC_g value, which is

about 4 for an area of a typical roof panel size, is significantly greater than mean of $\hat{C}_m$ shown in Table 4.8, and the implication on reliability will be shown shortly.

To evaluate P_f, we note that the annual maximum (hourly) mean wind speed U is commonly modeled as a Gumbel variate. The mean and cov of the annual wind speed for more than 230 locations, each having more than at least 10 years of record and provided by the Engineering Climatology Section of the Canadian Meteorological Centre in Downsview for the calibration of 2005 edition of NBCC, were considered. For the majority of these locations, the statistics indicate that the cov of U, v_U, ranges from 0.08 to 0.18 and an overall cov value of 0.13, and that the mean of U, m_U, varies from about 10 to 30 (m/s), and an overall mean of about 18 (m/s).

Using the afore-mentioned information, the characterizations of $F_{TF,E}$ and R_n given in the previous section, and considering that C_E in Eq. (5) is replaced by $\hat{C}_m$, the estimation annual probability of failure P_f based on the simple simulation technique can be carried out according to the following steps:

1) Sample $F_{TF,E}$ and U from their corresponding probability models;
2) Evaluate n using Eq. (10), and evaluate α_n and a_n using Eqs. (7) and (8), sample C_E according to the distribution shown in Eq. (6), and evaluate g;
3) Repeat Steps 1) to 2) n_s times and count number of times, n_f, that g is less than zero; and the estimated P_f equals n_f/n_s.

The reliability index β corresponding to the estimated P_f, equals $\Phi^{-1}\left(1-P_f\right)$, where $\Phi^{-1}(\,)$ denotes the inverse of the standard normal distribution function.

Table 4.8 Statistics of the peak of the absolute value of the negative wind pressure coefficients and parameters of Gumbel model (see Eq. (6)) for $\hat{C}_m$.

Panel	Statistics based on 5989 point-in-time samples		Probability distribution model parameters for $\hat{C}_m$ considering the duration of one hour and a reference hourly mean wind speed (at the average roof height) of U		Mean and cov of $\hat{C}_m$ for the duration of one hour		
	Mean m_{cm}	Standard deviation σ_{cm}	$\alpha_n = \pi/\left(\sqrt{6}\times\sigma_{cm}\right)$	$a_n = m_{cm} + \frac{1}{\alpha_n}\left(\ln\left(\frac{3010U}{5989}\right) - 0.577\right)$	For U = 20 m/s	For U = 25 m/s	For U = 30 m/s
S34	1.977	0.240	5.345	$1.977 + \frac{1}{5.345}\left(\ln\left(\frac{3010U}{5989}\right) - 0.577\right)$	2.408, 0.100	2.449, 0.098	2.484, 0.097
S35	2.635	0.237	5.416	$2.635 + \frac{1}{5.416}\left(\ln\left(\frac{3010U}{5989}\right) - 0.577\right)$	3.061, 0.077	3.102, 0.076	3.136, 0.076
S55	2.278	0.209	6.141	$2.278 + \frac{1}{6.141}\left(\ln\left(\frac{3010U}{5989}\right) - 0.577\right)$	2.654, 0.079	2.690, 0.078	2.720, 0.077

Table 4.9 Estimated annual failure probability for the selected panels for different wind hazard conditions.

Error Rate	Nail Correlation	Wind Hazard Condition		S34		S35		S55	
		Mean of U (m/s)	cov of U	P_f	β	P_f	β	P_f	β
0%	$\rho_{ij} = 0$	20	0.15	1.11×10^{-5}	4.24	7.28×10^{-5}	3.80	2.60×10^{-5}	4.05
		25	0.15	5.22×10^{-4}	3.28	2.43×10^{-3}	2.82	1.04×10^{-3}	3.08
		30	0.15	7.03×10^{-3}	2.46	2.53×10^{-2}	1.96	1.24×10^{-2}	2.24
		25	0.08	2.43×10^{-6}	4.57	3.70×10^{-5}	3.96	7.95×10^{-6}	4.32
		25	0.18	1.56×10^{-3}	2.96	5.80×10^{-3}	2.52	2.83×10^{-3}	2.77
	$\rho_{ij} = 1$	20	0.15	1.84×10^{-5}	4.13	1.16×10^{-4}	3.68	3.86×10^{-5}	3.95
		25	0.15	7.71×10^{-4}	3.17	3.26×10^{-3}	2.72	1.33×10^{-3}	3.00
		30	0.15	9.02×10^{-3}	2.36	3.00×10^{-2}	1.88	1.42×10^{-2}	2.19
		25	0.08	1.04×10^{-5}	4.26	1.01×10^{-4}	3.72	2.15×10^{-5}	4.09
		25	0.18	2.02×10^{-3}	2.88	6.96×10^{-3}	2.46	3.27×10^{-5}	2.72
1.5%	$\rho_{ij} = 0$	20	0.15	1.13×10^{-5}	4.24	1.08×10^{-4}	3.70	3.41×10^{-5}	3.98
		25	0.15	6.10×10^{-4}	3.23	3.31×10^{-3}	2.72	1.30×10^{-3}	3.01
		30	0.15	7.86×10^{-3}	2.41	3.21×10^{-2}	1.85	1.49×10^{-2}	2.17
		25	0.08	4.05×10^{-6}	4.46	6.47×10^{-5}	3.83	1.24×10^{-5}	4.22
		25	0.18	1.74×10^{-3}	2.92	7.43×10^{-3}	2.44	3.38×10^{-3}	2.71
	$\rho_{ij} = 1$	20	0.15	2.44×10^{-5}	4.06	1.60×10^{-4}	3.60	5.67×10^{-5}	3.86
		25	0.15	9.09×10^{-4}	3.12	4.06×10^{-3}	2.65	1.74×10^{-3}	2.92
		30	0.15	1.03×10^{-2}	2.32	3.54×10^{-2}	1.81	1.76×10^{-2}	2.11
		25	0.08	1.53×10^{-5}	4.17	1.66×10^{-4}	3.59	3.83×10^{-5}	3.95
		25	0.18	2.33×10^{-3}	2.83	8.34×10^{-3}	2.39	4.05×10^{-3}	2.65

By using this outlined procedure and the statistics of the uplift capacity shown in Table 4.4 with and without construction error, P_f and its corresponding β are estimated by considering a few combinations of values of m_U and v_U. For the analysis, a simulation cycle of 10^8 is employed, and the obtained P_f and β are shown in Table 4.9 for the considered Panels S34, S35 and S55. The table indicates that in all cases the estimated P_f for $m_U \geq 25$ (m/s) and $v_U \geq 0.15$ is greater than the tolerable annual failure probability level of about 5×10^{-5} to 10^{-6} (CSA S408 1980); the lowest reliability index equal to 1.81 is associated with the case with construction error $m_U = 30$ (m/s) and $v_U = 0.15$ for Panel S35. The results imply that use of the NBCC (2005) suggested fastening schedule to not ensure the roof panels meet the recommended target reliability level in the CSA S408 (1980). The ratio of the estimated P_f with construction error to that without construction error ranges from about 1.01 to about 1.75. Note that the mean of the uplift capacity for $\rho_{ij} = 1.0$ is greater than that for $\rho_{ij} = 0$, and the cov of the uplift capacity for $\rho_{ij} = 1.0$ is lower than that for $\rho_{ij} = 0$ (see Table 4.4). Their combination resulted in the estimated P_f for the case with $\rho_{ij} = 1.0$ that is greater than that for the case with $\rho_{ij} = 0$.

To investigate the impact of the mean of $\hat{C}_m$ on the estimated annual failure probability, a sensitivity analysis is carried out considering that the mean of $\hat{C}_m$ varies from 2.0 to 5.0 and the cov of $\hat{C}_m$ equals 0.05, 0.10 and 0.15. For the analysis, only the uplift capacity shown in Table 4.4 for Panel S35 is considered, as the statistics of $F_{TF,\,E}$ and the value of R_n for the three selected panels are similar. The consideration of the upper bound value of mean of $\hat{C}_m$ is based on the NBCC (2005) recommended C_pC_g values for the design of structural components and cladding. The estimated P_f is shown

in Figure 4.7 for m_U = 18 (m/s) and v_U = 0.05, 0.10 and 0.15. The results shown in the figure indicates that the estimated P_f is very sensitive to the mean of $\hat{C}_m$. If the mean of $\hat{C}_m$ is greater than 4.0, the estimated P_f is significantly higher than a tolerable annual failure probability of 10^{-5}. Therefore, for such a high mean value of $\hat{C}_m$, a more stringent fastening schedule should be considered to reduce the annual failure probability. In particular, if the more stringent fastening schedule with a nail spacing of 150 mm for both edge and intermediate supports is considered, by repeating the analysis that was carried out for Figure 4.7, the estimated P_f in all cases is less than 10^{-6} for mean value of $\hat{C}_m$ less than 5.0. This indicates that a significant increase of reliability level of roof panel can be achieved if the more stringent fastening schedule is adopted for the construction of light frame wood houses.

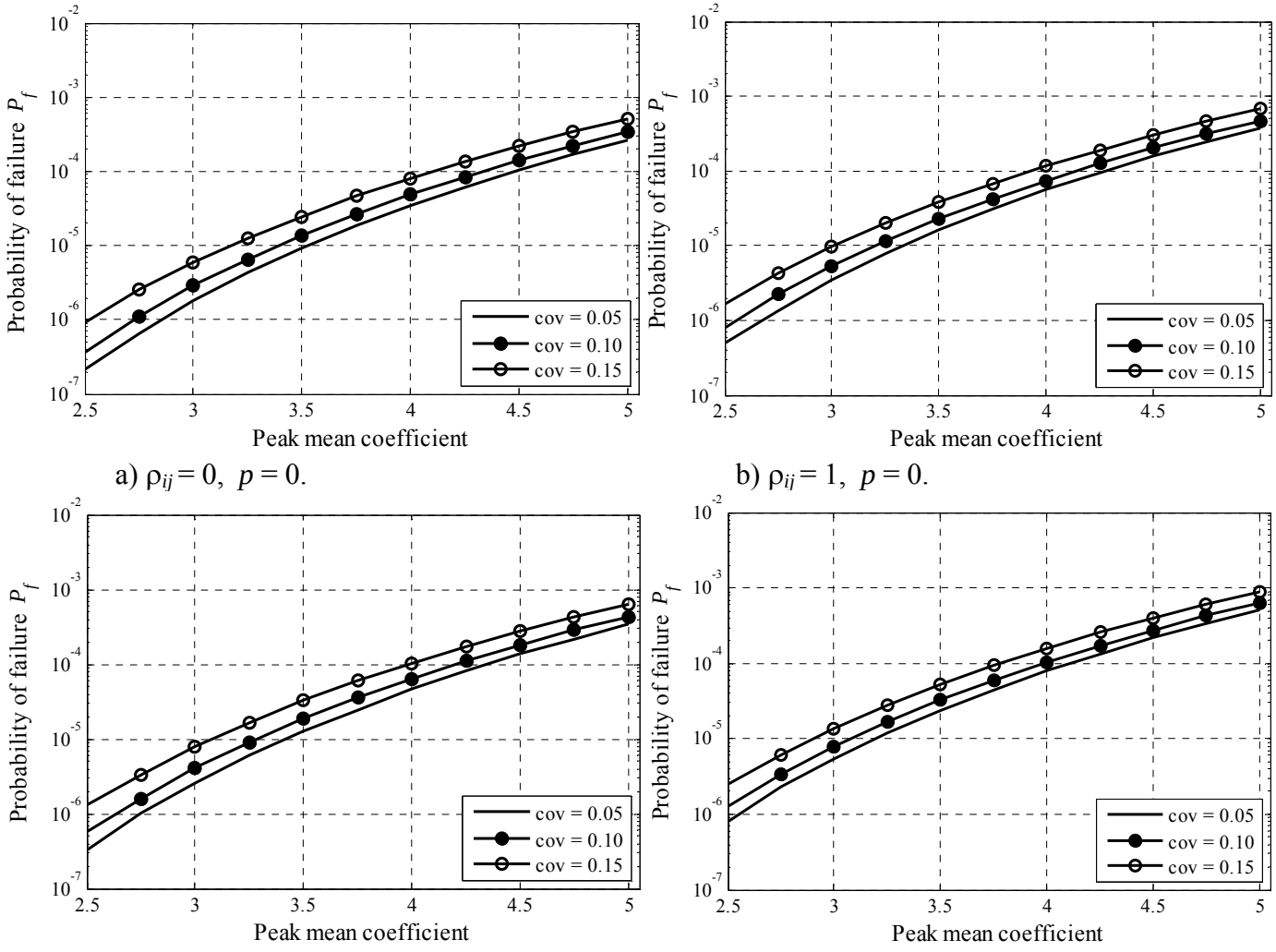

Figure 4.7 Estimated annual failure probability for nail spacing shown in Figure 2.

4.6. Conclusions

The occurrence of construction error on the fastening of roof panels for a full-scale two-story test house is described and used to develop a probability model. Statistics of roof panel uplift capacity are evaluated by considering and ignoring the missing nails, and the uncertainty in nail withdrawal behaviour. The results indicate that if the missing nail effect is ignored, an overestimation of the mean of the panel uplift capacity by about 4% can be observed. Also, the consideration of the construction error increases the coefficient of variation of the uplift capacity of the panel, especially if the withdrawal behaviour of the nails within the panel is fully correlated.

The estimated annual failure probability, P_f, of the roof panel fastened according to the NBCC (2005) requirement, for most considered wind hazard cases (representative of Canadian sites), is larger than the recommended tolerable annual failure probability level for calibrating design codes, which ranges from 5×10^{-5} to 1×10^{-6}. The ratio of the estimated P_f with construction error to that without construction error is up to 1.75.

If the code specified gust wind pressure coefficients for the design of structural components and cladding is considered, the obtained P_f is further increased. In such a case, it is suggested that a more stringent fastening schedule with a spacing of 150 mm for the edges and intermediate supports is to be adopted for the construction of light frame wood houses.

Reference:

Allen, D.E. (1986a). Tornado damage in the Barrie/Orangeville area, Ontario, May 1985. Building Research Note No. 240, National Research Council Canada.

Allen, D.E. (1986b). Human error and structural practice, in Modeling human error in Structural Design and Construction, Building Research Note No. 240, National Research Council Canada.

ANSYS Inc. (2005), ANSYS User's Manual, Version 10.0, Canonsburg, PA.

Atkinson, A. (1998). Human error in the management of building projects, Construction Management and Economics, 16: 339-349.

Bartlett, F.M., Galsworthy, J.K., Henderson, D., Hong, H.P., Iizumi, E., Inculet, D.R., Kopp, G.A., Morrison, M.J., Savory, E., Sabarinathan, J., Sauer, A., Scott, J., St. Pierre, L.M. and Surry, D. (2007). The Three Little Pigs Project: A New Test Facility for Full-Scale Small Buildings. In: International Conference on Wind Engineering, Cairns.

Benjamin, J.R. and Cornell, C.A. (1970). Probability, Statistics and Decision for Civil Engineers, McGraw-Hill, New York.

Canadian Plywood Association (2005). Plywood Design Fundamentals, www.canply.org

Dao, T.N. and van de Lindt, J.W. (2009). New Nonlinear Roof Sheathing Fastener Model for Use in Finite-Element Wind Load Applications, Journal of Structural Engineering, ASCE, 134(10): 1668-1674.

Ellingwood, B. (1987). Design and construction error effects on structural reliability, Journal of structural engineering New York, N.Y., 113(2), 409-422.

Ellingwood, B.R., Rosowsky, D.V., Li, Y. and Kim, J.H. (2004). Fragility assessment of

light-frame wood construction subjected to wind and earthquake hazard, Journal of Structural Engineering, 130(12): 1921-1930.

Foschi, R.O. (2000). Modeling the hysteretic response of mechanical connections for wood structures, Proc., World Conf. on Timber Engrg., Dept. of Wood Sci., ed., University of British Columbia, Vancouver.

Groom, K.M. and Leichti, R.J. (1993). Load withdrawal displacement characteristics of nails, Forest Products Journal, 43(1), pp. 51-54.

Gurley, K., Davis Jr, R.H., Ferrera, S.P., Burton, J., Masters, F., Reinhold, T. and Abdullah, M.P. (2004) Hurricane field survey - An evaluation of the relative performance of the standard building code and the Florida building code. St. Louis, MO, United states, 8.

Jordaan, I. (2005) Decision under uncertainty – Probabilistic analysis for engineering decisions, Cambridge University Press.UK.

Kopp, G.A., Morrison, M.J., Gavanski, E., Henderson, D. and Hong, H.P. (2010). The "Three Little Pigs" Project: Hurricane Risk Mitigation by Integrated Wind Tunnel and Full-Scale Laboratory Tests, Natural Hazards Review, http://dx.doi.org/10.1061/(ASCE) NH.1527-6996.0000019.

Kopp, G.A., Surry, S. and Mans, C. (2005). Wind effects of parapets on low buildings: Part 1. Basic aerodynamics and local loads, Journal of Wind Engineering and Industrial Aerodynamics, 93: 817-841.

Lee, K. H. and Rosowsky, D.V. (2005). "Fragility assessment for roof sheathing failure in high wind regions." Engineering Structures, 27(6), 857-868.

Madsen, H.O., Krenk, S. and Lind, N.C. (1986). Methods of Structural Safety, Prentice-

Hall, Inc., Englewood Cliffs, New Jersey.

Matousek, M. (1982). Measures against Errors in the Building Process. Institute of Structural Engineering, Swiss Federal Institute of Technology, Zurich, Switzerland (Translation No. 2067, National Research Council of Canada, 1983).

Melchers, R.E. (1989) Human error in structural design tasks. Journal of Structural Engineering, 115(7): 1795- 807.

Mizzell, D.P. (1994). Wind Resistance of Sheathing for Residential Roofs, Civil Engineering Department, MS Thesis Clemson, Clemson University.

NAHB Research Center. (2003). Roof sheathing connection tolerances, U.S. Department of Housing and Urban Development Office of Policy Development and Research, Washington, DC.

NBCC. (2005). National Building Code of Canada 1995. Institute for Research in Construction, National Research Council of Canada, Ottawa, Ont.

Nowak, A.S. and Collins, K.R. (2000). Reliability of structures. McGraw-Hill, New York.

Rosowsky, D. V. and Ellingwood, B. R. (2002). Performance-based engineering of wood frame housing: Fragility analysis methodology. Journal of Structural Engineering, 128(1), 32-38

Rosowsky, D.V. and Schiff, S.D. (1996) Probabilistic modeling of roof sheathing uplift capacity, Proceedings of the 1996 7th Specialty Conference on Probabilistic Mechanics and Structural Reliability, p 334-337

Rubinstein, R.Y. and Kroese, D.P. (2007). Simulation and the Monte Carlo Method (2nd ed.). New York: John Wiley & Sons.

Simiu, E. and Scanlan R.H. (1996). Wind Effects on Structures, Fundamentals and

Application to Design, New York: John Wiley.

Simiu, E. and Stathopoulos. T. (1997). Codification of wind loads on buildings using bluff body aerodynamics and climatological data bases. Journal of Wind Engineering and Industrial Aerodynamics, 69-71: 497-506.

Sparks, P.R., Schiff, S.D. and Reinhold, T.A. (1994). Wind damage to envelopes of houses and consequent insurance losses, Journal of Wind Engineering and Industrial Aerodynamics, 53(1-2): 145-155.

Stewart, M.G. (1993) Structural reliability and error control in reinforced concrete design and construction. Structural Safety, 12, 277- 92.

Surry, D. and Stathopoulos, T. (1978). An experimental approach to the economical measurement of spatially - Averaged Wind Loads, Journal of Ind. Aerodynamics, 2: 385-397.

Surry, D., Kopp, G.A., and Bartlett, F.M. (2005). Wind load testing of low buildings to failure at model and full scale, ASCE Natural Hazards Review, 6: 121-128.

Sutt, E.G. (2000). The Effect of Combined Shear and Uplift Forces on Roof Sheathing Panels, PhD thesis, Dept. of Civil Engineering, Clemson University, Clemson, S. C.

Rosowsky, D.V. and Lee, K.H. (2005). Fragility assessment for roof sheathing failure in high wind regions, Engineering structures, 27: 857-868.

Rosowsky, D.V. and Cheng N. (1999) Reliability of light-frame roofs in high-wind regions. II: Reliability analysis, Journal of Structural Engineering, 125(7): 734-739.

Shanmugam, B., Nielson, B.G. and Prevatt, D.O. (2009). Statistical and analytical models for roof components in existing light-framed wood structures, Engineering Structures, 31(11): 2607-2616.

CHAPTER 5

CONCLUSIONS AND FUTURE WORK

5.1 Summary and Conclusions

The main objectives of the present study are to assess the statistics of the roof panel uplift capacity, and to estimate the reliability of roof panel with typical fastening schedule under wind loading. For the analysis and estimation uncertainty in nonlinear nail withdrawal behaviour and the spatially and temporally varying wind pressure coefficients. The analysis also incorporates the construction error (i.e., effect of missing or improperly installed nails to fasten the roof panel). For the analyses, the panel is modeled using a finite element model, the nail withdrawal behaviour is modeled using a nonlinear spring, and the reliability of the roof panel under wind loading is estimated using the simulation technique. The conclusions that can be drawn from the numerical analysis are given below.

I) Based on the analysis for roof panel subjecting to time-varing uniform wind pressure, the conclusions are list below from I.1 to I.5.

I.1) The nonlinear static pushover (NSP) analysis and nonlinear incremental dynamic analysis were adopted for assessing the roof panel uplift capacity. It was observed that the use of the NSP analysis is adequate for estimating the uplift capacity of the panel.

I.2) The consideration of statistical correlation of nail withdrawal behaviour for the nails used to fastening the roof panel affects the mean of uplift capacity about 5%, and it reduces the coefficient of variation (cov) of the uplift capacity significantly as the degree of correlation between the nail behaviour decreases. The uplift

capacity of roof panel can be modeled adequately as a lognormal variate.

I.3) In general, the use of the simple tributary area approach underestimates the mean of the uplift capacity by 10% to 22% (for different nail correlation) as compared to that estimated using the NSP analysis. This underestimation is also about 10% if the panel is modeled using the finite element model and the nail withdrawal behaviour is modeled using (equivalent) linear-brittle spring. The difference of estimated panel uplift capacity using tributary area method and linear finite element model is not significant, and the difference is due to the fact that the tributary area method does not consider the load sharing among nails with different stiffness.

I.4) Sensitivity analysis indicates that missing a single nail could reduce the mean of the panel uplift capacity by 10%, and missing two nails could reduce the mean of R by as much as about 20%.

I.5) By using a more stringent nail schedule with the nails spacing of 6 inches on the edge and intermediate supports, the mean of uplift capacity is about twice of that obtained by using a nail spacing of 6 inches for edge supports and of 12 inches for intermediate support, which is a recommended practice by the 2005 edition of the National Building Code of Canada (NBCC 2005).

II) Based on the analysis results for roof panel subjecting to spatially and temporally varying wind pressure, the conclusions are list below from II.1 to II.5.

II.1) The statistics of the panel uplift capacity in terms of the (ultimate) total reacting force are not sensitive to the spatially varying wind, but are significantly

influenced by the adopted probabilistic model and correlation of nail withdrawal behaviour. This is especially true for the coefficient of variation (cov) of the total reacting force.

II.2) The use of the equivalent uniformly distributed wind loading, with the pressure coefficient equal to the weighted average wind pressure coefficient, provides sufficiently accurate estimates of the statistics of the uplift capacity of panel. This approximate approach is therefore recommended for assessing the panel uplift capacity as it simplifies the analysis. The approximation introduces a modeling error with a bias close to unity and a cov of only 4% which is much smaller than those associated of the ultimate total reacting force ranging from 7% to 20%.

II.3) The spatial correlation coefficient of the instantaneous pressure coefficients can be modeled using an exponential model with correlation length within 1.5 m to 3.0 m.

II.4) The ultimate total reacting force (i.e., the uplift capacity of the panel) of the panel could be modeled as lognormal variate. The investigation of the effect of missing nail on the uplift capacity indicates that missing a single critical nail could reduce the mean of the panel uplift capacity by about 10%.

II.5) The panel uplift capacity can also be characterized by the critical reference mean wind speed. As expected, the statistics of the speed depend on the location of the roof panel because the magnitude of and uncertainty in the pressure coefficients are location dependent. In all cases, the statistics represent the uplift capacity of the panel associated with the instantaneous pressure coefficients, and they do not incorporate the gust effect or exposure factor.

III) Based on analysis results by considering or ignoring construction error and reliability analysis results, the conclusions are list below from III.1 to III.5.

III.1) Survey and inspection of nails used to fastening the roof panels for a full-scale two-story test house is carried out. Simple statistical analysis indicates that the missing or improperly installed nails (i.e., construction error) can be modeled as a binomial process with a defect rate of 1.5%.

III.2) Results of the estimated uplift capacity by considering/ignoring the construction error indicate that if the construction error is not considered, on average, the uplift capacity is overestimated by about 6%. The consideration of the construction error increases the coefficient of variation of the uplift capacity of the panel, especially if the withdrawal behaviour of the nails within the panel is fully correlated.

III.3) To carry out reliability assessment of the roof panel under wind loading, an extreme analysis of the pressure coefficients was carried out, indicating that the magnitude of the mean of the peak wind pressure coefficients for the considered time histories is significantly lower than the pressure-gust coefficients (i.e., C_pC_g) recommended by the NBCC (2005) for the design of structural components and cladding. We attribute this to that the considered wind direction acting on the test model may differ from the critical wind direction for the considered pressure taps and panels, the location of the panel that was selected is not the location where subjecting highest wind pressure, and that the available wind pressure record employed in the extreme analysis may not be sufficiently long

III.4) By using these extreme value statistics of wind pressure coefficients, the estimated annual failure probability of the roof panel, P_f, for most considered wind hazard cases is smaller than the recommended tolerable annual failure probability level for calibrating design codes, which ranges from 1.6×10^{-4} to 7×10^{-7}. The ratio of the estimated P_f with construction error to that without construction error ranges from about 1 to about 1.75.

III.5) If the code value of the pressure-gust coefficients (i.e., C_pC_g) for the design of structural components and cladding is considered, the obtained P_f can be higher than the tolerable annual failure probability level. In such a case, it is suggested that a more stringent fastening schedule with a spacing of 150 mm for the edges and intermediate supports is to be adopted for the construction of light frame wood houses.

5.2. Suggested future work

It is suggest that the analyses presented in the present study is to be repeated for the whole roof system. This is likely to be very intensive computing time consuming task. The obtained results can be used to aid the development of simple approach to estimating the reliability of roof system. They can also be used to aid the calibration of design code.

Also, the analysis can be extended to include the roof trusses and impact of the construction error associated with the toe nails used to fastening the trusses on the reliability of the roof system.

APPENDIX A

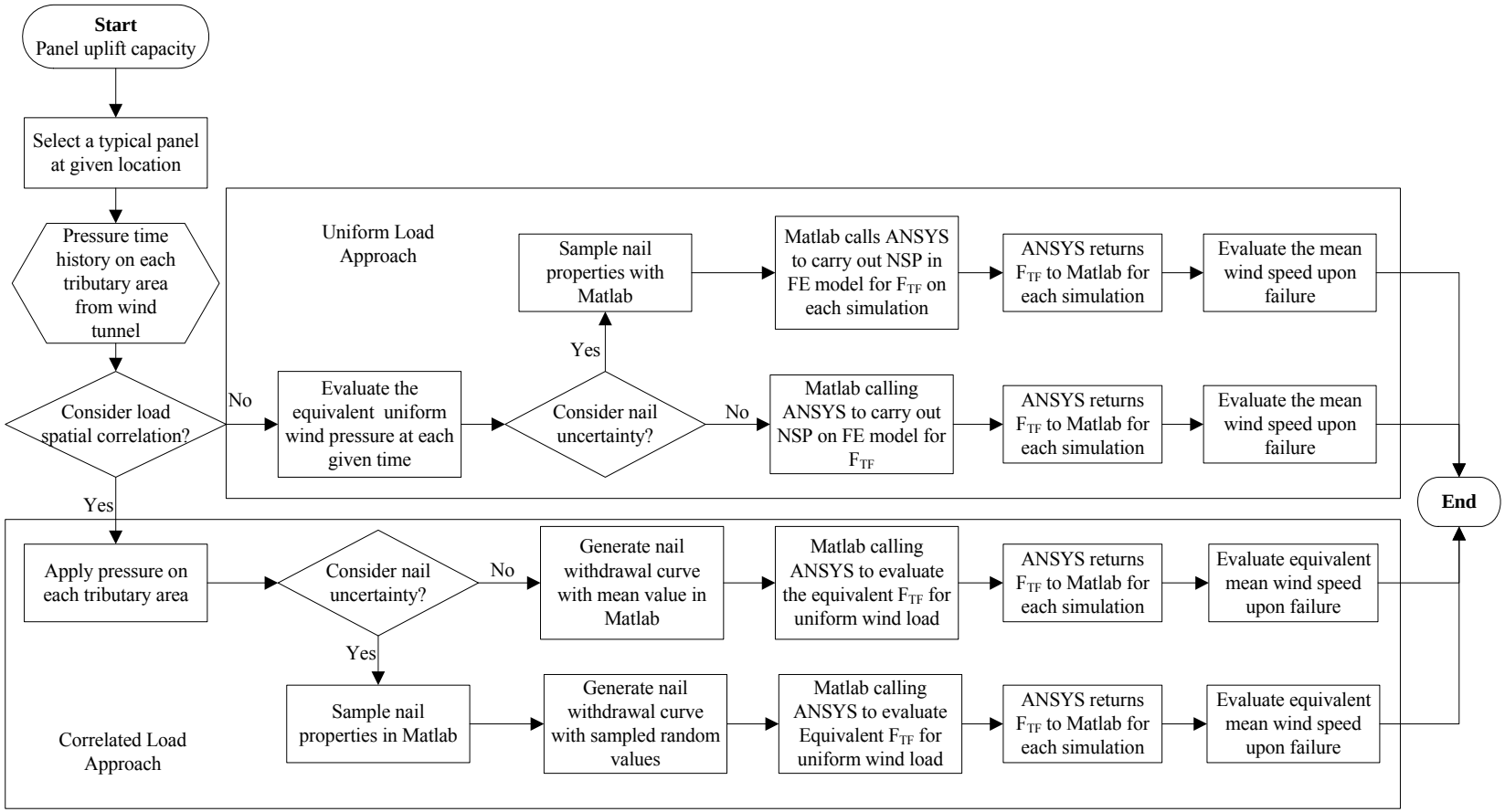

Figure A.1. The detailed flow chart of the analysis using Matlab and ANSYS

CURRICULUM VITAE

Name:	Weixian He
Post-secondary Education and Degrees:	The University of Western Ontario London, Ontario, Canada 2006-2010, PhD (Structural Engineering) The University of Western Ontario London, Ontario, Canada 2004-2006, M.Eng.(Structural Engineering) Tongji University Shanghai, China 1992-1996, B.Eng.(Engineering Mechanics)
Related Work Experience:	Lecturer The University of Western Ontario London, Ontario, Canada, 2009 Research and Teaching Assistant The University of Western Ontario London, Ontario, Canada, 2006-2009 Structural Engineer Third Harbour Engineering Co., Ltd. Shanghai, China, 1996-2003